Mathematical Modelling and Numerical Simulation of Aromatic Nitrations by Mixed Acid in Discontinuous Reactors

J. M. Zaldivar

JOINT RESEARCH CENTRE
EUROPEAN COMMISSION

1995

EUR 16266 EN

Published by the
EUROPEAN COMMISSION
Directorate-General XIII
Telecommunications, Information Market and Exploitation of Research
L-2920 Luxembourg

Cataloguing data can be found at the end of this publication

Luxembourg: Office for Official Publications of the European Communities, 1995

ISBN 92-827-4107-9

Printed in Italy

MATHEMATICAL MODELLING AND NUMERICAL SIMULATION OF AROMATIC NITRATIONS BY MIXED ACID IN DISCONTINUOUS REACTORS

PROEFSCHRIFT

ter verkrijging van
de graad van doctor aan de Universiteit Twente,
op gezag van de Rector Magnificus,
prof.dr. Th.J.A. Popma,
volgens besluit van het College voor Promoties
in het openbaar te verdedigen
op donderdag 22 juni 1995 te 13.15 uur.

door

José Manuel Zaldívar Comenges

geboren op 7 june 1958
te Barcelona (Spain)

dit proefschrift is goedgekeurd door de promotor

Prof. dr. ir. K.R. Westerterp

MATHEMATICAL MODELLING AND NUMERICAL SIMULATION OF AROMATIC NITRATIONS BY MIXED ACID IN DISCONTINUOUS REACTORS

J. M. Zaldívar Comenges

en de referenten:
Dr. M. S. A. Vrijland
Dr. Ir. M. Steensma

en de deskundige:
Dr. E. Molga

Printing and binding Publications Service, Joint Research Center, Ispra, Italy

CIP - DATA KONINKLIJKE BIBLIOTHEEK, DEN HAAG

Zaldívar Comenges, José Manuel

Mathematical modelling and numerical simulation of aromatic nitrations by mixed acid in discontinuous reactors / José Manuel Zaldívar Comenges

Thesis Enschede. - With ref.

ISBN
Subject headings: liquid-liquid reactions/ aromatic nitrations / batch processes

SUMMARY AND CONCLUSIONS

This thesis deals with the mathematical modelling and numerical simulation of aromatic nitrations in discontinuous reactors, and the experimental work carried out to characterise the model, as well as to verify the simulated results. A general introduction about the main subjects discussed is given in Chapter 1.

In Chapter 2 the heat and mass balances for discontinuous - batch and semibatch - reactors are derived. Emphasis has been placed on a realistic description of such reactors by incorporating an accurate representation of all secondary heat effects like heat taken up by reactor wall, heat losses, stirring power supply and dilution heat; and a model of the heating/cooling circuits as well as their controllers. On the basis of the fundamental equations developed, the procedure followed to identify the model parameters, to implement the simulator and to validate it for a bench scale reactor using well-known reactions, is described. The numerical solution of the mass and heat balances yields the reaction temperature and conversion as functions of time. The simulated values are compared with those experimental. The results of the simulator are in excellent agreement with the experimental values. The main observed differences are attributable to the lack of appropriate data that frequently are only valid within a short range of process variables. Undoubtedly, the thermo-kinetic data are the most sensitive; for instance, even for a simple reaction such as a neutralisation between sodium hydroxide and hydrogen chloride the heat of solution is still not well known. Another problem concerns the definition of the mixture properties that usually, in absence of experimental data, are treated as ideal systems. To minimise the data problem the simulator is implemented allowing flexibility from the physico-chemical and thermokinetics viewpoints. The user according to the data available and his/her understanding of the process, may define the data complexity, that can vary from very simple, e.g. constant values, to more complex, e.g. temperature and concentration dependencies.

Compared with homogeneous systems, the analysis of heterogeneous liquid-liquid systems is still further complicated. The most common method of bringing about the contact of the two liquid phases is to disperse droplets of one within the other by mechanical agitation. In such systems, the rate of interphase mass transfer as well as chemical reaction is affected not only by the physical and chemical characteristics of the system but also by the mechanical features of the equipment. The former includes viscosities and densities of the phases, interfacial surface properties, diffusion coefficients, distribution coefficients of reagents and products between the phases and chemical reaction constants. The latter include, for example, the type and diameter of the impeller, vessel geometry, the flow rate of each phase and the rotational speed of the impeller. Furthermore, dispersion phenomena such as coalescence and breakage of droplets,

drop size distribution and phase inversion will affect the extent of conversion and selectivity of the reactions.

To take into account such parameters experiments have been performed to characterise separately their influence, when possible.

Aromatic nitrations are studied in Chapters 3 - 6. The first one studies the heat effects in aromatic nitrations. The knowledge of the rate of heat generation due to dilution is important in reaction calorimetry to calculate accurately the rate of heat generation due to nitration which can be obtained from adiabatic calorimetry.

Chapter 4 is devoted to the mechanistic aspects of homogeneous nitrations and to check the validity under heterogeneous conditions of the kinetic data derived in homogeneous conditions. For this reason the slow liquid-liquid reaction regime, i.e. low sulphuric acid strength, is studied. Chapter 5 is dedicated to study the aromatic nitrations in conditions of chemically enhanced transfer, i.e. high sulphuric acid strength. The instantaneous reaction regime is entered if the conversion rate becomes extremely high. Furthermore, interfacial area is studied separately, using a similar system, to estimate the values during nitration experiments.

The last Chapter is devoted to the study of phase inversion phenomena during semibatch nitrations. If more and more dispersed-phase material, as in the semibatch nitration processes, is added to the stirred system, a point is eventually reached at which the addition of more dispersed phase causes inversion: the continuous phase suddenly becomes the dispersed one and *viceversa*. Inversion of phases is frequently accompanied either by a decrease or by an increase in the interfacial area. This effect, if the conversion rate is mass transfer controlled, can produce an unexpected step change on the overall rate.

The model employed, based on the effective interfacial area between the two liquids and the description of mass transfer with reaction using the film model is used.

Theoretical model predictions are compared with experimental results and the effect of the different parameters is discussed. From the comparisons between model and experimental results it can be concluded that it is possible to extrapolate data from homogeneous nitration experiments and to interpret the dynamic behaviour of discontinuous nitration processes of benzene, toluene and chlorobenzene in the different reaction regimens. Furthermore, the accumulation of unreacted nitric acid in semibatch aromatic nitrations can be dangerous if accompanied by a phase inversion due to the fact that the heat rate production may increase suddenly, since the conversion rate is usually mass transfer controlled under industrial operating conditions. The main parameter resposible for this increase is the interfacial area that increases if the continuous phase changes to acid phase.

SAMENVATTING EN CONCLUSIES

Dit proefschrift behandelt de wiskundige modelering en numerieke simulatie van aromatische nitreringen in niet-continue reactoren, en het experimentele werk uitgevoerd ter characterisering van het model en ter verifiering van de gesimuleerde resultaten. Een algemene inleiding over de besproken hoofd onderwerpen wordt gegeven in Hoofdstuk 1. In Hoofdstuk 2 worden de warmte-en massa balansen afgeleid voor niet continue -batch en semibatch- reactoren. De nadruk wordt gelegd op een realistische beschrijving van dergelijke reactoren door het inbouwen van een accurate weergave van alle secondaire warmte effecten zoals door de reactorwand opgenomen warmte, warmteverliezen, toevoer van roervermogen en oploswarmte; en een model van de verwarmings- en koelcircuits met hun regelaars. Op basis van de ontwikkelde fundamentele vergelijkingen, wordt de de gevolgde procedure beschreven voor identificatie van de model parameters, voor implementatie van de simulator en voor het valideren ervan voor een "bench-scale" reactor met gebruikmaking van goed bekende reacties. De numerieke simulatie van de massa- en warmtebalansen leidt tot de reactietemperatuur en conversie als functie van de tijd. De gesimuleerde waarden worden vergeleken met de experimentele. De belangrijkste waargenomen verschillen kunnen toegeschreven worden aan het tekort aan juiste data die vaak slechts gelden binnen een klein bereik van procesvariabelen. De thermokinetische data zijn ongetwijfeld de meest sensitieve(gevoelige): bij voorbeeld, zelfs voor een eenvoudige reactie zoals de neutralisatie van natronloog met zoutzuur is de oploswarmte nog steeds niet goed bekend. Een ander probleem betreft de definitie van de mengeigenschappen die gewoonlijk, bij ontbreken van experimentele data, als ideale systemen worden behandeld. Om het data probleem te minimaliseren, wordt de simulator zo geimplementeerd dat flexibiliteit -bezien vanuit een fysisch-chemisch en thermokinetisch oogpunt - is toegestaan. In overeenstemming met de beschikbare data en zijn of haar begrip van het proces, kan de gebruiker de gecompliceerdheid van de data definieren, die kunnen varieren tussen erg eenvoudig, bijv. costante waarden, tot meer complex, bijv. temperatuur en concentratie afhankelijkheden.

Vergeleken met homogene systemen is de analyse van heterogene vloeistof-vloeistof systemen nog gecompliceerder. De meest gangbare methode van het in contact brengen van de twee vloeistoffasen is het dispergeren (van druppels) van de ene in de andere door mechanische menging. In dergelijke systemen wordt de snelheid van massaoverdracht tussen de fasen en de chemische reactie niet alleen beinvloed door de fysische en chemische characteristieken van het systeem, maar ook ook door de mechanische werking van de apparatuur. De laatste houdt in viscositeiten en dichtheden van de fasen, grensvlakeigenschappen, diffusiecoefficienten, verdelingscoefficienten van reagentia en producten tussen de fasen en chemische reactie constanten. De laatste houdt in, bijv, het type en de diameter van de roerder, de

reactorgeometrie, de stroomsnelheid van elke fase en de rotatiesnelheid van de roerder (toerental?). Verder zullen dispersie verschijnselen zoals coalescentie en opbreking van druppels, druppel grootte verdeling en faseinversie, de conversiegraad en de selectiviteit van de reacties beinvloeden. Om met deze parameters rekening te houden zijn er experimenten uitgevoerd om -indien mogelijk- apart hun effect te characteriseren. Aromatische nitreringen worden beschouwd in Hoofdstukken 3-6. De eerste beschouwd de warmte-effecten in aromatische nitreringen. Kennis van de snelheid van warmteontwikkeling door oplossen is belangrijk bij reactie calorimetrie om de snelheid van warmteontwikkeling door nitratie accuraat te kunnen berekenen, welke uit adiabatische calorimetrie verkregen kan worden.

Hoofdstuk 4 is gewijd aan de mechanistische aspecten van homogene nitreringen en aan de geldigheidscontrole van de kinetische data onder heterogene condities, afgeleid van homogene condities. Hiervoor is het langzame vloeistof-vloeistof reactie regiem - bij lage zwavelzuur sterkte- onderzocht. Hoofdstuk 5 is gewijd aan de aromatische nitrering onder condities van chemisch verbeterde overdracht, te weten, hoge zwavelzuur sterkte.Men komt in het instantane reactie regiem als de omzettingssnelheid extreem hoog wordt. Verder wordt het grensvlak afzonderlijk bestudeerd met gebruik making van een soortgelijk systeem om de waardes tijdens nitreer experimenten te schatten.

Het laatste hoofdstuk is gewijd aan het onderzoek naar fase inversie verschijnselentijdens semi-batch nitreringen. Indien meer en meer disperse fase materie wordt toegevoegd aan het geroerde systeem, zoals in het semi-batch proces, wordt er uiteindelijk een punt bereikt waarbij toevoeging van meer disperse fase inversie veroorzaakt: de continue fase wordt plotseling de disperse - en viceversa. Inversie van fases gaat vaak vergezeld van een toe- of afname van het grensvlak. Indien de omzettingssnelheid door massaoverdracht wordt bepaald, kan dit effect een onverwachte stap verandering in de totale snelheid tot gevolg hebben.

Het gebruikte model, gebaseerd op het effectieve grensvlak tussen de twee vloeistoffen en de beschrijving van massa overdracht met reactie volgens het film model wrodt gebruikt. Theoretische model voorspellingen worden vergeleken met experimentele resultaten en het effect van de verschillende parameters wordt besproken. uit de vergelijkingen tussen model en experimentele resultaten kan geconcludeerd worden dat het mogelijk is data te extrapoleren van homogene nitreerexperimenten en het dynamische gedrag te interpreteren van discontinue nitreerprocessen van bezeen, tolueen en cloorbenzeen in de verschillende reactie regimes. Verder kan ophoping van ongereageerd nitreerzuur in semibatch nitreringen van aromaten gevaarlijk zijn indien vergezeld van fase inversie. Deze wordt veroorzaakt door het feit dat de snelheid van warmte produktie plotseling kan toenemen, omdat de omzettingssnelheid bij industriele condities gewoonlijk door massaoverdracht wordt bepaald. De belangrijkste bepalende parameter voor deze toename is het grensvlak dat toeneemt als de continue fase verandert van de organische in de zure fase.

ACKNOWLEDGEMENTS

I am grateful to my Supervisor, Prof. K. R. Westerterp, for his guidance and many illuminating discussions in the field of mass transfer with chemical reaction. I am grateful also for his critical reading of the text and for his continuous encouragement.

I would like to express my appreciation to Prof. N. C. Marziano for her valuable comments and suggestions. I benefited from our discussions that helped to bring into focus many kinetic aspects of aromatic nitrations.

I would like to express my thanks to all the staff of the FIRES project at Ispra (Italy), without their help and collaboration this work never would have been done. Specially, I would like to thank my friends H. Hernández and E. Molga for many discussions and work concerning all the chapters in this thesis and countless other topics, that I prefer not mention here. I am particularly indebted to C. Bassani who in an association of several years has been a source of continual encouragement. Sincere appreciation is due to H. Nieman who helped me in the translation to Dutch. Thanks to C. A. Busse, J. M. Riego, I.M. Galván, J.A. Feliu, P. Pimenta, J. Sanders, G. Mertel, M. Morbello, H. Schönherr and M. Franzetti.

Sincere appreciation is due to C. Barcons, M. A. Alós, T. J. Snee and J. Ligthart for their careful work, patient collaboration and fruitful discussions in the experimental part.

I am grateful to F. Graham and T. D'Alton for their patient in correcting my frequent English mistakes.

Thanks to my friends Raoul, Marjolaine, Isabelle, Michael, Nadia, Alex, Sylviane, Marlen, Babis, Sergio, Emanuela, Isabel and Martin.

Finally, moral support was provided when needed most by my wife, my daughter and my family to whom this thesis is dedicated.

CONTENTS

GENERAL INTRODUCTION

The rapid development of the Chemical Industry in the past decades has increased the complexity of chemical plants, the diversity of products and the number of processes. This has produced a parallel increase of discontinuous reactors, which due to their versatility allow the production of special chemicals - with very good yields - in small amounts -when compared to those of continuous processes- and permit a rapid change from one process to other with minor modifications.

Unfortunately, the study of accident case histories, see Rasmussen (1989), shows that batch units are usually more frequently involved in accidents than continuous process plants. These results are not surprising because batch processes are usually very complex, with reaction systems that normally are not entirely known, they have also strongly nonlinear dynamics and their parameters are varying with time. Furthermore, the fact that in a batch cycle there is no steady state implies that the operator musts perform continuous corrections to control the process.

It has been argued that due to the small production levels, time constraints and the enormous variety of processes, the understanding of reactor dynamic behaviour is usually not economically justified. However, there are a considerable number of advantages. The more important is the optimisation of such processes. Such optimisation should take into account two different aspects: performance and safety. From the performance point of view, the optimal process design must allow the manufacture of products with the desired specifications in the minimum amount of time and with low operating costs. From the safety point of view, optimum process design must significantly reduce the risk of thermal runaway, avoiding intermediate accumulation of hazardous compounds and reducing the effects of cooling system malfunction or agitation stoppage. Obviously, the ideal situations would be those in which the process is inherently safe, see Regenass (1984), that means, where no disturbances, whatsoever, i.e. accumulation of reagents, failure of the cooling system, stirrer stoppage, etc. can cause an incident.

Mathematical modelling and dynamic simulation applied to these processes have demonstrated to be very useful tools to obtain optimal yields, see Cawthon and Knoebel (1989) and to carry out thermal hazard assessment, see Gordon *et al.* (1982). However, this type of applications has been performed mainly for specific reactions in which the thermo-kinetic model was well known. In the last years, due to the fast development of digital computers, on-line identification applications have appeared, see Bonvin *et al.* (1989). These applications are based on the fact that, normally, the possibilities to optimise and to control this type of reactors is limited, because the uncertainties that allow few state variables or parameters be measured and amongst these, only a few with sufficient time in advance to be incorporated in the control or/and decision chains. However, if by some procedure, i.e. estimation techniques, the state variables and fundamental parameters can be inferred, these new data can be used to perform predictive calculations about the future behaviour

of the system, to detect in advance dangerous situations, to improve the control algorithms, and to assist the plant operators in their decisions about the correct measures to be adopted under certain situations.

Although aromatic nitrations in mixed acid were one of the earliest unit processes to be operated on a large scale when the heavy organic chemical industry first developed last century, and that these reactions have played an equally important part in the development of our present understanding of the mechanism of organic reactions, offering a typical example of electrophilic substitution, see the classic investigations of Ingold and co-workers during the 1950's, many questions remain to be answered, particularly under the conditions employed in industry, and mainly in discontinuous reactors.

The dynamic behaviour of aromatic nitrations by mixed acid in discontinuous reactors involve a considerable number of problems because, in these heterogeneous liquid-liquid reactions, chemical reaction and mass transfer phenomena occur simultaneously. The occurrence of these phenomena leads to a complex problem while characterising and scaling-up these processes, due to the interdependence between fluid properties, operating conditions and equipment characteristics. Furthermore, nitrations involve high exothermicity and side reactions, which, besides the previous mentioned phenomena, have produced a considerable amount of incidents, see Barton and Nolan (1984).

Therefore, a better understanding of these kinds of processes is of great importance for the safe and economic design, as well as optimal operation of these plants.

The present investigation was undertaken with the main purpose of studying the dynamic behaviour and the influence of the initial and operating conditions in discontinuous nitration processes. To achieve this, a numerical simulator of a discontinuous reactor has been developed, see Zaldívar *et al.* (1990). This model has been formulated and characterised experimentally using a commercial bench-scale reactor, Mettler RC1, see Reisen and Grob (1985). Furthermore, the simulator has been validated using simple systems and reactions, i.e. neutralisation and esterifications.

In parallel, an experimental programme, to study aromatic nitrations: benzene, toluene and chlorobenzene, by mixed acid, has been carried out using adiabatic, heat flow calorimetry and pilot plant experiments, supported by chemical analysis. Adiabatic experiments were performed using a PHI-TEC calorimeter, see Singh (1989), isothermal and isoperibolic experiments were made using a RC1 reaction calorimeter, while pilot plant experiments were carried out in the FIRES facility, see Zaldívar *et al.* (1993).

As result, a mathematical model for predicting the overall reaction rate, within the range of experimental conditions studied, has been developed, see Zaldívar *et al.* (1992). This model has been introduced into the numerical simulator of the RC1 reaction calorimeter, to compare and validate it with the experimental results. Moreover, a special version of the simulator has been

applied on-line to estimate the reaction rate, see Hernández *et al.* (1993) and some parameters during nitration experiments.

REFERENCES

Barton, J.A. and P.F. Nolan, 1984, Runaway reactions in batch reactors, *The Protection of Exothermic Reactors and Pressurised Storage Vessels*, IChemE Symposium Series 85, 13-21 .

Bonvin, D., de Vallière, P. and Rippin, D.W.T., 1989, Application of estimation techniques to batch reactors- I. Modelling thermal effects, *Computer Chem. Engng.* **13**, 1-9.

Cawthon, G. D. and Knaebel, K.S., 1989, Optimization of semibatch polymerization reactions, *Computer Chem. Engng.* **13**, 63-72.

Gordon, M.H., O'Brien, G.J., Hensler C.J. and Marcali, K., 1982, Mathematical modelling in thermal hazards evaluation, *Plant/Operation Progress* **1**, 27-32.

Hernández, H., J.M. Zaldívar and C. Barcons, 1993, Development of a mathematical model and a numerical simulator for the analysis and optimization of batch reactors, *Computer Chem. Engng.* **17S**, 45-50.

Ingold, C.K., 1953, *Structure and Mechanism in Organic Chemistry*, ch. 6, Bell, London.

Rasmussen, B., 1988, Ocurrence and impact of unwanted chemical reactions, *J. Loss Prev. Process Ind.* **1**, 92-95.

Regenass, W., 1984, The control of exothermic reactors, *The Protection of Exothermic Reactors and Pressurised Storage Vessels*, IChemE Symposium Series, 85, 1-11.

Reisen, R. and B. Grob, 1985, Reaction calorimetry in chemical Process development, *Swiss Chem.* **7**, 39-43.

Singh, J., 1989, PHI-TEC: Enhanced vent sizing calorimeter, in *International Symposium on Runaway Reactions*, AIChE, New York, 313-330.

Zaldívar, J.M., H. Hernández and C. Barcons, 1990, Development of a numerical simulator for a reaction calorimeter. FISIM, RC1 version, *JRC Ispra, TN n° I.90.109.*, Italy.

Zaldívar, J.M., C. Barcons, H. Hernández, E. Molga and T.J. Snee, 1992, Modelling and optimization of semibatch toluene mononitration with mixed acid from performance and safety viewpoints, *Chem. Eng. Sci.* **47**, 2517-2522.

Zaldívar J.M., Hernández H., Nieman H., Molga E. and Bassani C., 1993, The FIRES project: experimental study of thermal runaway due to agitation problems during toluene nitration, *J. Loss Prev. Process Ind.* **6**, 319-326.

CHAPTER 2

DEVELOPMENT OF A MATHEMATICAL MODEL AND A NUMERICAL SIMULATOR FOR THE ANALYSIS AND OPTIMISATION OF DISCONTINUOUS REACTORS. EXPERIMENTAL MODEL CHARACTERISATION

ABSTRACT

The mathematical modelling of a bench-scale batch reactor is presented. The formulation of the mass and heat balances leads to a set of algebraic-differential equations which, when solved, produces the temperature and concentrations profiles as a function of time. Emphasis has been placed on a realistic description of such reactor by incorporating an accurate representation of heat effects like heat taken by reactor wall, heat losses, stirring power supply, heat of dilution, vortex influence on heat transfer area; and a model of the heating/cooling circuits as well as their controllers.

To obtain the data necessary to simulate the dynamic behaviour of the reactor a set of characterisation test was carried out. Once the different parameters of the model were evaluated, some experiments were performed to compare with the predicted dynamic behaviour obtained with the simulator. These experiments included: heating/cooling dynamic behaviour with different fluids, neutralisation reaction between sodium hydroxide and hydrogen chloride and esterification reaction between propionic anhydride and 2-butanol

Keywords

Mathematical Modelling, Numerical Simulation, Batch Reactors, Reaction Calorimetry

1. INTRODUCTION

The analysis of batch reactors is frequently limited by a poor understanding of the process chemistry and by the lack of basic data. It has been argued that due to the small production levels, time constraints, and the enormous variety of processes, the understanding of reactor dynamic behaviour is usually not economically justified. However, mathematical modelling and dynamic simulation of batch and semibatch processes has proved to be a very valuable tool for achieving optimal reactor performance, see Cawthon *et al.* (1988), and for carrying out thermal hazard evaluation, see Gordon *et al.* (1982).

In any case, a detailed dynamic model of the reactor, its accessories and its control system is a necessary prerequisite. Moreover, in order to achieve understanding of the basic phenomena involved, it is vital to study simultaneously three different parts: the thermo-kinetics phenomena occurring in the reaction mixture, its interaction with the equipment and the influence of the operating conditions.

The objective of this work is the development of a numerical simulator able to reproduce the behaviour of chemical processes carried out in a discontinuous chemical reactor. It is intended to serve as an aid to experiment design and data analysis allowing the determination of the optimal and safe operating conditions. Furthermore, this model is the basis for a posterior application of model-based estimation techniques to estimate different state variables or process parameters.

1.1. Generalities

The bench-scale reactor under consideration is described by Reisen and Grob (1985), see Appendix 1. In Figure 1, the principal elements included in the simulator are indicated: the reactor vessel, the heating/cooling circuits, the feeding device and the controllers.

The description of the mathematical model is divided in three parts: the fundamental equations obtained from mass and energy balances, and equilibrium relations; the thermo-kinetic models introduced in these equations; and the model of the heating/cooling circuits and the feeding device.

The basic mathematical model consider a general case with the following characteristics:

- Operating mode:
  - Batch or semibatch with any number of feeding streams.
  - Adiabatic, isothermic, isoperibolic or temperature-programme modes.
- Chemical reactions:
  - Any number, taking place only in the liquid mixture.
  - Homogeneous or heterogeneous liquid-liquid.
  - Irreversible, instantaneous or equilibrium types.
- Reactive mixture homogeneous or uniform for liquid-liquid systems.
- Heat effects:

- Inhomogeneous reactor wall.
- dynamics of the heating/cooling circuit
- exchange with the surroundings including losses and stirring supply.

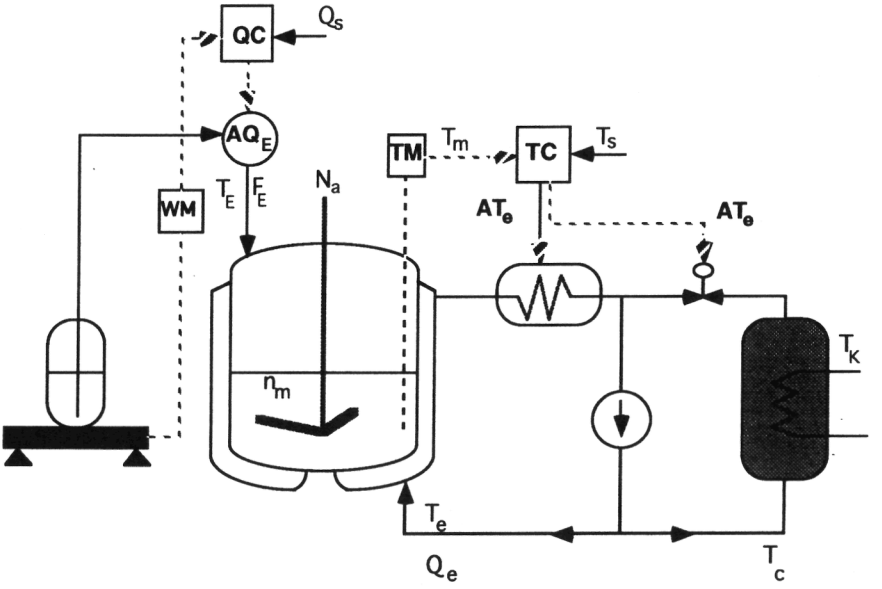

Figure 1. Schematic representation of the bench-scale reactor (Mettler RC1).

1.2. Approach

The following criteria were taken into account in the design of the simulator:

• A compromise between the phenomena complexity and the model representability. Nevertheless, it must be able to represent the influences of all the relevant operating conditions, to model the control functions and reactor accessories.

• A coherence between the level of knowledge of processes: availability, accuracy, and validity range of data, and the simulator input.

• A flexibility from a physico-chemical point of view in order to deal with the diversity of substances and processes carried out in a batch reactor.

• A user friendly and practical tool. As long as possible, it has to reproduce the functions of a real simulator: identity of task, of control, and of information generated.

2. FUNDAMENTAL EQUATIONS

Formulation of mass and energy balances for the reaction mixture provides the time-profile of molar hold-up for each specie present in the reaction mass and temperature:

$$\frac{dn_{m_j}}{dt} = F_{E_j} + R_j \cdot V_m \qquad ; j \in A_L(N_L) \tag{1}$$

$$\frac{dT_m}{dt} = \frac{1}{\Gamma_m} \left(q_x + q_E + q_{dil} + q_{0_w} + q_{0_d} + q_a + q_l \right) \tag{2}$$

where the different thermal flows included are:

- q_x = released by chemical reaction,
- q_E = due to mass addition,
- q_{dil} = due to heat of dilution of species,
- q_0 = exchanged with the heat transfer fluid (w refers to wetted and d stands for dry part)
- q_a = supplied by stirring,
- q_l = exchanged with the surroundings,

and Γ_m is the thermal capacity of the reaction mixture and devices wetted within.

Due to the importance of the reactor wall on the heat transfer from/to the reaction mixture, and in order to take into account the possibility of heat accumulation in the wall during fast transients, a complementary heat balance is formulated which considers axial (z) and radial (r) conduction into the wall, see Mc Adams (1954), including the bottom surface to the cylindrical part:

$$\frac{\partial T_w}{\partial t} = \frac{\lambda_w}{\Gamma_w} \left[\frac{1}{r} \frac{\partial}{\partial r} \left(r \frac{\partial T_w}{\partial r} \right) + \frac{\partial^2 T_w}{\partial z^2} \right] \tag{3}$$

With the boundary conditions:

$$\lambda_w \frac{dT_w}{dr}\Big|_{r = R_0} = h_0 \left(T_{0_w} - T_m \right) \tag{4}$$

$$\lambda_w \frac{dT_w}{dr}\Big|_{r = R_1} = h_1 \left(T_e - T_{1w} \right) \tag{5}$$

The partial differential eq. (3) is discretised spatially in order to obtain a set of ordinary differential equations consistent with the rest of the model. The number of discretisation points was chosen after an experimental study of the dynamics of the heating/cooling circuits, thus taking into account its smallest time-constant. The wall is divided axially in two parts according to the surface wetted by the reaction mixture, and radially in three equally spaced parts, as indicated in fig. 2.

The obtained time-profile temperatures through the reactor wall are:

Internal side, wetted part (T_{0w})

$$\frac{dT_{0_w}}{dt} = \frac{4}{\Gamma_w} \left[q_{0w} - q_{w1} - q_{w3} \right] \tag{6}$$

Center wall, wetted part (T_{w1})

$$\frac{dT_{w1}}{dt} = \frac{2}{\Gamma_w}\left[q_{w1} - q_{w4} - q_{w2}\right] \tag{7}$$

External side, wetted part (T_{1w})

$$\frac{dT_{1w}}{dt} = \frac{4}{\Gamma_w}\left[q_{w2} - q_{w5} - q_{1w}\right] \tag{8}$$

Internal side, dry part (T_{0d})

$$\frac{dT_{0d}}{dt} = \frac{4}{\Gamma_d}\left[q_{0d} + q_{w3} - q_{w6}\right] \tag{9}$$

Center wall, dry part (T_{w2})

$$\frac{dT_{w2}}{dt} = \frac{2}{\Gamma_d}\left[q_{w6} + q_{w4} - q_{w7}\right] \tag{10}$$

External side, dry part (T_{1d})

$$\frac{dT_{1d}}{dt} = \frac{4}{\Gamma_d}\left[q_{w7} + q_{w5} - q_{1d}\right] \tag{11}$$

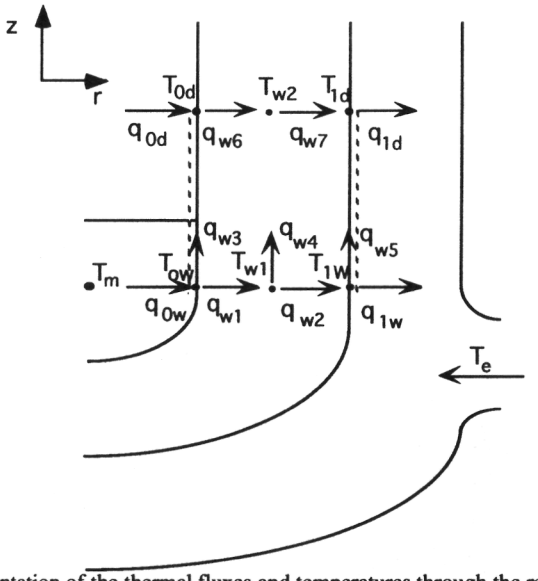

Figure 2. Representation of the thermal fluxes and temperatures through the reactor wall

3. THERMO-KINETIC MODELS

From a calorimetric point of view, it is interesting to divide the thermo-kinetic phenomena according to their participation in the two main terms of the heat balance: heat production within the reaction mass, q_{rxn}, and exchange of heat with the surroundings, q_{ex}.

$$q_{rxn} = q_x + q_{dil} \tag{12}$$

$$q_{ex} = q_{0w} + q_{0d} + q_l + q_E + q_a \tag{13}$$

3.1. Heat production within the reaction mass

In this term are considered the enthalpy changes due to chemical reactions and physical phenomena taking place within the reactor contents, i.e. dilution, evaporation, etc.

The heat released by chemical reaction is calculated from the rate of reactions and their respective enthalpy change. When the rate of reaction is defined per unit of mixture volume, the rate of heat generated is:

$$q_x = - V_m \sum_{i=1}^{N_R} \Delta H_i \cdot r_i \tag{14}$$

where N_R is the number of independent chemical reactions.

Expressions for the rate of reaction, r, are defined in the most flexible way, in order to cover the diversity of cases. Reactions may be homogeneous or heterogeneous depending on the medium where they take place, or may be irreversible or instantaneous depending on the phenomena controlling the rate. The rate of reactions allows also the calculation of the net rate of transformation of each species, necessary to solve the mass balance:

$$R_j = \sum_{i=1}^{N_R} \nu_{ij} \cdot r_i \tag{15}$$

The enthalpy change which accompanies the mixing or dilution of two or more substances is called the heat of dilution, and it may be calculated in the integral form as the change between the final and the initial state (before and after mixing) of the sum of the relative partial molar enthalpies times the number of mole of each component, see Glasstone (1947). Thus,

$$\Delta H_{dil} = \sum_{k=1} \Delta(n_k \cdot L_k) \tag{16}$$

where n_k and L_k are the number of moles and the relative apparent molar enthalpy of the kth-component respectively.

In order to obtain the rate of heat generation due to dilution, it is necessary to consider a differential change with respect to time of the heat of dilution, see Zaldívar *et al.* (1992), hence,

$$q_{dil} = \frac{dH_{dil}}{dt} = \sum_{k=1} \left(n_k \frac{dL_k}{dt} + L_k \frac{dn_k}{dt} \right) \tag{17}$$

3.2. Heat exchanged with the surroundings

The reaction mixture exchanges heat mainly with the heat transfer fluid that circulates in the jacket. The other terms considered in the heat balance are the enthalpy change due to mass addition, heat losses through the cover andpower supplied by stirring.

The rate of heat exchanged with the heat transfer fluid is calculated taking into account all the thermal resistances, see Bird *et al.* (1960). The heat balance described above considers the thermal fluxes through the internal and external resistance films,

- Convective flux through the internal resistance film:

$$q_{0w} = h_{0w} \cdot S_w \, (T_m - T_{0w}) \tag{18}$$

The internal heat transfer coefficient, h_{0w}, may be expressed as a function of operating conditions and fluid properties. It is deduced using dimensional analysis from: Nu = f(Re,Pr,Vi) and can be represented as a function of the stirring speed, n_a, by the following equation, see Uhl and Gray (1966):

$$h_{0w} = \alpha_0 \cdot n_a^{\theta_{20}} \tag{19}$$

where α_0 is defined as a function of mixture properties:

$$\alpha_0 = \theta_{10} \frac{\lambda_m}{D_R} \, Pr^{\theta_{30}} \cdot Vi^{\theta_{40}} \left[\frac{D_a^2 \cdot \rho_m}{\mu_m} \right]^{\theta_{20}} \tag{20}$$

where θ_{10}, θ_{20}, θ_{30}, θ_{40} are constant for each agitator, see Section 4.

The wetted surface is calculated as a function of the reaction mixture volume and the effect of stirring (vortex), see Holland (1973):

$$S_w = S_B + \frac{2\,(V_m - V_B)}{R_0} + \Delta S_v \tag{21}$$

where S_B is the bottom surface, see Appendix 1, and ΔS_v is the surface increase due to the vortex.

- Conductive radial flux through the reactor wall:

The conductive radial flux from the reactor through the wall to the jacket is modelled with the following equations:

- Wetted part by the reaction mass:

$$q_{w1} = \frac{2 \cdot S_w \cdot \lambda_w}{e_w} \, (T_{0w} - T_{w1}) \tag{22}$$

$$q_{w2} = \frac{2 \cdot S_w \cdot \lambda_w}{e_w} \, (T_{w1} - T_{1w}) \tag{23}$$

- Dry part of the reactor wall:

$$q_{w6} = \frac{2 \cdot S_d \cdot \lambda_w}{e_w} \, (T_{0d} - T_{w2}) \tag{24}$$

$$q_{w7} = \frac{2 \cdot S_d \cdot \lambda_w}{e_w} \, (T_{w2} - T_{1d}) \tag{25}$$

where e_w is the wall thickness, λ_w is the thermal conductivity of the wall and S_d is the exchange surface not wetted by the mixture, i.e. $S_T - S_w$, see Appendix 1.

- Conductive axial flux through the reactor wall:

Hereafter is described the conductive axial flux. This term, due to the low thermal conductivity of glass, has small influence in the energy balances.

$$q_{w3} = \frac{4 \cdot S_x \cdot \lambda_w}{H_m} (T_{w1} - T_{1w}) \tag{26}$$

$$q_{w4} = \frac{2 \cdot S_x \cdot \lambda_w}{H_m} (T_{w1} - T_{w2}) \tag{27}$$

$$q_{w5} = \frac{4 \cdot S_x \cdot \lambda_w}{H_m} (T_{1w} - T_{1d}) \tag{28}$$

where:

$$S_x = \pi (R_1^2 - R_0^2) \tag{29}$$

$$H_m = H_T - \frac{V_m}{\pi \cdot R_0^2} \tag{30}$$

- Convective fluxes through the external resistance film:

$$q_{1w} = h_1 \cdot S_w (T_{1w} - T_e) \cdot \Psi_1 \tag{31}$$

$$q_{1d} = h_1 \cdot S_d (T_{1d} - T_e) \cdot \Psi_2 \tag{32}$$

Replacing the relevant dimensionless numbers in the Nusselt equation, see Bondy and Lippa (1983), the external heat transfer coefficient, h_1, may be expressed as a function of the heat transfer fluid flow, Q_e, as:

$$h_1 = \alpha_1 \cdot Q_e^{\theta_{21}} \tag{33}$$

where α_1 is defined as a function of heat transfer fluid properties and jacket characteristics:

$$\alpha_1 = \theta_{11} \frac{\lambda_e}{D_t} Pr^{\theta_{31}} \cdot Vi^{\theta_{41}} \left[\frac{\rho_e \cdot D_t}{S_t \cdot \mu_e} \right]^{\theta_{21}} \tag{34}$$

where θ_{11}, θ_{21}, θ_{31}, θ_{41} are constant for each reactor and fluid-dynamic regime, see Section 2.Ψ_1 and Ψ_2 are correction factors to take into account the change of heat transfer fluid temperature through the jacket:

$$\Psi_1 = \left[\frac{1 - \exp\left(\frac{-h_1 \cdot S_w}{Q_e \cdot Cp_e} \right)}{\frac{h_1 \cdot S_w}{Q_e \cdot Cp_e}} \right] \tag{35}$$

$$\Psi_2 = \left[\frac{1 - \exp\left(\frac{-h_1 \cdot S_d}{Q_e \cdot Cp_e} \right)}{\frac{h_1 \cdot S_d}{Q_e \cdot Cp_e}} \right] \tag{36}$$

Thermal capacity of the wall

The thermal capacity of the reactor wall is divided in the wetted part by the reactant mass and the part that is maintained dry inside the reactor:

$$\Gamma_{w_w} = \Gamma_w \cdot x_w \tag{37}$$

$$\Gamma_{w_d} = \Gamma_w - \Gamma_{w_w} \tag{38}$$

where x_w is the wetted surface fraction, $x_w = S_w/S_T$.

Heating/cooling by mass addition

During a semibatch process, frequently the added mass is not at the same temperature as the reactor, contributing to cooling or heating of the reactant mass. Then, this enthalpy difference must be taken into account in the energy balance.

$$q_E = -\sum_{j \in A_L}^{N_L} F_{E_j} \int_{T_m}^{T_{E_j}} Cp_j \cdot dT \tag{39}$$

where F_{Ej} is the molar input flow of j.

$$F_{E_j} = \sum_{j \in A_L}^{N_L} Q_k \cdot C_{E_j} \quad ; \quad k=1,...,N_E \tag{40}$$

where Q_k is the mass flow of k input stream and C_{Ej} is the molality of j

Heat losses

The importance of heat losses increases with the temperature difference between the system and the surroundings, depending also on how isolated (U) the system is.

$$q_l = US_l \, (T_a - T_m) \tag{41}$$

where US_l is the effective heat transfer coefficient for losses through the top of the reactor and T_a the ambient temperature

Power supplied by stirring

Using dimensional analysis it is possible to obtain an empirical law for the power introduced by the stirrer, see Uhl and Gray (1966):

$$Po = f(Re,Fr, S_1, S_2,... S_n) \tag{42}$$

For agitated vessels, the dimensionless numbers can be defined as:

$$Po = \frac{q_a}{\rho_m \cdot n_a^3 \cdot D_a^5} \tag{43}$$

$$Re = \frac{\rho_m \cdot n_a \cdot D_a^2}{\mu_m} \tag{44}$$

$$Fr = \frac{n_a^2 \cdot D_a}{g} \tag{45}$$

S_1, S_2,...,S_n are shape factors, defined as the ratio between different characteristic geometric measures of the reactor related to the position of the stirrer, its diameter, the number of blades, etc.

From geometric similarity, equation (42) is reduced to:

$$Po = K_2 \cdot Re^{K_3} \cdot Fr^{K_4} \tag{46}$$

where K_2 is an overall dimensionless shape factor, and K_3 and K_4 are constants. Replacing the relevant terms of eqs. (43) - (45) in eq. (46), it is possible to obtain different situations for Newtonian fluids, see Tavlarides and Stamatoudis (1981): At low impeller Reynolds numbers, Re<15, the flow is laminar around the impeller and stagnant away from it. At higher Reynolds number, Re>15, discharge flow develops. This region is mostly laminar and extends up to Re≈200 for turbine impellers. Beyond this point, the transition region begins with the flow becoming turbulent around the impeller, while further away the flow is still laminar. The transition region for impellers extends up to Re≈10^4. Thus, the average power input in an agitated vessel operating in the laminar region is given by:

$$q_a = \phi'' \cdot \mu_m \cdot n_a^2 \cdot D_a^3 \tag{47}$$

In the transition range flow, the average power input in the vessel over short ranges is given by:

$$q_a = \phi' \cdot \rho_m \cdot n_a^3 \cdot D_a^5 \left(\frac{\rho_m \cdot n_a \cdot D_a^2}{\mu_m} \right)^n \tag{48}$$

where ϕ' and ϕ'' can be considered constants, see Section 4.3, and n is the slope of the plot of log of power number versus of Re. With increasing Re, n continuously increases from -1 (Re≈15) to 0.16 (Re≈300) and then decreases, approaching 0 (Re≈11000).

Modification of the heat transfer area due to stirring (vortex)

The heat transfer area is the surface wetted by the reaction mixture and can be calculated as a function of the reaction mixture volume and the effect of stirring (vortex) by the following expression:

$$S_w = S_B + \frac{2\,(V_m - V_B)}{R_0} + \Delta S_v \tag{21}$$

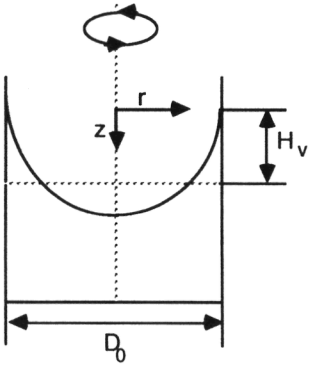

Figure 3. Modification to the exchange surface due to stirring.

In order to take into account the influence of the stirrer speed in the wetted surface due to the vortex produced by the agitator, the following correlation relating the increase in height of the exchange heat transfer area with the reactor radio and the stirrer speed was found in literature, see Holland (1973):

$$H_v = \frac{n_a^2 \cdot R_0^2}{2 \cdot g} \tag{49}$$

where H_v is the increase in height due to stirring. Hence,

$$\Delta S_v = 2 \cdot \pi \cdot R_0 \cdot H_v \tag{50}$$

This correlation is only valid for Newtonian fluids with no vertical or radial velocity. Experimental results shown that this increase in the heat exchange area is not independent on liquid volume, type of agitator, and physical fluid properties. In order to correct the idealities of such assumption the value of n_a in the eq. (49) was multiplied by factor, f, that depends empirically on all the characteristics mentioned above. Hence, eq. (50) can be write, for a determined reactor and geometry, as follows,

$$\Delta S_v = K_1 \cdot f \cdot n_a^2 \tag{51}$$

where K_1 is a constant that depends on the geometry of the reactor and f is the factor that correct for the non-idealities

According to Uhl and Gray (1966) the factor must be correlated with the discharge rate that depends on the power number given by eq. (46). Substituting f by this term and rearranging eq. (51) the following relationship is obtained:

$$\Delta S_v = C_1 \cdot Re^{C_2} \cdot Fr^{C_3} \cdot n_a^2 \cdot g(V_m) \tag{52}$$

Where $g(V_m)$ is a function that depends on the reaction mass volume. Intuitively, this function has to follow an exponential inverse behaviour, that means with less volume the increase in height must be bigger than with more volume present in the reactor. The correlation that better fitted the experimental data is:

$$g(V_m) = \left(\frac{V_T - V_m}{V_T} \right)^{C_4} \tag{53}$$

where C_1, C_2 , C_3 and C_4 are constants that were calculated experimentally for different fluids and agitators, modifying the liquid volume, the temperature and the stirrer speed,see Section 4.

Heat accumulation within the reactor

This term is calculated as the product of the molar hold-up with the specific heat of species in the reactor, including the thermal capacity of the devices wetted by the mixture:

$$\Gamma_m = \sum_{j \in A_L}^{N_L} n_{m_j} \cdot Cp_{L_j} + \Gamma_b \tag{54}$$

where Γ_b is the thermal capacity of devices wetted, see Appendix 1.

4. CHARACTERISATION OF THE EFFECTIVE HEAT TRANSFER COEFFICIENT AND SECONDARY HEAT EFFECTS

4.1. Introduction

The most usual method to control temperature in batch reactors is by means of removing the heat generated by exothermic reactions during a process through a cooled heat transfer fluid that circulates in a jacket, see fig. 4. The heat flow is proportional to the driving force (temperature difference between the reactor, T_m , and the jacket, T_e):

$$q_0 = U \cdot S \ (T_m - T_e) \cdot \Psi \tag{55}$$

where the proportional factor U·S, called the effective heat transfer coefficient, depends on the fluids properties, operating conditions and the geometry of the system. Ψ is a correction factor to take into account the change of the heat transfer fluid temperature between the inlet and the outlet of the jacket.

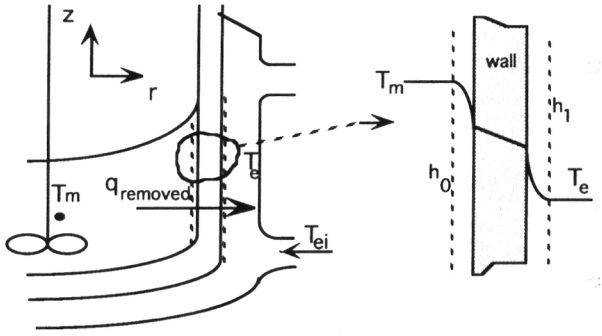

Figure 4. Heat transfer from a chemical reactor to an external jacket.

The knowledge of U·S is of great importance for the design of batch reactors and it is decisive for its optimisation from performance and safety point of views. Different experimental and empirical methods have been proposed to evaluate the effective heat transfer coefficient amongst heat flow calorimetry has demonstrated to be an useful technique, see Bourne *et al.* (1981), and it is widely used. The method consists in introducing a known thermal power in the reaction mass, q_i, by means of an electrical resistance and comparing the area under the curve of a plot of $(T_m-T_e)\Psi$ against time over the period of the calibration, see RC1 user's manual, while using the control system to keep the reactor temperature constant accelerating the process:

$$U \cdot S = \frac{q_i}{(T_m - T_e) \cdot \Psi} \tag{56}$$

4.2. Experimental description

In order to validate experimentally the model for the calculation of U·S, see Section 3, a set of experiments with five different fluids - isopropanol, tetrachloromethane, ethylene glycol, water

and toluene - was carried out in the RC1, see Zaldívar *et al.* (1990). The type of stirrers used were anchor, and two turbines for L/L and G/L mixtures with a speed range of 50-250 rpm for the anchor, and of 200-800 rpm for the turbines. The temperature and volume ranges were 273-323 K and 0.7-1.8 l respectively. The experimental results for the tetrachloromethane are shown in Table 1 as an example.

Table 1. U·S for tetrachloromethane with the anchor, turbine G/L and turbine L/L stirrers as a function of temperature and stirrer speed.

Anchor stirrer					
rpm T_m(°C)	50	100	150	200	250
0.0	4.158	4.947	5.573	6.132	6.737
15.0	4.328	5.116	5.781	6.337	6.918
25.0	4.370	5.260	5.829	6.421	7.038
35.0	4.483	5.358	6.051	6.569	7.149
50.0	4.643	5.634	6.384	6.865	7.416
Turbine G/L stirrer					
rpm T_m(°C)	200	300	400	500	600
0.0	4.799	5.190	5.537	5.959	6.419
15.0	4.950	5.402	5.778	6.256	6.657
25.0	5.080	5.524	5.892	6.379	6.803
35.0	5.213	5.642	6.064	6.542	6.993
50.0	5.381	5.957	6.432	6.977	7.357
Turbine L/L stirrer					
rpm T_m(°C)	200	300	400	500	600
0.0	4.849	5.244	5.583	6.026	6.516
15.0	5.041	5.406	5.790	6.257	6.703
25.0	5.141	5.522	5.839	6.405	6.862
35.0	5.235	5.665	6.064	6.639	7.031
50.0	5.436	5.947	6.464	7.096	7.499

The influence of exchange surface in U·S was investigated for the cases of water and toluene, carrying out a series of evaluations adding periodically a certain amount of the liquid and with different type of stirrer. Table 2 shows the experimental results for water.

The values, obtained in the experiments described previously, were employed to evaluate the participation of resistances involved in the overall heat transfer coefficient, and to adjust the expression for the wetted surface.

The parameters for the internal heat transfer coefficient, see Table 3, were found in literature, see Bourne *et al.* (1981) and validated by Wilson's plots; whereas the θ_{12} and θ_{21} of the external heat transfer coefficient, h_1, and C_1, C_2, C_3 and C_4 - eqs. (52) and (53) - for each stirrer were adjusted using a multivariable non-linear regression method, see Press *et al.* (1986). This values are shown in Tables 4 and 5. The results form a comparison between the experimental evaluation and predicted values are: maximum error 10.3 % , average error 2.3 %, standard deviation 2.8 %. Figure 5 shows experimental and calculated results for toluene and water respectively.

Table 2. Variation of U·S for water as a function of the volume in the reactor for the anchor stirrer at 250 rpm and for the turbine G/L and L/L at 500 rpm and 308 K.

mass of water (Kg)	U·S anchor	U·S turbine G/L	U·S turbine L/L
0.717	6.769	6.071	5.835
0.767	6.901	6.077	5.946
0.817	7.153	6.289	6.102
0.867	7.378	6.387	6.264
0.917	7.492	6.571	6.409
0.967	7.620	6.696	6.614
1.017	7.699	6.806	6.705
1.067	7.879	6.949	6.860
1.117	7.919	7.187	7.082
1.167	8.128	7.325	7.217
1.217	8.195	7.469	7.338
1.267	8.340	7.587	7.544
1.317	8.451	7.793	7.669
1.367	8.556	7.923	7.848
1.417	8.568	7.969	7.965
1.467	8.666	8.163	8.130
1.517	8.736	8.414	8.232
1.567	8.845	8.512	8.393
1.617	8.898	8.648	8.556
1.667	-	8.777	8.661
1.717	-	8.927	-
1.767	-	8.959	-
1.817	9.180	9.073	8.953

Table 3. Coefficients for the exponents of h_0, eqs. (26)-(27).

Coefficients	Anchor	Turbine
θ_{10}	0.29	0.42
θ_{20}	0.678	0.694
θ_{30}	1/3	1/3
θ_{40}	0.14	0.14

Table 4. Coefficients for the exponents of h_1, eqs. (40)-(41).

Coefficients	Annular jacket, no baffles
θ_{11}	1.14
θ_{21}	0.29
θ_{31}	1/3
θ_{41}	0.14

Table 5. Values of the constants of eqs. (52) - (53) for the RC1 reactor.

Constant	Anchor	G/L Turbine	L/L Turbine
C_1	$1.251 \cdot 10^{-3}$	$0.917 \cdot 10^{-5}$	$1.36 \cdot 10^{-5}$
C_2	-0.0145	0.325	0.284
C_3	-0.309	-0.395	-0.486
C_4	1.11	1.66	1.80

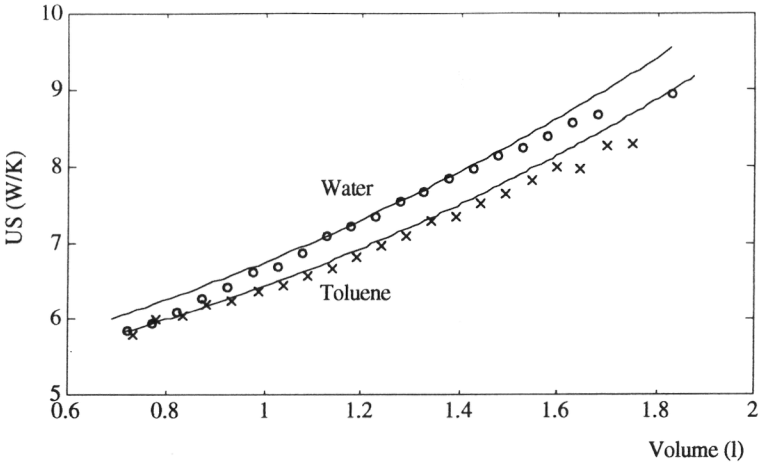

Figure 5. Experimental and calculated effective heat transfer coefficient for pure water and toluene. Periodical additions were carried out followed by evaluation of US. T_m= 308 K, and n_a=8.33 s^{-1}.

4.3. Power introduced by stirring into the reaction mass

Different experiments were performed with water in order to determine if the data obtained were consistent with literature correlations. The experiments consisted in follow the increase of temperature during one day maintaining adiabatic conditions. For the two type of agitators tested (anchor and turbine) the agreement was satisfactory and consequently the data from Uhl and Gray (1966), and Bourne *et al.* (1981) have been employed for calculating the power introduced by stirring into the reaction medium.

Table 6. ϕ for different agitators tested, eq. (47).

Type of agitator	ϕ
Anchor	0.5
Turbine Gas/Liquid	2.2
Turbine Liquid/Liquid	2.2
Pfaudler	1.0

4.4. Heat Losses

The following expression, see de Valliere *et al.* (1986) was used in order to take into account the heat looses, mainly, from the reactor cover through the surroundings:

$$q_l = (8.1 \cdot 10^{-3} \cdot T_m - 2.348) \cdot (T_a - T_m) \qquad (57)$$

5. MODELLING AND CHARACTERISATION OF THE HEATING/COOLING CIRCUITS AND CONTROLLERS

5.1. Introduction

The thermostat consists basically on two different loops in whose silicone oil, used as heat transfer fluid, circulates at high speed. The first loop contains an electrical heater, that can give a power up to 2000 W, and is connected to the jacket in which the silicone oil is pumped (≈3 l capacity). The second loop is the cooling circulation system, with a larger capacity (≈5 l), connected to the heating loop by a control valve and containing a coil heat exchanger attached to an external cold source, see figure 6. To follow a programme, the temperature of the heat transfer fluid in the jacket is adjusted by manipulating the electrical heater and/or the control valve.

The cooling flow, Q_c, and the electrical heating power, q_h, are manipulated by the controller according to a cascade control scheme described in figure 7.

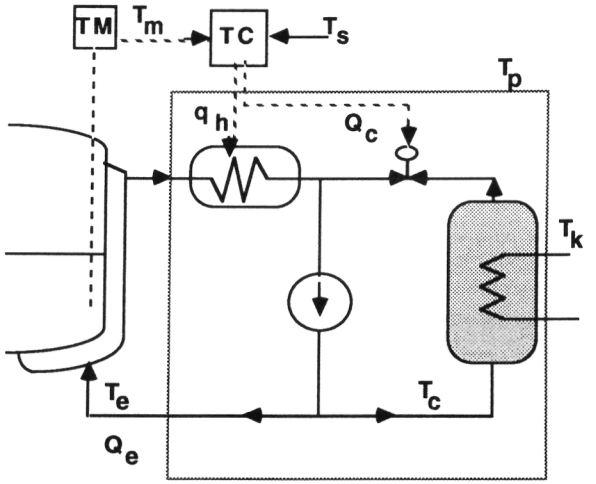

Figure 6. Thermostat of the RC1 Calorimeter.

The controller of the outer loop (C1) corrects deviations of the reactor temperature from the set value T_s, following a P (Proportional) criterion using a P_1 value defined beforehand by the user to calculate the set-point of jacket temperature:

$$T_{e_s} = T_s + P_1 (T_s - T_m) \qquad (58)$$

providing the set value for the heat transfer fluid temperature, T_{e_s}, which is adjusted by the inner loop controller (C2) by means of a self-adaptive PI (Proportional-Integral) criterion. Controller C2 uses a model based algorithm that carries out an energy balance in the heated

loop at each sampling time, calculating the power necessary to reach or maintain the required temperature

$$q_n = P_2 (T_{es}-T_e)+I_2\int(T_{es}-T_e)\,dt - q_{pumps}-q_{losses} \qquad (59)$$

where respectively q_{pumps} and q_{losses} take into account the power introduced due to friction by the recirculating pumps, and the heat losses of the thermostat to the surroundings, see Table 7.

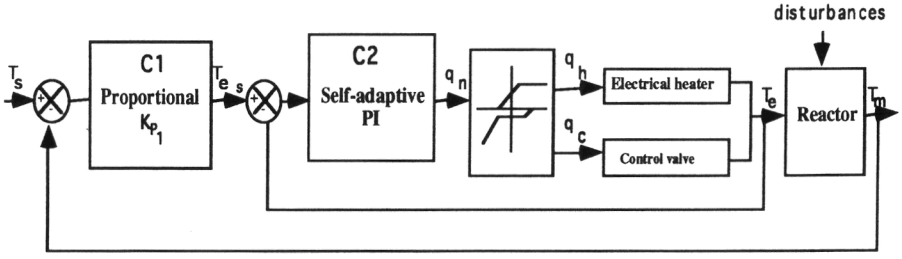

Figure 7. Temperature control scheme

Table 7. Characteristic values of the controllers (from Mettler A.G.)

Parameter	Value
P_1	3 - 12
P_2	700
I_2	4.5
q_{pumps} (W)	120.0
q_{losses} (W)	6.6 (298.0-T_e)

The controller distributes this power by acting either on the electrical resistance or on the control valve according to an empirical criterion, see Regenass *et al.* (1984), which decomposes the needed power, q_n, into the two different components, i.e. heating power, q_h, and cooling power, q_c, see fig. 8.

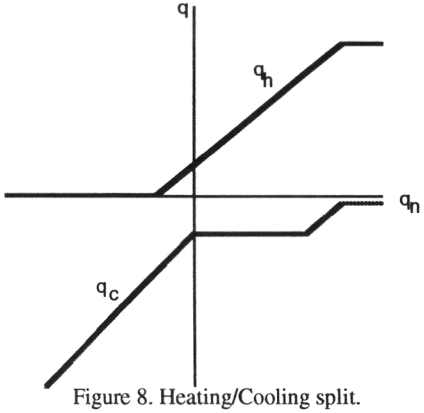

Figure 8. Heating/Cooling split.

5.2. Modelling the heating/cooling circuits

In order to reproduce the behaviour of the RC1 under any operating mode, the simulator has to predict the evolution of the heat transfer fluid temperature and consequently a model of the thermostat functioning was developed. According to the characteristics of the heating/cooling circuits, and after having tested different types of modelling, it was found that a model consisting of three thermally homogeneous subsystems described adequately the behaviour of these circuits: The heated and cooled loops with temperatures T_e and T_c respectively, and the container of the heat loop with uniform temperature T_p. Energy balances in the three subsystems permitted the time-profile of temperatures T_e, T_c and T_p to be mathematically modelled, and the control algorithm to be applied:

$$\frac{dT_e}{dt} = \frac{1}{\Gamma_e}\left[q_0 + Q_c \cdot \rho_e \cdot Cp_e (T_c - T_e) + q_h + q_{p_e} \right] + \frac{(T_P - T_e)}{\tau_{e_1}} \qquad (60)$$

$$\frac{dT_c}{dt} = \frac{1}{\Gamma_c}\left[-Q_c \cdot \rho_e \cdot Cp_e (T_c - T_e) - US_c \cdot \Delta T_{ln} + q_{p_c} + US_{lc} (T_a - T_c) \right] \qquad (61)$$

$$\frac{dT_P}{dt} = \frac{T_a - T_P}{\tau_P} + \frac{T_e - T_P}{\tau_{e_2}} \qquad (62)$$

where Γ_e, Γ_c are the overall thermal capacities (oil+inserts) of the heating and cooling loops; q_0 is the heat exchanged with the reactor wall = $q_{0w} + q_{0d}$; q_{pe}, q_{pc} are the thermal fluxes due to the recirculating pumps; US_c is the effective heat transfer coefficient between the cooling loop and the external cold source, i.e. cryostat; ΔT_{ln} is the logarithmic average temperature of heat exchange between the cooling loop and the external cold source; τ_{e1} and τ_{e2} are time-constants of heat exchange between the heated loop and its container; τ_P is the time-constant of heat losses of the container of the heated loop ; and US_{lc} is the overall heat losses coefficient in the cooled circuit.

5.3. Heating/Cooling circuits Characteristics

Different aspects has been studied in this part with the aim of characterise completely the different variables and parameters of the model of the heating/cooling circuit above formulated. These are:

a/ Power introduced by the centrifugal pumps (q_{p_e} and q_{p_c}): The power introduced to the heat transfer fluid from the centrifugal pumps due to friction effects, can be described as a function of the viscosity by the following equations:

$$q_{p_e} = 59.14 + 0.86 \cdot 10^3 \cdot \mu_e \qquad (63)$$

$$q_{p_c} = 24.63 + 0.37 \cdot 10^3 \cdot \mu_c \qquad (64)$$

where μ_e and μ_c are the viscosities of the heating and cooling circuits respectively, see Appendix 1.

b/ Flow of the heat transfer fluid (Q_e) : The hydraulic characteristics of the heating/cooling circuit were experimentally determined, see Chenneaux *et al.* (1990). An hysteresis behaviour was observed: for a given temperature, the flow characteristics were

different for the cases where the steady state was reached from increasing or from decreasing the temperature of the heat transfer fluid.

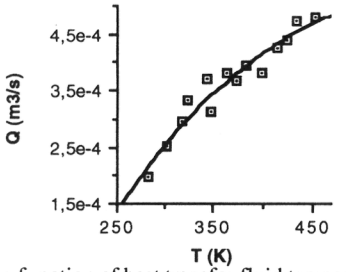

Figure 9. Volumetric flow as a function of heat transfer fluid temperature, see Chenneaux *et al.* (1990).

For simulation purposes, the following correlation, see fig. 9, was used in the evaluation of the heat transfer coefficients:

$$Q_e = -7.565 \cdot 10^{-4} + 4.631 \cdot 10^{-6} \cdot T_e - 4.238 \cdot 10^{-9} \cdot T_e^2 \qquad (65)$$

c/ Steady State experiments: Experiments to determine some characteristic parameters of the heating/cooling circuits, were performed in steady state conditions, i.e.,

$$\frac{dT_e}{dt} = 0 \ , \ \frac{dT_c}{dt} = 0 \ , \ \text{and} \ \frac{dT_P}{dt} = 0 \qquad (66)$$

The first set of experiments were carried out introducing a constant power by means of the electrical heater, maintaining a constant external cryostat temperature, and forcing the control valve to be fully open by a fictitious set-point value. For each experiment the system was brought to a steady state after a certain period of time. The experimental values found are listed in Table 8.

Another set of experiments were carried out in the same way, but forcing the control valve to be fully closed and without introducing any power. In this case, the different steady states were reached by changing the temperature of the external cold source (T_K). For each experiment the system was brought to a steady state after a certain period of time. The experimental values found are listed in Table 9.

Replacing the steady state condition, eq. (66), into eqs. (60) - (62), the following equations are obtained,

$$Q_c \cdot \rho_e \cdot Cp_e (T_c - T_e) + q_h + q_{p_e} + \frac{\Gamma_e (T_P - T_e)}{\tau_{e_1}} = 0 \qquad (67)$$

$$-Q_c \cdot \rho_e \cdot Cp_e (T_c - T_e) - US_c \cdot \Delta T_{ln} + q_{p_c} + US_{lc}(T_a - T_c) = 0 \qquad (68)$$

$$\frac{T_a - T_P}{\tau_P} + \frac{T_e - T_P}{\tau_{e_2}} = 0 \qquad (69)$$

Using eq. (69) to obtain an expression for T_P,

$$T_P = \frac{\tau_{e_2} \cdot T_a + \tau_P T_e}{\tau_{e_2} + \tau_P} \qquad (70)$$

Replacing this equation in eq. (67) and rearranging,

$$T_e = \frac{q_h + q_{p_e} + K_1 \cdot T_a}{Q_c \cdot \rho_e \cdot Cp_e + K_1} + \frac{Q_c \cdot \rho_e \cdot Cp_e}{Q_c \cdot \rho_e \cdot Cp_e + K_1} T_c \qquad (71)$$

where K_1 is defined as,

$$K_1 = \frac{\tau_{e_2} \cdot \Gamma_e}{\tau_{e_1} (\tau_p + \tau_{e_2})} \qquad (72)$$

As a first approximation, this term was considered a constant related to the properties of the system (masses and heat capacities) and the heat losses of the heating loop.

Table 8. Steady state values with fully open control valve.

q_h (W)	T_K (°C)	T_a (°C)	T_e (°C)	T_c (°C)	ΔT_K
1796.0	11.9	24.5	66.15	24.0	3.590
1973.0	0.0	24.7	59.30	14.05	4.320
1974.0	-7.8	24.5	52.50	6.9	4.835
1327.0	-8.0	24.5	32.50	2.8	3.420
980.4	-8.2	24.0	23.40	0.47	2.690
700.1	-8.2	24.0	15.50	-1.40	2.020
412.7	-8.3	24.0	8.16	-3.25	1.430
1976.0	-15.5	24.5	45.50	0.10	5.760
1642.0	-15.5	25.5	35.90	-2.00	4.580
1329.0	-15.6	24.5	26.32	-4.10	4.230
988.6	-15.7	24.5	16.90	-6.40	3.390
698.1	-15.8	24.0	9.20	-8.30	2.640
418.7	-15.81	24.5	1.56	-10.30	1.910
207.7	-15.85	24.5	-4.00	-11.75	1.310
54.4	-15.9	24.2	-7.94	-12.90	0.860
693.6	-19.8	22.0	5.58	-12.10	2.980
412.7	-19.9	21.0	-2.12	-14.10	2.140
204.4	-20.0	21.0	-7.61	-15.60	1.550
66.5	-20.0	21.0	-11.20	-16.60	1.160
16.8	-20.0	21.0	-12.58	-17.00	0.961
0.0	-20.0	21.0	-12.97	-17.10	0.940
700.0	-23.7	23.5	2.45	-15.45	3.630
417.6	-23.85	23.5	0.31	-17.80	2.670
207.7	-23.9	23.5		-19.50	1.850
1266.0	10.0	25.1	47.70	19.00	
1266.0	2.0	25.1	40.13	11.65	
1266.0	-6.0	25.2	32.70	4.20	
1266.0	-15.0	25.0	25.25	-3.70	
1266.0	-22.0	25.0	19.60	-9.50	
1266.0	-30.0	25.0	18.80	-10.10	
0.0	19.6	21.3	23.33	21.29	
0.0	17.7	21.5	21.54	19.39	

Table 9. Steady state values with fully close control valve.

q_h (W)	T_K(°C)	T_a (°C)	T_e (°C)	T_c (°C)
0.0	0.0	19.14	38.27	1.302
0.0	-10.0	19.23	34.79	-8.47
0.0	-20.0	18.88	30.81	-17.97
0.0	-30.0	18.75	27.02	-27.20
0.0	-30.0	10.42	24.18	-27.20

d/ Maximum and minimum flow through the control valve ($Q_{c_{max}}$ and $Q_{c_{min}}$) and K_1: In order to evaluate the maximum flow trough the control valve, eq. (71) was

applied with the experimental points of Table 8. Representing T_e as a function of T_c, assuming that $Q_{c_{max}}$ and K_1 are constants and the heat transfer fluid properties (Cp_e, ρ_e) do not change appreciably in the temperature range considered, the experimental values should give different straight lines for each constant power input (q_h) at the same ambient temperature. The figure 10 seems to confirm such a hypothesis.

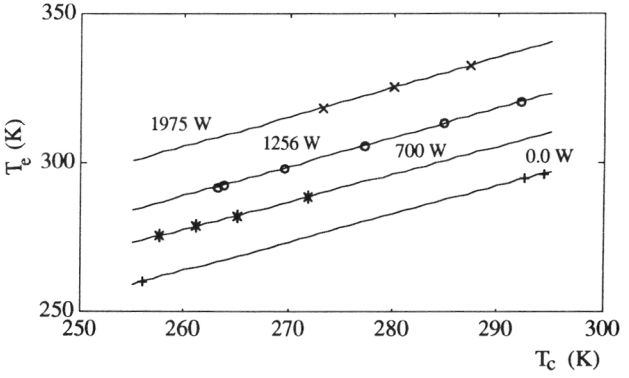

Figure 10. T_e versus T_c for different power inputs with opened control valve

The values obtained for the different straight lines are:

$$T_{e\,(1975.0)} = 48.52 + 0.989\ T_c \quad (73)$$

$$T_{e\,(1266.0)} = 33.10 + 0.984\ T_c \quad (74)$$

$$T_{e\,(700.0)} = 36.13 + 0.929\ T_c \quad (75)$$

$$T_{e\,(415.0)} = 25.99 + 0.946\ T_c \quad (76)$$

$$T_{e\,(0.0)} = 18.05 + 0.946\ T_c \quad (77)$$

From these series of experiments, replacing the values of eqs. (73)-(77) in eq. (71), the value calculated for $Q_{c_{max}}$ was:

$Q_{c_{max}} = (3.09 \pm 0.42) \cdot 10^{-5}\ m^3/s$

The same procedure was followed in order to calculate the minimum flow through the control valve using the experimental results of Table 9. Representing T_e as a function of T_c, see figure 11, the straight line was fitted to:

$$T_e = 202.64 + 0.397\ T_c \quad (78)$$

and replacing the values of eq. (78) in eq. (71) the value obtained for $Q_{c_{min}}$ was:

$Q_{c_{min}} = (7.34 \pm 0.04) \cdot 10^{-7}\ m^3/s$

The corresponding values of K_1 were also determined following the same procedure:

$K_1 = 2.2 \pm 1.6$

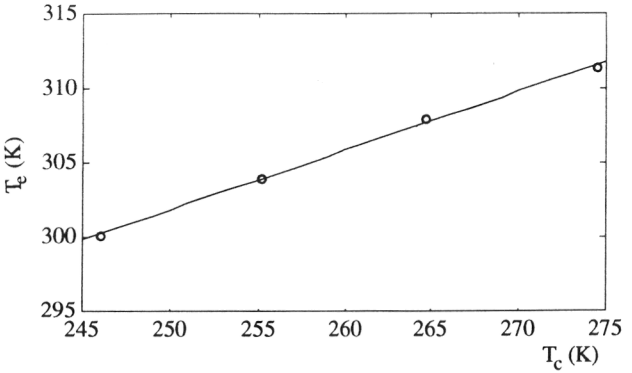

Figure 11. T_e versus T_c with control valve closed.

e/ Cooling provided by the external source and US_{Ic}: The heat exchanged by the cooling loop through the external cold source can be expressed as:

$$q_{exchanged} = US_c \cdot \Delta T_{ln} \tag{79}$$

where US_c is the overall heat transfer coefficient for the internal coil of the cooling circuit times the exchange area, and ΔT_{ln} is the logarithmic average temperature of heat exchange between the cooling loop and the external cold source.

ΔT_{ln} can be calculated using the following expression:

$$\Delta T_{ln} = \frac{T_{K_o} - T_{K_i}}{\ln\left(\frac{T_c - T_{K_i}}{T_c - T_{K_o}}\right)} \tag{80}$$

Hence, T_{K_o} is the only unknown. From a heat balance in the coil of the cooling loop, and neglecting the accumulation term:

$$T_{K_o} = T_c + (T_{K_i} - T_c) \exp\left(\frac{-US_c}{Q_K \cdot \rho_K \cdot Cp_K}\right) \tag{81}$$

The exponential term depends on the cryostat properties and characteristics of the cooling loop. In the normal operation mode, the cryostat conditions should be more or less constants and therefore the exponential term can be assumed constant as first approximation. Then eq. (81) reduces to:

$$T_{K_o} = T_{K_i} \cdot E_1 + T_c\,(1-E_1) \tag{82}$$

with,

$$E_1 = \exp\left(\frac{-US_c}{Q_K \cdot \rho_K \cdot Cp_K}\right) \tag{83}$$

Hence, rearranging eq. (83) it is possible to find:

$$E_1 = \frac{T_{K_o} - T_c}{T_{K_i} - T_c} \tag{84}$$

This assumption was validated experimentally, in the experiments at steady state. In these experiments ΔT_K was measured by means of a precise device: Hewlett Packard mod. 2804A. The experimental data found are listed in Table 10.

Table 10. Experiments to determine the cooling provide by the external source.

T_c (°C)	T_{Ki} (°C)	T_{Ko}(°C)	E_1
24.0	11.90	15.49	0.703
14.1	0.00	4.32	0.694
6.9	-7.80	-2.97	0.671
2.8	-8.00	-4.58	0.683
0.5	-8.20	-5.51	0.691
-1.4	-8.20	-6.18	0.703
-3.3	-8.30	-6.87	0.714
0.1	-15.50	-9.74	0.631
-2.0	-15.50	-10.92	0.661
-4.1	-15.60	-11.37	0.632
-6.4	-15.70	-12.31	0.635
-8.3	-15.80	-13.16	0.648
-10.3	-15.81	-13.90	0.653
-11.8	-15.85	-14.54	0.677
-12.9	-15.90	-15.04	0.713
-12.1	-19.80	-16.82	0.613
-14.1	-19.90	-17.76	0.631
-15.6	-20.00	-18.45	0.648
-16.6	-20.00	-18.84	0.659
-17.0	-20.00	-19.04	0.680
-17.1	-20.00	-19.06	0.676
-15.5	-23.70	-20.07	0.557
-17.8	-23.85	-21.18	0.559
-19.5	-23.90	-22.05	0.580

Taking the average, $E_1 = 0.655$, eq. (82) becomes:

$$T_{K_o} = 0.655 \cdot T_{K_i} + 0.345 \cdot T_c \tag{85}$$

By manipulating eq. (68), it is possible to obtain the following expression for the evaluation of US_c:

$$T_e = \frac{US_c \cdot \Delta T_{ln} - q_{p_c} - US_{ic}\, T_a}{Q_c \cdot \rho_e \cdot Cp_e} + \frac{Q_c \cdot \rho_e \cdot Cp_e + US_{ic}}{Q_c \cdot \rho_e \cdot Cp_e} T_c \tag{86}$$

The slope of the correlations for the experimental values (see figure 10) suggest that the evaluation of US_{ic} from this data will be difficult since $Q_c \cdot \rho_e \cdot Cp_e >> US_{ic}$. This implies that in the second term of eq. (86), the factor that multiplies T_c is approx. equal to 1. Using this simplification, and rearranging eq. (86) becomes:

$$US_c \cdot \Delta T_{ln} - Q_c \cdot \rho_e \cdot Cp_e\,(T_e - T_c) - q_{p_c} - US_{ic}\; T_a = 0 \tag{87}$$

In order to evaluate the evolution of US_c as a function of the temperature of the external cryostat (T_K) and the internal cooling loop (T_c) the following assumption was made:

$$US_c = A + B \cdot T_{cK} + C \cdot T_{cK}^2 \tag{88}$$

where T_{cK} is an average temperature defined as,

$$T_{cK} = \frac{\left(\frac{T_{K_i} + T_{K_o}}{2}\right) + T_c}{2} \tag{89}$$

From regression analysis, the parameters of eqs. (86) and (87) were obtained:

Table 11. Parameters for the calculation of US_c and US_{lc}.

A	$-2.670 \cdot 10^3$
B	19.36
C	$-3.262 \cdot 10^{-2}$
US_{lc}	0.435

f/ Experiments in dynamic conditions, thermal capacities and time constants (Γ_e, Γ_c, τ_P, τ_{e1}, τ_{e2})**:** A set of curves, see fig. 12, at reactor empty were generated by means of jumps in the temperature set values on the RC1 reaction calorimeter in order to characterize the thermal capacities and time constants of the different parts of the heating/cooling loop.

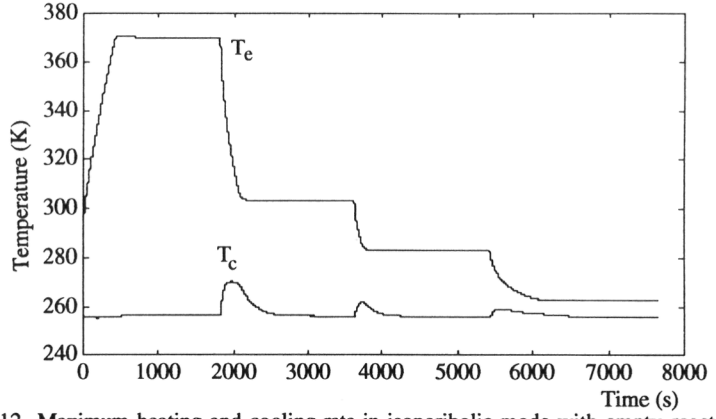

Figure 12. Maximum heating and cooling rate in isoperibolic mode with empty reactor. $T_{set\text{-}point} \rightarrow 293.2 \rightarrow 370.2 \rightarrow 283.2 \rightarrow 263.2$ K.

It is possible to obtain the eqs. (90)-(91) from the start of the heating period (maximum heating) and eqs. (92)-(93) from the start of the cooling period (maximum cooling) part of the curves, with the following assumptions :

- Thermal equilibria at the beginning of the experiments, that means no heat accumulation on the wall of the main loop.
- Starting of the heating: the system control closes completely the regulation valve ($Q_c = Q_{c_{min}}$) and the electrical heater introduces the maximum power (q_h=2000 W).

- Starting of the cooling: The system control opens completely the regulation valve ($Q_c=Q_{c_{max}}$) and the electrical heater is close ($q_h=0$ W)

- $(T_p-T_e) \cong 0$

$$\Gamma_e \left(\frac{dT_e}{dt} \right)_{max} = Q_{c_{min}} \cdot \rho_e \cdot Cp_e (T_c-T_e) + 2000. + q_{p_e} \tag{90}$$

$$\Gamma_c \left(\frac{dT_c}{dt} \right)_{min} = -Q_{c_{min}} \cdot \rho_e \cdot Cp_e (T_c-T_e) - US_c \cdot \Delta T_{ln} + q_{p_c} + US_{lc}(T_a-T_c) \tag{91}$$

for the maximum heating period, and

$$\Gamma_e \left(\frac{dT_e}{dt} \right)_{min} = Q_{c_{max}} \cdot \rho_e \cdot Cp_e (T_c-T_e) + 0.0 + q_{p_e} \tag{92}$$

$$\Gamma_c \left(\frac{dT_c}{dt} \right)_{max} = -Q_{c_{max}} \cdot \rho_e \cdot Cp_e (T_c-T_e) - US_c \cdot \Delta T_{ln} + q_{p_c} + US_{lc}(T_a-T_c) \tag{93}$$

for the maximum cooling period.

Unfortunately the derivative and in particular the search of its maximum and minimum is very sensitive to noise and the type of filtering and/or data treatment, but the following approximate values were obtained:

$\Gamma_e \approx 5.0 \cdot 10^3$ J/K

$\Gamma_c \approx 2.0 \cdot 10^4$ J/K

The time constants τ_{e1},τ_{e2},and τ_P are difficult to evaluate from experiments due to the fact that T_P is not measured and probably not constant. However, orders of magnitude can be calculated with the data available (assuming a certain weight for the container of the heated loop made of stainless steel) and considering the following relationships:

$$\tau_{e_1} = \frac{\Gamma_e}{US_P} \quad , \quad \tau_{e_2} = \frac{\Gamma_P}{US_P} \quad \text{and} \quad \tau_P = \frac{\Gamma_P}{US_a} \tag{94}$$

$\tau_{e1} \approx 20.0$ s

$\tau_{e2} \approx 30.0$ s

$\tau_P \approx 2000.0$ s

In order to fit the heating/cooling model to the experimental results the set of curves generated at isoperibolic mode, i.e. constant jacket temperature, were used to obtain the remainder unknowns. After an optimisation procedure, see Press *et al.* (1986), the results obtained are listed in Table 12.

Table 12. Results of the optimisation procedure

Constants	value	units
Γ_e	$3.59 \cdot 10^3$	J/K
Γ_c	$1.7 \cdot 10^4$	J/K
τ_P	7747.0	s
τ_{e1}	18.07	s
τ_{e2}	38.82	s

Using eq. (72) with the values of Table 12, the value found for $K_1 \approx 1$ is consistent with the values calculated from steady-state experiments.

6. IMPLEMENTATION OF THE NUMERICAL SIMULATOR

According to the objectives and the requirements, the simulator was developed in terms of independent modules as shown in fig. 13. The physico-chemical properties of the substances dealt with, the stoichiometry and the thermo-kinetical parameters of reactions are introduced beforehand by the user. Concerning this aspect, full flexibility is permitted, e.g. any number of components and complex reaction schemes. This information, as well as the equipment characteristics of the reaction calorimeter are managed and stored in the DATA LIBRARY block.

For a given case, the user introduces an operating procedure which is validated and interpreted by the algorithms of the INPUT block, that by accessing the respective libraries, generate a matrix structure containing all the information necessary for the simulation and used by the SEQUENCER.

The SEQUENCER controls the simulation and sends the results to the OUTPUT block. This control consists of timing the simulation and updating the matrix structure by interacting with the MODEL GENERATOR and the SOLVER.

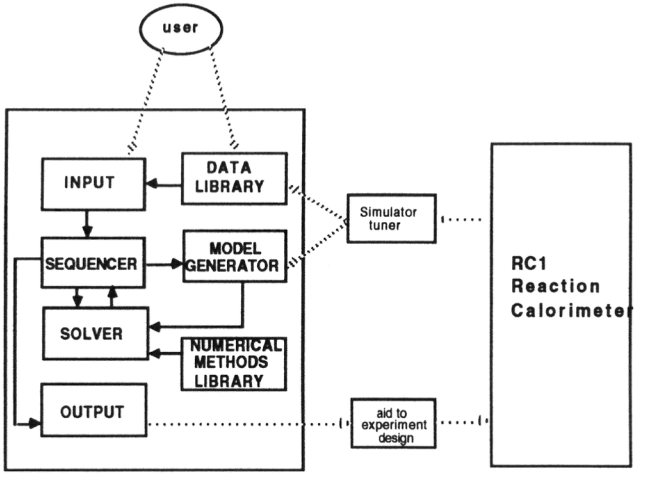

Figure 13. Block diagram of the simulator and its interaction with the RC1.

The MODEL GENERATOR constructs a set of algebraic-differential equations whose number depends on the specific case and administers any modification of the model during simulation. Mathematical models implemented in the simulator comprise a basic model considering

homogeneous mixture and ideal behaviour, and alternative models, which are collected cases of particular interest or systems for which the assumptions of the basic model are not valid.
The basic model consists of fundamental equations like heat and mass balances, and equilibrium relations, reproducing the behaviour of the state vector, and of thermo-kinetic models representing all the thermal fluxes involved in the process. Special emphasis has been placed on the evaluation of physico-chemical and transport properties. Correlations obtained by dimensionless analysis are used in order to follow the influence of the main operating variables such as stirrer speed, reactant feeding rate, temperature and flow of the heat transfer fluid.
The simulator also includes models for the controllers of temperature, and reactant flows. Due to the complexity and fast response of the cooling/heating circuit and in order to reproduce the isothermal-controlled operating mode, it was necessary to model the dynamic behaviour of the heat transfer fluid.
The numerical resolution of the set of equations is done by the SOLVER block, which uses numerical tools available in the NUMERICAL METHODS LIBRARY.
The results presented by the OUTPUT block, in tabulated or graphic format, are the profiles of temperature, pressure, volume, composition and thermal fluxes as function of time.
The whole code was implemented in FORTRAN-77 on a PC, see Zaldívar *et al.* (1990).

7. MODEL VALIDATION TESTS

A set of different experiments were carried out in order to examine the assumptions in the model and to compare the experimental and predicted dynamic behaviour. The first set consisted of heating/cooling the reactor by means of jumps in the temperature set values of the reaction calorimeter. In the second set a very simple reaction, i.e. neutralisation, was chosen and several experiments modifying the operating conditions, such as temperature, concentrations, feeding rate, etc. were carried out. Finally, the esterification between propionic anhydride and 2-butanol was studied.

7.1. Heating/Cooling Tests

With the reactor filled with 1.00 l of water, different heating and cooling experiments were carried out by the same procedure followed at section 5.3. The aim of these tests was to compare experimental behaviour of the RC1 with the behaviour predicted by the simulator for some step changes on temperature set-point. The temperature of the cryostat was maintained constant and equal to -20°C.

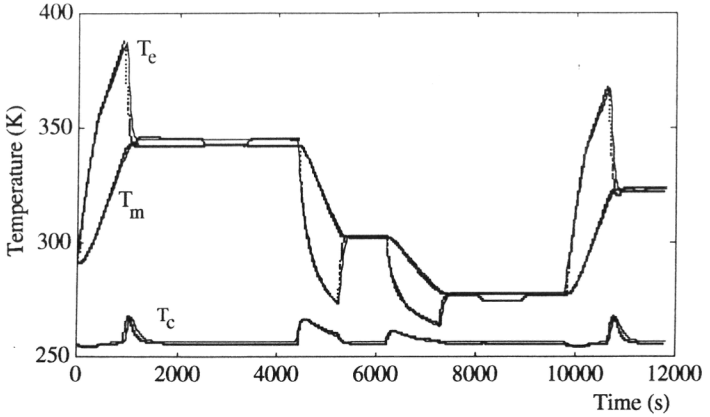

Figure 14. Experimental (dotted lines) and simulated (continuous lines) behaviour of different steps with water. $T_{set\text{-}point} \rightarrow 291.7 \rightarrow 343.2 \rightarrow 283.2 \rightarrow 262.2 \rightarrow 323.2$ K.

Note that during the experiments some calibrations that were not simulated were carried out. The same types of experiments were performed filling the reactor with 0.6 l of 2-butanol. In this case, the capacity for predicting the internal heat transfer coefficient as a function of the physical properties for a liquid that was not used in the U·S characterisation experiments was also evaluated.

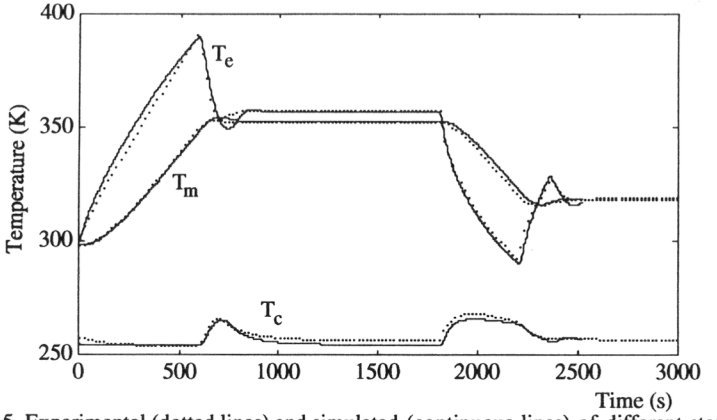

Figure 15. Experimental (dotted lines) and simulated (continuous lines) of different steps with 2-butanol. $T_{set\text{-}point} \rightarrow 298.2 \rightarrow 353.2 \rightarrow 318.2$ K.

7.2. Neutralisation Reaction

The neutralisation reaction between the sodium hydroxide and chloridric acid is an example of an instantaneous and irreversible chemical reaction i.e. the power generated by the reaction medium is proportional to the speed of introduction of reactants.

$$HCl_{aq} + NaOH_{aq} \rightarrow NaCl_{aq} + H_2O$$

The heat of neutralisation at 25 °C, see Hougen *et al.* (1954) is -55.9 kJ/mol. Due to the reaction being instantaneous, the rate reaction is defined as follows,

$$r(t) = \frac{Q_{E_j} \cdot C_{E_j}}{V_m(t)} = \frac{F_{E_j}}{V_m(t)} \qquad (95)$$

Operating conditions: An aqueous solution of chloridric acid (≈2 M) was added to the reactor. Thereafter, the sodium hydroxide solution (≈2 M) was introduced at different rates, cooling and stirring at the same time. Two different operating modes were carried out with the purpose of testing the dynamics of the simulator. In isoperibolic mode T_e was maintained constant, and a certain amount of NaOH was dosed at constant rate until the complete neutralisation of the hydrochloric acid (pH=7).

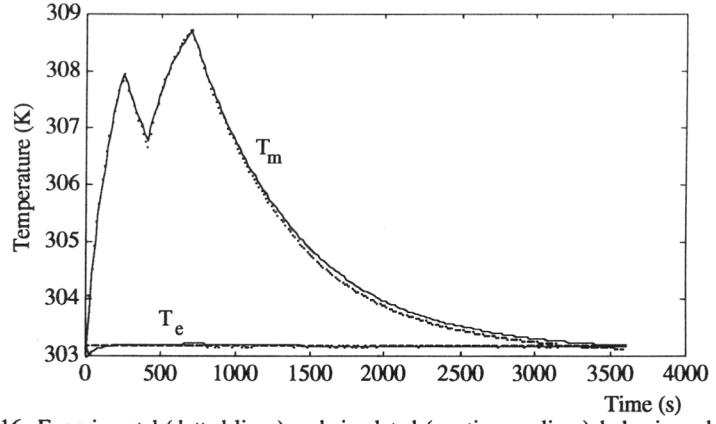

Figure 16. Experimental (dotted lines) and simulated (continuous lines) behaviour during an isoperibolic experiment. Initial conditions: 1.3 mol HCl, 32.7 mol H_2O and T_e=constant=303.2 K, anchor stirrer 200 rpm. Two additions of NaOH solution at 1.3 g/s of dosing rate. First addition: 0.6 mol NaOH and 15.9 mol of H_2O. Second addition: 1.6 mol NaOH and 46.2 mol H_2O.

In the isothermic mode, the same type of procedure was followed but the temperature of the reactor Tm was kept at the specified set-point by the control system. In these experiments the dynamic behaviout of the simulated heating/cooling circuits is also tested.

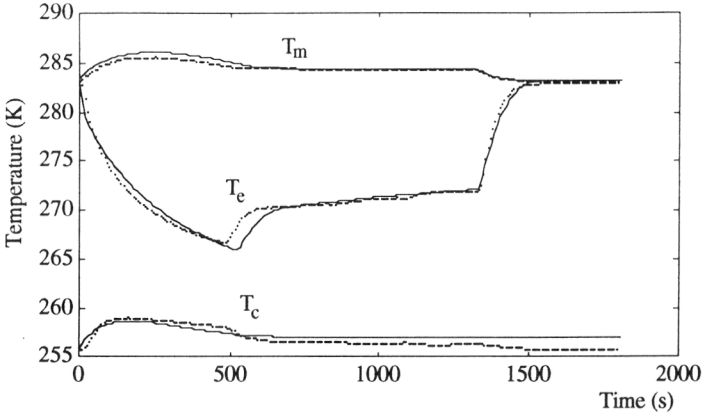

Figure 17. Experimental (dotted lines) and simulated (continuous lines) behaviour during an isothermal experiment. Initial conditions: 1.6 mol HCl, 41.5 mol H_2O and $T_{mset\text{-}point}$ = 283.2 K, turbine G/L stirrer 500 rpm, P-control = 10. Additions of NaOH solution at 0.6 g/s of dosing rate during 35.2 min., 1.4 mol NaOH and 38.0 mol of H_2O.

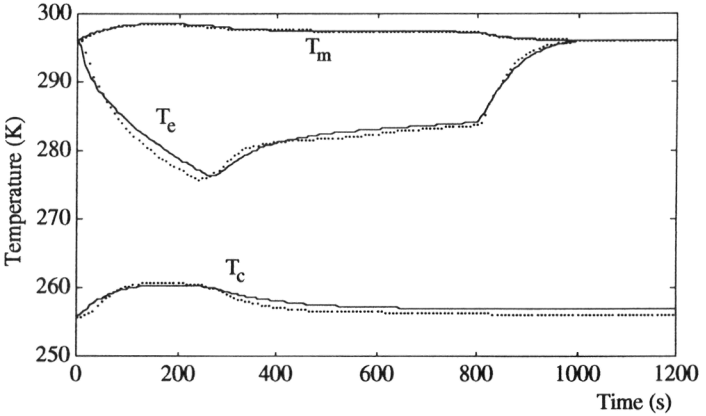

Figure 18. Experimental (dotted lines) and simulated (continuous lines) behaviour during an isothermal experiment. Initial conditions: 1.8 mol HCl, 45.6 mol H_2O and $T_{mset\text{-}point}$ = 296.2 K, turbine G/L stirrer 500 rpm, P-control = 10. Additions of NaOH solution at 1.2 g/s of dosing rate during 13.3 min., 1.8 mol NaOH and 49.4 mol of H_2O.

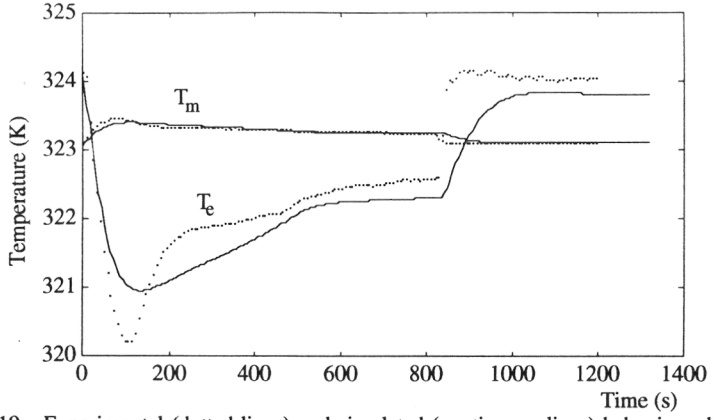

Figure 19. Experimental (dotted lines) and simulated (continuous lines) behaviour during an isothermal experiment. Initial conditions: 1.6 mol HCl, 41.4 mol H_2O and $T_{mset\text{-}point}$ = 323.2 K, turbine G/L stirrer 500 rpm, P-control = 10. Additions of NaOH solution at 1.0 g/s of dosing rate during 13.9 min., 1.6 mol NaOH and 44.9 mol of H_2O.

7.3. Esterification Reaction

The system 2-butanol/propionic anhydride (acid) which has been studied by Snee et al. (1992) in safety assessment was selected as a specific case. This homogeneous reaction has some characteristics that make it very interesting for testing studies: moderately exothermic with no danger of decomposition reactions; reaction rate variable as a function of catalyst (strong acid, i.e. sulphuric acid); the reaction exhibits a second-order kinetics when no strong acid is present and a kind of autocatalytic behaviour when sulphuric acid is introduced, see Zaldívar *et al.* (1993).

$$(CH_3\text{-}CH_2\text{-}CO)_2O + CH_3\text{-}CHOH\text{-}CH_2\text{-}CH_3 \xrightarrow{H^+} CH_3\text{-}CH_2\text{-}COOH + CH_3\text{-}CH_2\text{-}COOCH(CH_2)\text{-}CH_2\text{-}CH_3$$

7.3.1. Experimental part

An extensive experimental programme was carried out using adiabatic and heat flow calorimetry supported by chemical analysis. The adiabatic experiments were performed using a PHI-TEC calorimeter, see Singh (1989), while the isothermal and isoperibolic experiments were made using a RC1 reaction and a small jacketed vessel of approx. 200 ml capacity. GC was used for the concentration analysis of different species.

The adiabatic experiments are summarised in Table 13. A series of measurements in the PHI-TEC were made using different molar ratio between propionic anhydride (A), 2-butanol (B) and propionic acid (C) catalysed by various concentrations of sulphuric acid (S) with a total

sample mass of approx. 60 g. Reagents were added with the sample container positioned inside the calorimeter and adiabatic conditions were established from ambient temperature without using the 'heat-wait-search' mode of operation.

Table 13. Adiabatic experiments: initial conditions.

Ex.	$n_A:n_B:n_C$	$x_S \cdot 10^3$
1	1:1:2	0.0
2	1:1:0	0.0
3	1:2:0	0.0
4	1:1:0	2.2
5	1:1:0	2.9
6	1:1:0	3.6
7	1:1:0	4.3
8	1:1:0	5.9
9	1:1:2	1.5
10	1:2:0	1.9
11	1:3:0	1.5
12	1:2:1	1.4

The isothermal variation of the rate of heat generation with time was measured using the Mettler RC1 calorimeter. Table 14 summarises the isothermal experiments. During this experiments, the concentration of 2-butanol and the ester was measured by GC. The alcohol was added to the reactor and time was allowed for the control system to achieve the temperature selected for isothermal measurement. Propionic anhydride (or propionic acid, or a mixture) at ambient temperature was then added quickly to the reactor and the reaction was allowed to proceed until completion.

Table 14. Isothermal experiments: initial conditions.

Ex.	T_{sp} (K)	$n_A:n_B:n_C$	$x_S \cdot 10^3$
13	343.2	0:1:1	0.0
14	343.2	0:1:1	3.0
15	343.2	0:1:1	6.0
16	343.2	1:1:0	0.0
17	331.6	1:1:0	0.0
18	303.2	1:1:0	3.0
19	303.2	1:1:1	2.0
20	303.2	1:1:2	1.5
21	303.2	2:2:1	2.4

The isoperibolic experiments carried were carried out in the same way than the isothermal tests in the bench-scale reactor by configuring it to operate at constant jacket temperature. Experiments were performed at a series of fixed jacket temperatures with an equimolar mixture of propionic anhydride/2-butanol catalysed by the addition of the same amount of sulphuric acid, see Table 15.

The data from adiabatic -temperature versus time - and isothermal -concentrations versus time - experiments were used to fit the kinetic expressions whereas the isoperibolic data were used to test the accuracy of such kinetics through the comparison of experimental versus the theoretical by simulation.

Table 15. Experimental isoperibolic test matrix: initial conditions.

Ex.	T_e (K)	$n_A:n_B:n_C$	$x_S \cdot 10^3$
22	293.9	1:1:0	3.0
23	295.7	1:1:0	3.0
24	298.2	1:1:0	3.0
25	300.7	1:1:0	3.0
26	303.2	1:1:0	3.0
27	308.2	1:1:0	3.0

7.3.2. Identification of Kinetic Scheme

The esterification mechanism involving acidic catalysis have been studied in detail and a number of general possibilities have been recognised, see March (1992). There are four possible mechanisms depending on the following criteria: unimolecular or bimolecular, and acyl or alkyl cleavage. All four of these are SN1, SN2 or tetrahedral mechanisms. This applies to the reaction between 2-butanol and propionic anhydride as well as propionic acid. Moreover, in this relatively simple reaction system another group of reactions have been recognised:

- The reaction between the sulphuric acid and the 2-butanol to form the mono-alkyl sulphuric acid which acts as a different catalyst of the reaction, see Dhanuka *et al.* (1977) and can favour the ionisation of the alcohol to carbonium and in consequence the alkyl cleavage, see Deno and Newman (1951).
- The reaction between the sulphuric acid and the propionic anhydride to form the propyl sulphate which acts as a different catalyst of the reaction, see Yvernault (1955).

In addition, different authors, see Haldar and Rao (1992a, 1992b), have shown the influence of the Hammett's acidity function on the reaction rate which depend on the sulphuric and propionic acid concentrations, and temperature.

For all these reasons, only empirical kinetic models can be found in literature, in which the reaction rate constant depend of the sulphuric acid concentration, the initial ratio between reagents concentrations, the organic acid concentration, etc. see Sreeramulu and Rao (1973), Troupe and Kobe (1950), amongst others.

a/ The reaction rate without sulphuric acid:

The analysis of experiments without sulphuric acid, Ex. 1-3, 16 and 17, showed that in this particular case the reaction rate followed a second-order expression, see fig. 22a,

$$r = k_0 \cdot C_A \cdot C_B \qquad (96)$$

where $k_0 = 5.36178 \cdot 10^7 \cdot \exp(-80.47864/R \cdot T_m)$. Furthermore, the propionic acid seemed not to influence the reaction mechanism.

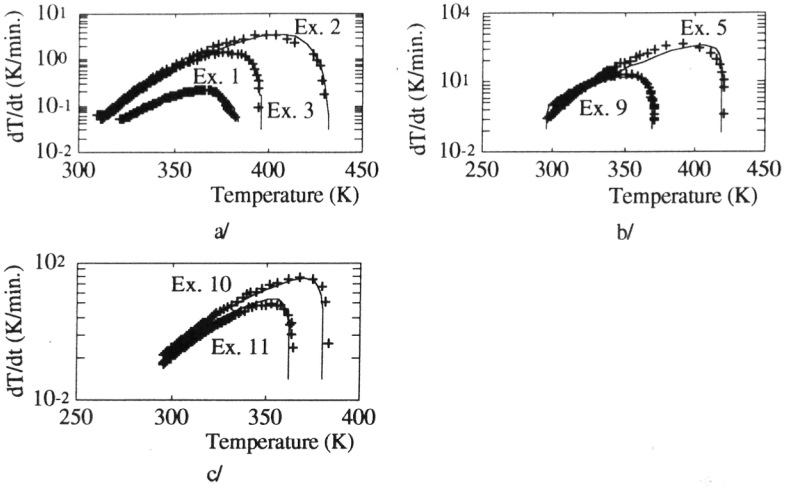

Figure 22. Experimental (+) and simulated (continuous lines) rates of self-heating for the esterification a/without sulphuric acid (see eq. 96); b/ and c/ with sulphuric acid (see eqs. 102-104).

b/ The reaction rate between propionic acid and 2-butanol:

In a separate set of experiments, Ex. 13-15, it was demonstrated that the reaction rate between the propionic acid and 2-butanol was negligible in presence of propionic anhydride - the constant rate is approx. 200 slower- and the reaction could be fitted using an elementary reversible second-order kinetics,

$$r = k_1 \cdot C_B \cdot C_C - k_{-1} \cdot C_E \cdot C_W \qquad (97)$$

in which the sulphuric acid influence could be correlated by the following expressions, see Dhanuka *et al.* (1977),

$$k_1 = \alpha_1 + \beta_1 \cdot x_S \qquad (98)$$

$$k_{-1} = \alpha_{-1} + \beta_{-1} \cdot x_S \qquad (99)$$

where α was the specific reaction rate constant for non-catalytic reaction and β was a constant ($\alpha_1 = 1.4813 \cdot 10^{-7}$, $\alpha_{-1} = 3.8072 \cdot 10^{-8}$, $\beta_1 = 3.746.10^{-3}$, $\beta_{-1} = 1.4863 \cdot 10^{-3}$ at $T_m = 343$ K).

c/ The sulphuric acid as catalyst:

The following experimental observations were found during the reaction between 2-butanol and propionic anhydride catalysed by sulphuric acid:

- The initial reaction rate from adiabatic experiments seems proportional to the concentration of sulphuric acid. In addition, the heat of reaction does not change, between the experimental error, with the addition of sulphuric acid, see Snee and Hare (1992).
- The propionic acid concentration increases the reaction rate, producing a sort of autocatalytic behaviour only if there is sulphuric acid.

- After some concentration level the propionic acid seems not to increase the reaction rate anymore.

Different kinetic schema were tested, but the elucidation of the real pathway was to complex. In consequence, the formulation of elementary reactions that would explain this behaviour was abandoned for another more empirical approach.

Since the elucidation of the real pathway was so complex, it was abandoned for another more empirical approach. The existence of two catalysts was postulated, see Dhanuka *et al.* (1977). The former accelerating the second order reaction and the latter producing a first order reaction expression. Furthermore, the transformation of the catalysts was correlated with the acidity function, see Haldar and Rao (1992a), and the concentration of 2-butanol. This empirical model can be written as:

$$A + B \rightarrow C + E \tag{100}$$

$$Cat._1 \rightarrow Cat._2 \tag{101}$$

where the main reaction can be expressed as,

$$r_2=\left(k_0+k_2\cdot C_{Cat._1}\right)C_A C_B+k_3\cdot C_{Cat._2} C_A \tag{102}$$

$$r_3 = k_4\cdot 10^{-H_R}\cdot C_{Cat_1}\cdot C_B \tag{103}$$

and H_R is related to the acidity function, see Rochester (1970) and is correlated as:

$$H_R=-\left(p_1\cdot C_{Cat._1}+p_2\cdot C_C\right)\left(p_3+\frac{p_4}{T_m}\right) \tag{104}$$

Table 16. Kinetic parameters of eqs. (102)-(104).

A_2	$2.8074\cdot10^{10}$
Ea_2	79.1595
A_3	$3.9480\cdot10^{10}$
Ea_3	69.9746
A_4	$1.4031\cdot10^{8}$
Ea_4	76.6172
p1	$2.002\cdot10^{-1}$
p2	$3.205\cdot10^{-2}$
p3	-21.3754
p4	12706.0

The parameters for these expressions were obtained by minimisation trough the complete set of experimental data from Tables 13-14, see fig. 23.

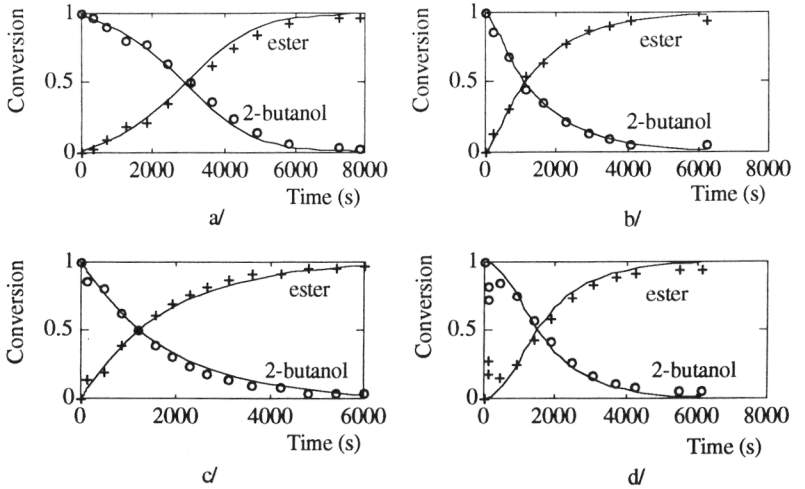

Figure 23. Experimental(+ and o) and simulated (continuous lines) conversion profiles for the esterification with sulphuric acid. a/ Ex. 18 ; b/ Ex. 19; c/ Ex. 20; d/Ex. 21.

Afterwards, the isoperibolic experiments were used to check its validity. In figure 24 are plotted the temperature profiles of six isoperibolic experiments at different T_e set-point. The initial drop in reactor temperature is due to the endothermic mixing of the reagents. As can be seen, the behaviour of the reaction mass shows that in these conditions we are working in a parametric sensitivity region, defining sensitivity as the the variation of the maximum of reactor temperature with respect to that of the jacket, i.e. dT_m/dT_e. In Ex. 22 at jacket temperature of 293.9 K the maximum temperature reached by the reaction mass is 310.5 K whereas in Ex. 27 with a jacket temperature of 308.2 K the maximum temperature is 407.5 K, i.e. a change of 14.3 degrees in jacket temperature produces a change of 97 K in the maximum temperature reached by the reaction mass. This shows how an exothermic reaction can proceed under subcritical (controlled) and supercritical (runaway) conditions. In the latter, the reaction stops when all reagents have been consumed.

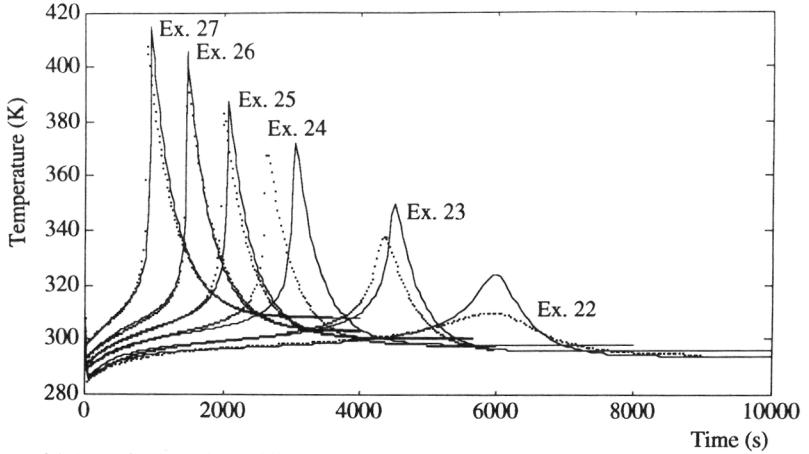

Figure 24. Experimental (dotted lines) and simulated (continuous lines) reactor temperatures of isoperibolic batch experiments of Table 16 using the empirical model (eqs. 102-104). 884.0 g. of propionic anhydride were added to 503.2 g. of 2-butanol. The molar fraction of sulphuric acid was $3.0 \cdot 10^{-3}$.

8. CONCLUSIONS

The formulated mathematical model adequately describes the significant process behaviour of the RC1 reaction Calorimeter. The model of the reaction mass with lumped parameters satisfies the level of knowledge of fine chemical processes. The modelisation of heat transfer through the reactor wall assuming thermal inhomogeneity is important whenever fast transients take place. Furthermore, to simulate all the thermal operating modes, it has been necessary to model accurately the temperature controller of the RC1, including the dynamics of the heating/cooling circuits.

Considerable effort has been devoted to the characterisation of the equipment. Fortunately, only few parameters of the model are specific of the Reaction Calorimeter RC1 and , in consequence, the simulator can be easily applied to other equipment of similar characteristics. Concerning the external cold source, an additional adjustment should be made to calculate the heat removed. Furthermore, it has been observed that the values of the heat transfer coefficient differ, under the same conditions, between apparatus of the same model. However, following the procedures described in this work, the adjustment of these thermal effects can be easily performed.

One of the most important features of the implementation of this simulator is the flexibility from the physico-chemical and thermokinetics viewpoints. The user according to the data available and his understanding of the process, may define the data complexity, that can vary

from very simple, e.g. constant values, to more complex, e.g. temperature and concentration dependencies.

The results of the simulator of the RC1 are, in general, in excellent agreement with the experimental values. The main observed differences are attributable to the lack of appropriate data that frequently are only valid within a short range of process variables. Undoutely, the thermo-kinetic data are the most sensitive; for instance, even for a simple reaction such as a neutralisation between sodium hydroxide and hydrogen chloride the heat of solution is still not well known. Another problem concerns the definition of the mixture properties that usually, in absence from experimental data, are treated as ideal systems.

NOTATION

A	Frequency factor, depends on kinetics
A_L	Set of chemical species
AQ	Flow actuator
AT	Temperature actuator
B	Control signal for reactant feeds, dimensionless
C	Molar concentration, kmol/m^3
Cp	Specific heat capacity, $J \cdot Kg^{-1} \cdot K^{-1}$
Cp_L	Molar heat capacity of a chemical species, $J \cdot mol^{-1} \cdot K^{-1}$
D	Diameter, m
E_a	Activation energy, J/mol
e	thickness, m
F	Molar flow, mol/s
h	partial heat transfer coefficient, $W \cdot m^{-2} \cdot K^{-1}$
H	height, m
H_R	Acidity function
K	Coefficient of heat losses, W/K
k	Reaction velocity constant, depends on kinetics
L	Relative apparent molar enthalpy, J/mol
n_a	Stirrer speed, s^{-1}
N_E	Number of reactant feed streams
N_L	Number of liquid species
N_R	Number of independant reactions
n	Molar Hold-up, mol
Q	Volumetric flow, m^3/s
QC	Flow controller
q	Thermal flow, W
r	Rate of reaction, $mol \cdot l^{-1} \cdot s^{-1}$
R	Rate of chemical production or consumption, $mol \cdot l^{-1} \cdot s^{-1}$
R	Radius, m
S	Surface, m^2
T	Temperature, K
TC	Temperature controller
TM	Temperature measurement
U	Overall heat transfer coefficient, $W \cdot m^{-2} \cdot K^{-1}$
US	Effective heat transfer coefficient, W/K
v	Molar volume, m^3/kmol

V Volume, m^3
WM Weight measurement
x Molar fraction or fraction of wetted heat exchange surface

Greek symbols

Γ Thermal capacity, J/K
ΔH Enthalpy of reaction, J/mol
θ Parameter of a heat transfer correlation
λ Thermal conductivity, $W \cdot m^{-1} \cdot K^{-1}$
μ Dynamic viscosity, $kg \cdot m^{-1} \cdot s^{-1}$
ν Stoichiometric coefficient, reactant(-), product(+)
partial order of reaction
ρ Density, kg/m^3
τ Time constant, s
ϕ Constant in stirrer power correlation, eqs. (54-55)
ψ Correction factor for the heat exchange model

Subscripts

0 reactor, internal side
1 reactor, external side
A Propionic Anhydride
a Stirrer or ambient
B bottom
A Propionic Anhydride
b inserts
C Propionic Acid
c Heat transfer fluid, cooled loop
d Dry part
dil Dilution
E Feed of reactants
E 2-butyl propionate
e Heat transfer fluid, heated loop
h Heating
k Kryostat
L Liquid
l losses
lc losses cooled loop
ln logarithmic average
M Measurement
m Reaction mixture
P container heated loop
p pumps or proportional
R Reactor
r radial
S Sulphuric Acid
s Set-point
T Total
t Hydraulic
v Vortex
W water
w Wall or Wetted part
z Axial

Dimensionless groups

Fr	Froude number	$N_a^2 \cdot D_a \cdot g^{-1}$
Nu	Nusselt number	$U \cdot D \cdot \lambda^{-1}$
Pr	Prandtl number	$\mu \cdot Cp \cdot \lambda^{-1}$
Re	Reynolds number	$\rho_m \cdot Q \cdot D \cdot S^{-1} \cdot \mu^{-1}$
	for stirred tank	$\rho_m \cdot N_a \cdot D_a^2 \cdot \mu_m^{-1}$
Po	Power number	$q_a \cdot \rho_m^{-1} \cdot N_a^{-3} \cdot D_a^{-5}$
S_k	Shape factors	D_a / D_k (internal geometry)
Vi	Viscosity ratio	$\mu_{bulk} / \mu_{at\ wall}$

REFERENCES

Bird, R.B., Stewart, N.E. and Lighfoot, E.N., 1960, *Transport Phenomena*, John Wiley, New York.

Bondy F. and Lippa S., 1983, Heat transfer in agitated vessels, *Chem. Eng.* **4**, 62-66.

Bourne J.R., Buerli M. and Regenass W., 1981, Heat transfer and power measurements in stirred tanks using heat flow caloirimetry, *Chem. Eng. Sci.* **36**, 347.

Cawthon, G. D. and Knaebel, K.S., 1989, Optimization of semibatch polymerization reactions. *Computer Chem. Engng.* **13**, 63-72.

Chenneaux, F., Ohlmer, E., Schultze, W. and Van Gerwen, I., 1990, Flow Characterisation of the Mettler Calorimeter RC1. *Technical Note n° I.90.46*, Joint Research Center of C.E.C., Ispra (Italy).

de Vallière, P. and Bonvin, D., 1986, On the dynamics of a bench-scale calorimeter. *IFAC Control of Distillation Columns and Chemical Reactors*, 301-310.

Deno, N.C., and M.S. Newman ,1951, The Racemization of alkyl hydrogen sulpates in sulfuric acid, *J.A.C.S.* **73**, 1920-1923.

Dhanuka, V.R., V.C. Malshe and S.B. Chandalia, 1977, Kinetics of the Liquid Phase Esterification of Carboxylic Acids with Alcohols in the presence of Acid Catalysts: Re-interpretation of Published Data, *Chem. Eng. Sci.* **32**, 551-556.

Glasstone S. , 1947, *Thermodynamics for Chemist*, Van Nostrand Inc., New York.

Gordon, M.H., O'Brien, G.J., Hensler C.J. and Marcali, K., 1982, Mathematical modelling in thermal Hazards Evaluation. *Plant/Operation Progress* **1**, 27-32.

Haldar R. and D. P. Rao, 1992a, Experimental studies on parametric sensitivity of a batch reactor. *Chem. Eng. Technol.* **15**, 34-38.

Haldar, R., and D. P. Rao, 1992b, Experimental studies on semibatch reactor parametric sensitivity. *Chem. Eng. Technol.* **15**, 39-43.

Holland F.A., 1973, *Fluid flow for Chemical Engineers*, Edward Arnold, London.

Hougen O.A., Watson K.M. and Ragatz R.A., 1954, *Chemical Process Principles*, Part I, John Wiley, New York.

March, J., 1992, *Advanced Organic Chemistry: Reactions, Mechanisms, and Structure*, 4th Edition, Wiley & Sons, New York.

McAdams W.H., 1954, *Heat Transmission*, 3rd ed., Mc Graw-Hill, New York.

Press W.H., Flannery, B.P., Teukolsky, S.A., and Vetterling, W.T., 1986, *Numertical Recipies*, Cambridge University Press, New York.

RC1 Operating Instructions, 1989, Mettler AG, Switzerland.

Regenass W. et al., 1984, United States patent 4, 456,386; Jun.26.

Reisen, R. and B. Grob, 1985, Reaction calorimetry in chemical process development, *Swiss Chem.* **7**, 39-43.

Rochester C. H., 1970, *Acidity Functions*, Academic Press, London.

Singh, J.(1989). PHI-TEC: Enhanced Vent Sizing Calorimeter, in *International Symposium on Runaway Reactions,* AIChE, 313-330.

Snee T.J., C. Barcons, H. Hernández, and J.M. Zaldívar, 1992, Characterisation of an exothermic reaction using adiabatic and isothermal calorimetry, *Journal of Thermal Analysis* **38**, 2729-2747.

Snee T. J. and J. A. Hare, 1992, Development and application of a pilot scale facility for studying runaway exothermic reactions. *J. Loss Prev. Process Ind.* **5**, 46-54.

Sreeramulu,,V., and P.B. Rao (1973). Kinetics of esterification of isobutyl alcohol with palmitic acid using sulfuric acid catalyst. *Ind. Eng. Chem. Process Des. Develop.* **12**, 483-485.

Tavlarides, L. L. and Stamatoudis, M., 1981, The Analysis of Interphase Reactions and Mass Transfer in Liquid-Liquid Dispersions, in *Advances in Chemical Engineering*, vol 11, Eds. T.B. Drew, G. R. Cokelet, J. W. Hoopes Jr. and T. Vermeulen, Academic Press, New York.

Troupe,,R.A., and K. Kobe (1950). Kinetics of methanol-lactic acid reaction. *Ind. Eng. Chem.* **42**, 801-810.

Uhl V.W. and Gray J.B. (eds), 1966, *Mixing: Theory and Practice*, vol. 1 and 2, Academic Press, New York.

Yvernault, T. (1955). Acid catalysis of the hydrolysis of acetic anhydride in acetic acid.*Compt. rend.* **241**, 485-487.

Zaldívar, J.M., Hernández , H., and Barcons, C., 1990, Development of a mathematical model and numerical simulator for a reaction calorimeter. FISIM, RC1 version. *Technical Note N° I.90.109*, Commission of The European Communities, Joint Reasearch Centre, Ispra (Italy).

Zaldívar, J.M., Hernández, H., Barcons, C., and Nomen, R., 1992, Heat effects due to dilution during aromatic nitrations by mixed acid in batch conditions. *J. of Thermal Analysis* **38**, 2575-2582.

Zaldívar J.M., Hernández H., Molga E., Galvan I.M. and Panetsos F., 1993, The use of neural networks for the identification of kinetic functions of complex reactions. *Proc. of the 3rd European Symposium on Computer Aided Process Engineering*, Graz, Austria.

Appendix 1: The METTLER RC1 reaction calorimeter

- Reaction Calorimetry: Reaction Calorimetry has proved to be an important technique in chemical process optimisation from safety and performance viewpoints. The method provides information measured under conditions very similar to industrial situations which permits the gaining of knowledge about the process and the influence of the operating conditions on its behavoiur, see Reisen and Grob (1985).

The principle of such as calorimeter is based on the measurement of a time-dependent temperature difference. Normally, three methods are implemented: adiabatic, isoperibolic and heat flow calorimetry. These methods can be defined using the following simplified energy balance for a calorimeter, see fig. A1:

a/ Heat flow calorimetry ($q_{acc} \approx 0$, hence $q_{rxn} \approx q_{ex}$)

In an ideal heat flow calorimeter, exchange of the heat produced by reaction, q_{rxn}, with the surroundings is infinitely fast, hence there is no accumulation in the reaction medium. This methods allows to work in isothermic or temperature programmed modes.

b/ Adiabatic calorimetry ($q_{ex} \approx 0$, hence $q_{rxn} \approx q_{acc}$)

In an ideal case, the total amount of heat produced by reaction, q_{rxn}, is accumulated in the reactor, which means that no heat exchange occurs between reaction mass and surroundings. Normally, this is implemented by controlling the temperature of the surroundings.

c/ Isoperibolic calorimetry ($q_{acc} \neq 0$ and $q_{ex} \neq 0$)

The term isoperibolic means uniform surroundings, that implies constant temperature. Hence, the heat exchange depends only on the reaction mixture and the interface resistance.

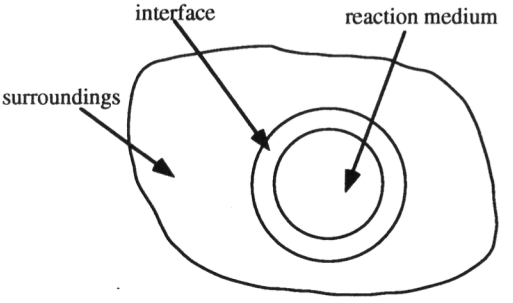

Figure A1. Schematic representation of a calorimeter

- The METTLER RC1 Reaction Calorimeter: The RC1 is a computer-controlled batch reactor, see fig. A2, able to carry out isothermal, adiabatic, isoperibolic, and temperature programmed experiments, see RC1 user's manual.

The stirred galss reactor is surrounded by a jacket in which heat transfer fluid circulates at very high rate. In typical operating conditions, a controller adjust the temperature of the heat transfer fluid to follow the required temperature programme.

The calorimetric principle implemented in the RC1 is based on the continuous measurement of the temperature difference between the reaction medium and the heat transfer fluid.

The use of a powerful thermostat allows rapid adjustment of the jacket temperature, which is essential to deal with fast transients into the reaction mass.

The main characteristicas are:

- Glass reactor of similar geometry to industrial vessels (effective volume 0.5-2 l).
- RD10 dosing controller with two independent control loops for automatic weight and additional inputs and outputs for other measurements (pH, pressure, etc.)
- Stirrer motor with adjustable speed control.
- Temperature working range from -20 to 200 °C.

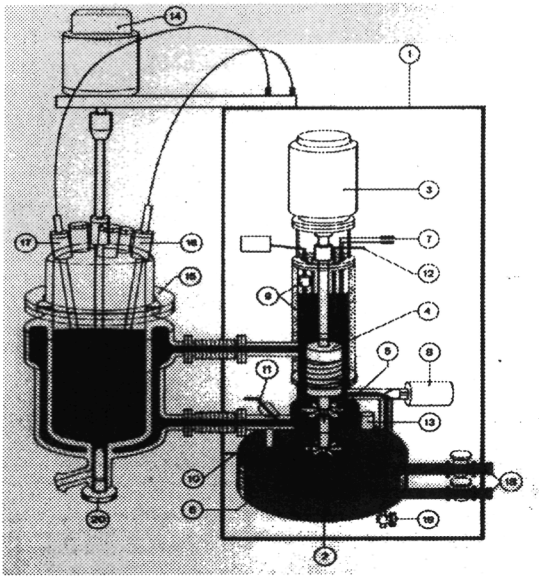

1. Housing
2. Cooling oil container
3. Pump motor
4. Displacement body
5. Pump impellers of the heated circulation
6. Pump impellers in cooling oil container
7. Connection for electrical heating
8. Stepper motor regulated control valve
9. Float switches for detection of the oil level
10. Tc sensor
11. T_e sensor
12. T_{es} sensor
13. Safety valve
14. Stirrer motor
15. Reactor
16. T_m/T_{ms} sensors
17. Calibration heater
18. External coolant connection
19. Oil drain cock
20. Bottom valve of the glass reactor vessel

Figure A2. Schematic illustration of the RC1 Calorimeter system (from the RC1 users manual)

The complete operatiopn of the RC1 is menu-supported and experiments can be run either under direct control or -if preprogrammed- in fully automatic mode, following a recipe introduced beforehand by the operator. During the experiment the values of selected variables can be displayed on the screen and/or plotted, and/or recorded on a diskette. The information stored allows subsequent evaluation of parameters such as heat of reaction, heat transfer coefficient, heat capacity of reaction mass, etc.

- Reactor Characteristics: The main dimensions of the reactor are described in fig. A3. D_0, D_i, D_a, and D_t are the external, internal, stirrer and hydraulic diameters respectively; and e_w is the wall thickness.

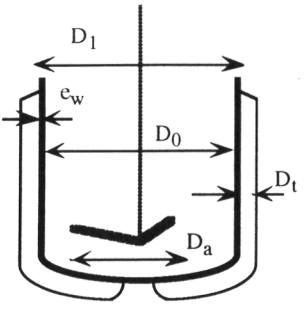

$D_0 = 0.125$ m
$D_1 = 0.115$ m
$D_a = 0.105$ m (anchor)
0.059 m (turbine)
$e_w = 0.005$ m
$D_t = 0.007$ m

Figure A3. Dimensions of the standard glass reactor

The total heat transfer surface, S_T, is equal to $7.47 \cdot 10^{-2}$ m^2, whereas the term $[S_B - 2 \cdot V_B/R_0]$ (eq. 28 in Chapter 1) is equal to $6.545 \cdot 10^{-3}$ m^2. The height of the reactor (eq. 37 in Chapter 1) , H_T, is equal to 0.193 m, and the total volume (eq. 60 in Chapter 1), V_T, is 2 l.

The thermal conductivity (λ_w) and specific heat capacity (Cp_w) of the wall can be correlated using the following expressions:

$$\lambda_w = 0.827 + 5.0 \cdot 10^{-4}(T_m + T_e) \quad \text{(A1)}$$

$$Cp_w = 354.9 + 1.41 \cdot T_w \quad \text{(A2)}$$

and the density is $\rho_w = 2600$ Kg/m^3. The total mass of the glass is 1.11 kg.

- Heat Transfer Fluid Properties: The heat transfer fluid is a silicon oil, Rhodorsil 47V20. The variation of its properties as a function of temperature can be correlated by means of the following expressions:

$$\ln \mu_e = 1.5692 \cdot 10^3 \left(\frac{1}{T_e} - \frac{1}{7.052 \cdot 10^2} \right) \quad \text{(A3)}$$

$$\rho_e = 1.758 \cdot 10^3 - 4.96 \cdot T_e + 9.8 \cdot 10^{-3} \cdot T_e^2 - 7.34 \cdot 10^{-6} \cdot T_e^3 \quad \text{(A4)}$$

$$Cp_e = 9.614 \cdot 10^2 + 1.8 \cdot T_e \quad \text{(A5)}$$

$$\lambda_e = 2.205 \cdot 10^{-1} - 2.33 \cdot 10^{-4} \cdot T_e \quad \text{(A6)}$$

CHAPTER 3

AROMATIC NITRATIONS BY MIXED ACID: HEAT EFFECTS

ABSTRACT

Although the heat produced by aromatic nitration is relatively large in comparison to the heat produced by dilution, knowledge of the rate of heat generation due to dilution of the mixed acid is important for predicting the dynamic behaviour of discontinuous nitration processes. In this paper a mathematical model, its implementation and experimental validation of the heat effects due to dilution are described and discussed.

Furthermore, adiabatic experiments were carried out to study the stability of the reacting mixtures, with accumulations up to 25% equimolar nitric acid. No secondary or decomposition reaction was detected in such experiments.

Keywords

heat of dilution, adiabatic nitrations

1. INTRODUCTION

In the nitration of an aromatic compound by means of a mixture of concentrated nitric and sulphuric acids (mixed acid), the total heat liberated is equal to the heat of nitration plus the heat of dilution due to change in composition of the mixed acid. Although the heat produced by aromatic nitration is relatively large in comparison to the heat produced by dilution, the knowledge of the rate of heat generation due to dilution is important in discontinuous nitration processes to calculate accurately the rate of heat generation due to reaction. In addition, calculation of heat of dilution is complicated since the mixed acid composition varies as the reaction goes on, generating water and consuming nitric acid, also fresh mixed acid is introduced in semibatch conditions.

The objectives of this preparatory experimental programme were to separate the heat of nitration from the heat of dilution, and to develop a model to calculate the rate of heat generation due to dilution during discontinuous nitrations with different mixed acid composition. Furthermore, a study, using adiabatic calorimetry, to check the heat of nitration and the possible secondary or decomposition reactions in case of accumulation of unreacted nitric acid was performed.

2. RATE OF HEAT GENERATION DUE TO DILUTION

2.1. Mathematical modelling of rate of heat generation due to dilution

The enthalpy change that accompanies the mixing or dilution of two or more substances is called the heat of dilution, and it may be calculated in the integral form as the change between the final and the initial state (before and after mixing) of the sum of the relative partial molar enthalpies times the number of mole of each component, see Glasstone (1947). Thus,

$$\Delta H_d = \sum_{k=1}^{n} \Delta(n_k \cdot L_k) \qquad (1)$$

where n_k and L_k refer to the number of moles and the relative partial molar enthalpy of the kth component (pure compounds are used as standard states of reference), respectively.

In order to obtain the rate of heat generation due to dilution, it is necessary to consider a differential change with respect to time of the heat of dilution, hence,

$$q_d = \frac{dH_d}{dt} = \sum_{k=1}^{n} \left(n_k \frac{dL_k}{dt} + L_k \frac{dn_k}{dt} \right) \qquad (2)$$

In the particular case of a discontinuous nitration process there are two possible contributions: the addition of a constant composition of mixed acid to the reacting mass and the dilution by water which is produced as nitric acid is consumed by the chemical reaction, see fig. 1.

Introducing these terms into eq. (2), it is possible to obtain

$$q_d = \sum_{k=1}^{3} \left[n_k \frac{dL_k}{dt} + L_k \left(\frac{dn_k^{(a)}}{dt} + \frac{dn_k^{(r)}}{dt} \right) - L_k^{(a)} \frac{dn_k^{(a)}}{dt} \right] \qquad (3)$$

where $dn^{(a)}/dt$ refers to the mole change due to the addition of mixed acid whereas $dn^{(r)}/dt$ stands for the production or consumption by chemical reaction.

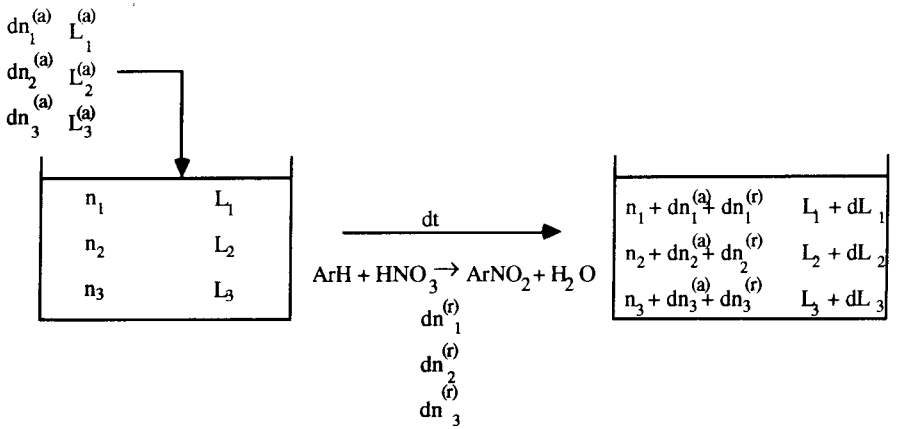

Figure 1. Differential energy balance. The subscripts' 1,2 and 3 refer to water, nitric and sulphuric acids respectively, whereas the superscripts (a) and (r) refer to addition and reaction.

Using experimental data from different authors, i.e. McKinley and Brown (1942), Giauque *et al.* (1950) and Perry and Chilton (1973), the values of L_k's were correlated as a function of molar percentages using a polynomial equation of type,

$$L_k = \prod_{i=1}^{3}\left(\sum_{j=1}^{3} a_{k_{ij}} \cdot x_i^{j-1}\right) \qquad (4)$$

where the x_i's are the molar percentages of the three components: water, nitric and sulphuric acids. The a_{kij} parameters, see Tables 1-3, were estimated by conjugate gradient methods, see Press *et al.* (1986) minimising the objective function:

$$\text{Error} = \sum_{l=1}^{m}\left(H_{d_l}^{exp.} - H_{d_l}^{calc.}\right)^2 \qquad (5)$$

where m is the total number of experimental points, m=311.

A comparison between the experimental data from McKinley and Brown (1942) and the enthalpy-concentration diagram that was calculated using eq. (4) and the estimated parameters is given in fig. 2. In general, a good agreement is obtained over the whole range of concentrations.

Table 1. a_{kij} parameters in the polynomial expression of the L_k for the water.

i \ j	1	2	3
1	-23.646	$3.861 \cdot 10^{-1}$	$-1.491 \cdot 10^{-3}$
2	430.578	-13.675	$1.396 \cdot 10^{-1}$
3	$1.360 \cdot 10^{-3}$	$9.780 \cdot 10^{-5}$	$-9.678 \cdot 10^{-7}$

Table 2. $a_{k_{ij}}$ parameters in the polynomial expression of the L_k for the nitric acid.

i \ j	1	2	3
1	-26.721	$-2.666 \cdot 10^{-1}$	$-1.951 \cdot 10^{-2}$
2	-214.103	-3.163	$4.922 \cdot 10^{-2}$
3	$-5.500 \cdot 10^{-4}$	$-8.859 \cdot 10^{-6}$	$-9.495 \cdot 10^{-8}$

Table 3. $a_{k_{ij}}$ parameters in the polynomial expression of the L_k for the sulphuric acid.

i \ j	1	2	3
1	-24.125	$-5.786 \cdot 10^{-1}$	$-1.530 \cdot 10^{-2}$
2	-284.162	3.189	$-1.921 \cdot 10^{-2}$
3	$-1.110 \cdot 10^{-3}$	$1.155 \cdot 10^{-5}$	$-7.325 \cdot 10^{-9}$

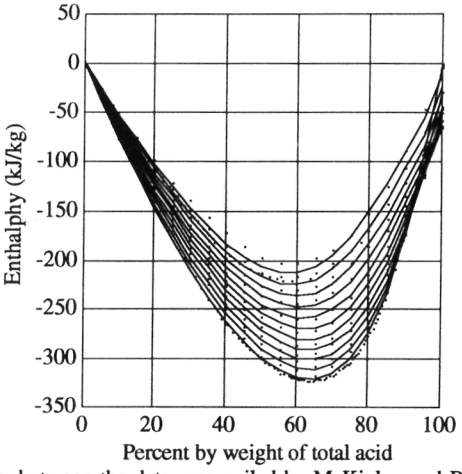

Figure 2. Comparison between the data recompiled by McKinley and Brown (1942) and the values calculated using the correlation's for L_k. In this enthalpy-concentration diagram the enthalpy in kJ/kg for a specific composition of solution is obtained by interpolation between the lines of indicated nitric acid composition (starting from the top that refers to pure HNO_3 and decreasing at 10% intervals up to pure H_2SO_4), based on anhydrous acid (HNO_3+H_2SO_4).

Equation (4) can be differentiated to be used in the calculation of eq. (3) applying the chain rule:

$$\frac{dL_k}{dt} = \left(\frac{\partial L_k}{\partial x_1}\right)_{x_2,\, x_3} \frac{dx_1}{dt} + \left(\frac{\partial L_k}{\partial x_2}\right)_{x_1,\, x_3} \frac{dx_2}{dt} + \left(\frac{\partial L_k}{\partial x_3}\right)_{x_1,\, x_2} \frac{dx_3}{dt} \tag{6}$$

hence,

$$\frac{dL_k}{dt} = \sum_{i=1}^{3} \left\{ \left(a_{k_{i2}} + 2 \cdot a_{k_{i3}} \cdot x_i \right) \prod_{j=1,\, j\neq i}^{3} \left(\sum_{l=1}^{3} a_{k_{il}} \cdot x_j^{l-1} \right) \right\} \frac{dx_i}{dt} \tag{7}$$

and dx_i/dt can be expressed on function of n_i as,

$$\frac{dx_i}{dt} = \frac{100}{n_{Tot.}}\left(\frac{dn_i}{dt} - \frac{n_i}{n_{Tot.}}\frac{dn_{Tot.}}{dt}\right) \qquad (8)$$

2.2. Experimental model validation

In order to check the validity of the dynamic model to predict the heat evolution due to dilution during an aromatic nitration, different experiments were carried out in a reaction calorimeter, see Reisen and Grob (1985). Unfortunately during nitration it is not possible to separate both heat effects, therefore the preparation of different mixed acids in the reaction calorimeter was used to validate experimentally the model developed. Figure 3 show the comparison between experimental and simulated rate of heat generation for two experiments in which mixed acid of different compositions were prepared. In the first experiment 1592 g of sulfuric acid 96 wt. % were added in two hours to 1200 g of nitric acid 70 wt. %; whereas in the second experiment 1754 g of sulfuric acid 96 % wt were added in two hours to 740 g of nitric acid 43.5 wt %.

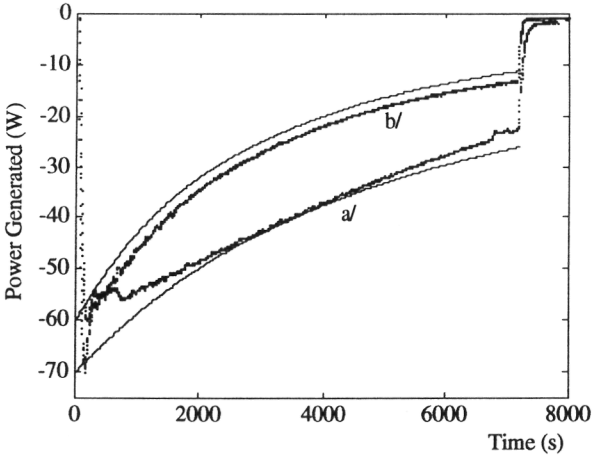

Figure 3. Experimental (dotted lines) and simulated (continuous lines) rates of heat generation during the preparation of mixed acid in the RC1.

3. HEAT OF NITRATION: ADIABATIC EXPERIMENTS

PHI-TEC is a computer controlled adiabatic calorimeter shown schematically in fig. 4, see Singh (1989). The operation of this device is similar to the accelerating rate calorimeter, ARC, see Townsend and Tou (1980) and the vent sizing package, VSP, see Fauske and Leung (1985).

The sample is held in a stainless steel container provided with a magnetic stirrer and with thin walls in order that the experimental results are not strongly influenced by the heat capacity of the container. Adiabatic conditions are maintained by using electrical heaters to match the temperature of the surroundings to that of the sample. A separate heater is used to raise the

temperature of the sample to the selected initial temperature and then adiabatic conditions are maintained as the temperature and pressure increases due to exothermic reaction of the sample. If there is no increase temperature due to exothermic reaction, the instrument can operate in 'heat-wait-search' mode by using the sample heater to produce a series of temperature steps until exothermic reaction is detected. Rupture of the thin-walled sample container is prevented by automatically applying nitrogen pressure to the outside of the container to compensate for internal pressure generated due to exothermic reaction.

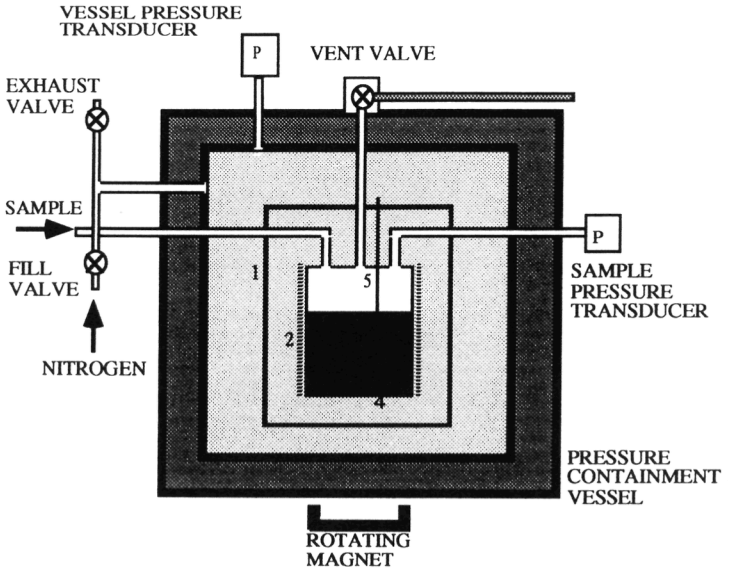

1 RADIANT HEATERS
2 SAMPLE HEATER
3 MAGNETIC STIRRER
4 SAMPLE CONTAINER
5 SAMPLE THERMOCOUPLE

Figure 4. Schematic diagram of PHI-TEC adiabatic calorimeter.

The nitration experiments were carried out by injecting mixed acid to the organic compound and starting the mixing. The resulting reactions were allowed to go to completion. Figures 5-7 show the temperature-time data for the nitration of benzene, toluene and chlorobenzene. The shape of these curves is totally different to homogeneous reactions where the initial rate is slow and then builds up with temperature, i.e. typical exponential behaviour. The difference is due to the fact that the nitration conversion rate, at the above mentioned experimental conditions, is mass transfer controlled.

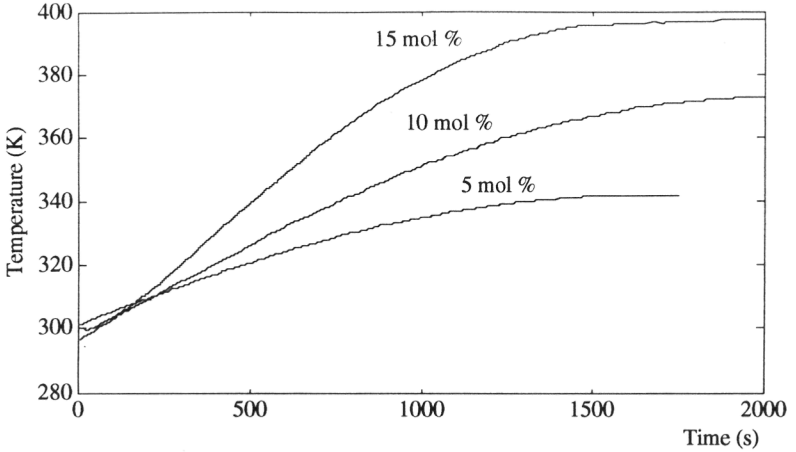

Figure 5. Benzene. Adiabatic temperature rise PHI-TEC experiments. 5, 10, and 15 mol % nitric acid related to the equimolar quantity were added to 50 g. of benzene. Mixed acid wt %: 61.2 H_2SO_4 and 22.1 HNO_3.

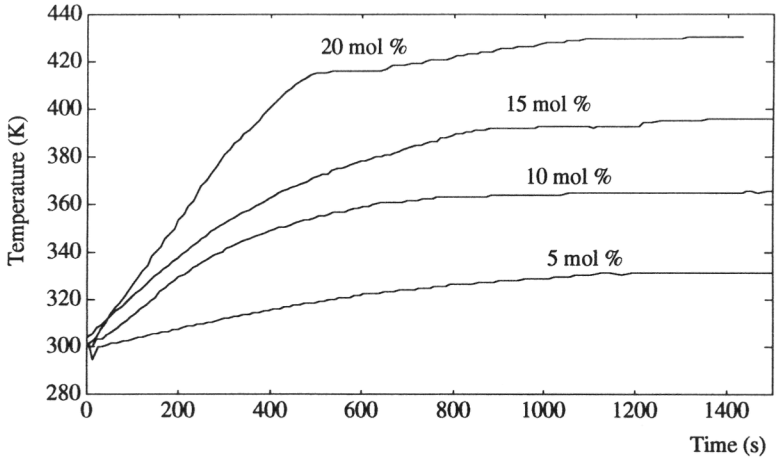

Figure 6. Toluene. Adiabatic temperature rise PHI-TEC experiments. 5, 10, 15 and 20 mol % nitric acid related to the equimolar quantity were added to 50 g. of toluene. Mixed acid wt %: 56.2 H_2SO_4 and 28.8 HNO_3.

The heat of reaction was calculated assuming constant Cp from the adiabatic temperature rise, see Snee *et al.* (1992). The calculated heats of reaction, see Table 4, are in agreement with literature data, see Groggins, (1958) : 113 kJ/mol for benzene; 106, 123 and 141 kJ/mol for nitration of toluene in ortho, meta and para position respectively.

Table 4. Calculated heats of reaction from adiabatic experiments

Compound	$\Delta H_{PHI-TEC}$ (kJ/mol)
Benzene	128
Toluene	148
Chlorobenzene	124

Adiabatic experiments can simulate the cooling failure scenario while accumulation of unreacted mixed acid. From the temperature and pressure profiles, and GC analysis of final products it was found that no secondary reaction was triggered off and therefore the RC1 calorimeter experiments could be carried out allowing certain accumulation of unreacted nitric acid to study the dynamic behaviour in conditions with low sulphuric acid strength, i.e. low reaction rate.

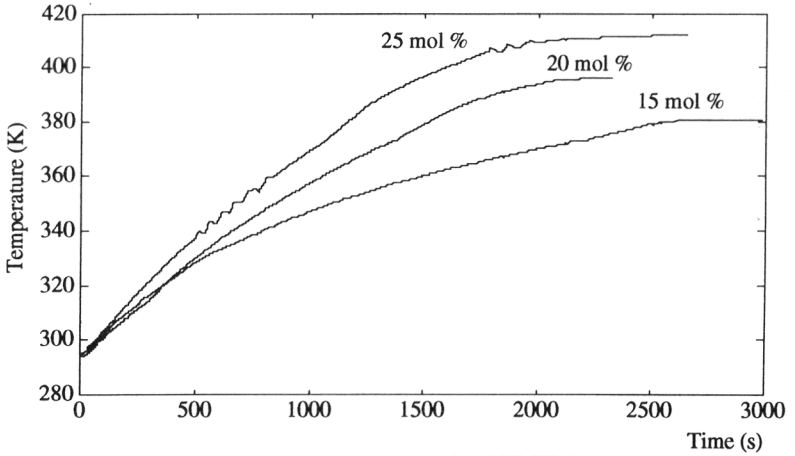

Figure 7. Chlorobenzene. Adiabatic temperature rise PHI-TEC experiments. 15, 20, and 25 mol % nitric acid related to the equimolar quantity were added to 50 g. of chlorobenzene. Mixed acid wt %: 61.2 H_2SO_4 and 22.1 HNO_3.

4. CONCLUSIONS

Although the heat of dilution is approximately 7% of the heat of nitration, its evolution is important when simulating the dynamic behaviour of a discontinuous nitration process because it changes over time and is related to the rate of reaction and concentration of the mixed acid. From the comparison between experimental and model predicted results it has been demonstrated that the general approach to the mathematical modelling of the rate of heat generation due to dilution, leads to a satisfactory agreement when preparing different mixed acids within the range of experimental conditions studied. Thus, the presented model can be introduced into the general modelling for the simulation of aromatic nitration reactions.

Furthermore, adiabatic experiments were carried out to study the stability of the reacting mixtures, with accumulations up to 25% equimolar nitric acid. No secondary or decomposition reaction was detected in such experiments.

REFERENCES

Fauske, H.K. and Leung, J.C., 1985, New experimental technique for characterizing runaway chemical reactions. *Chemical Engng. Progress* **81**, 39-46.

Giauque, W.F., Horning, E.W., Kunzler, J.E. and Rubin, T.R., 1950, The thermodynamic properties of aqueous sulphuric acid solutions and hydrates for 15 to 300 K. *J. Amer. Chem. Soc.* **82**, 62-70.

Glasstone S., 1947, *Thermodynamics for chemists*, Van Nostrand Inc., New York.

Groggins, P.H., 1958, *Unit processes in organic synthesis*, McGraw-Hill, New York.

McKinley, C. and Brown, G.G., 1942, Thermal properties of mixed acids, *Chem. & Met. Eng.* **5**, 142-.

Perry, R.H. and Chilton, C.H.(eds), 1973, *Chemical Engineers' Handbook*, 5th Ed., MacGraw-Hill, New York.

Press W.H., Flannery, B.P., Teukolsky, S.A., and Vetterling, W.T., 1986, *Numerical recipies*, Cambridge University Press, New York.

Reisen, R. and B. Grob, 1985, Reaction calorimetry in chemical process development, *Swiss Chem.* **7**, 39-43.

Singh, J., 1985, PHI-TEC: Enhanced vent sizing calorimeter application and comparison with existing devices. International Symposium on Runaway Reactions, AIChE, 313-330.

Townsend, D.T. and Tou, J.C. , 1980, Thermal hazard evaluation by an accelerating rate calorimeter. *Thermochim. Acta* **37**, 1-30.

NOTATION

L	Relative apparent molar enthalpy, J/mol
n	Molar Hold-up, mol
q	Thermal flow, W
t	time, s
T	temperature, K
x	molar percentage
ΔH	molar enthalpy, J/mol

Subscripts and superscripts

a	addition
d	Dilution
r	reaction
Tot.	total

CHAPTER 4

AROMATIC NITRATIONS BY MIXED ACID: SLOW LIQUID-LIQUID REACTIONS

ABSTRACT

Aromatic nitrations by mixed acid have been selected as a specific case of a heterogeneous liquid-liquid reaction. An extensive experimental programme has been followed using adiabatic and heat flow calorimetry and pilot reactor experiments, supported by chemical analysis. A series of nitration experiments have been carried out to study the influences of different initial and operating conditions such as temperature, stirring speed, feed rate and sulphuric acid concentration. In parallel a mathematical model to predict the overall conversion rate has been developed. In this paper the mathematical modelling and the implementation and experimental validation for benzene, toluene and chlorobenzene mononitration in the kinetic control regime (slow liquid-liquid reaction) is presented and discussed.

Keywords.
Aromatic nitrations, slow liquid-liquid reactions

1. INTRODUCTION

Many questions remain to be answered for aromatic nitrations in mixed acid, particularly under the conditions employed in industry, and mainly in discontinuous reactors, despite the fact that nitration was one of the earliest unit processes to be operated on a large scale when the heavy organic chemical industry first developed last century. These reactions have played an equally important part in the development of our present understanding of the mechanism of organic reactions, offering a typical example of electrophilic substitution, see the classic investigations of Ingold and co-workers during the 1950's.

The dynamic behaviour of aromatic nitrations by mixed acid in discontinuous reactors involve a considerable number of problems due to the fact that, in these heterogeneous liquid-liquid reactions, chemical reaction and mass transfer phenomena occur simultaneously. The occurrence of these phenomena lead to a complex problem while characterising and scaling-up these processes, due to the interdependence between fluid properties, operating conditions and equipment characteristics. Furthermore, nitrations involve high exothermicity and side reactions, which, in addition to the previously mentioned phenomena, have produced a considerable amount of incidents, see Barton and Nolan (1984). Therefore, a better understanding of this kind of processes is of great importance for the safe and economic design as well as the optimal operation of nitration plants.

The present investigation was undertaken with the main purpose of studying the dynamic reactor behaviour and the influence of the different initial and operating conditions in discontinuous nitration processes. To achieve this, an extensive experimental programme has been carried out using adiabatic and heat flow calorimetry and pilot plant experiments, supported by chemical analysis. The adiabatic experiments were performed using a PHI-TEC calorimeter, see Singh (1989), and the isothermal and isoperibolic experiments using a RC1 reaction calorimeter, see Reisen and Grob (1985), while the pilot plant experiments were carried out in the FIRES facility, see Hernández and Zaldívar (1990). Chemical analysis was done by Gas Chromatography, see Molga *et al.* (1993).

In parallel, a mathematical model for predicting the overall conversion rate, within the range of experimental conditions studied, has been developed. This model has been introduced into the numerical simulator of the RC1 reaction calorimeter, see Zaldívar *et al.* (1990), in order to compare and validate it with the experimental results. Furthermore, a special version of the simulator is applied on-line to estimate the reaction rate during nitration experiments, see Hernández *et al.* (1993). These data are compared to those from chemical analysis and simulation.

In this paper two kinetic expressions, based on different acidity functions, are described and implemented to interpret literature data from homogeneous nitration experiments with one liquid phase and low nitric acid concentration, C_{HNO_3} of around 10^{-2} M. These kinetic expressions are extended to predict the dynamic behaviour of discontinuous nitrators under industrial conditions with two liquid phases and high nitric acid concentrations C_{HNO_3} of

around 5M. Also they are compared to experimental results from the mononitration of benzene, toluene and chlorobenzene in the kinetic regime of slow liquid-liquid reaction as a first step for the development of an overall conversion rate expression in the mass transfer control region.

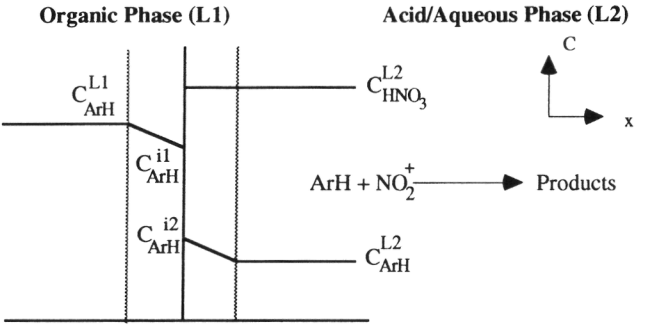

Figure 1. Schematic representation of mass transfer with chemical reaction during the nitration of an aromatic compound, according to the stagnant film theory. Concentration profiles near the liquid-liquid interface for a slow reaction and low solubility.

2. INTERPRETATION OF HOMOGENEOUS KINETIC DATA

As it is well known from literature, a.o. by Schofield (1980) and Olah *et al.* (1989), the nitration of aromatic compounds by a mixture of nitric and sulphuric acids, called "mixed acid", occurs in the aqueous acid phase (L2); and proceeds through the intermediation of the nitronium ion NO_2^+ :

$$NO_2^+ + ArH \rightarrow \text{Products} \qquad (1)$$

Hence, if the interaction of the nitronium ion with the aromatic substrate is the rate-limiting step, see Albright and Hanson (1976), the reaction rate in the acid phase, using a Brønsted-Bjerrum rate law or transition-state theory, can be written as:

$$r = k_2' \cdot C^{L2}_{ArH} \cdot C^{L2}_{NO_2^+} \frac{\gamma_{ArH} \cdot \gamma_{NO_2^+}}{\gamma^{\ddagger}} \qquad (2)$$

Hence, the aromatic compound diffuses through the organic phase to the interface and into the aqueous phase; whilst it is diffusing it reacts in the boundary layer and/or in the bulk of the aqueous phase with the nitronium ion to form the nitrocompounds,see fig 1.

From homogeneous nitration experiments, it has been found, a.o. by Deno and Stein (1956); Coombes et al. (1968), that second-order kinetics hold, and rate coefficients were determined related to stoichiometric concentrations of reagents as:

$$r = k_2 \cdot C^{L2}_{HNO_3} \cdot C^{L2}_{ArH} \qquad (3)$$

Plots of the observed rate constant, k_2, versus sulphuric acid composition, see benzene in fig. 2, show that k_2 is a strong function of the sulphuric acid strength and that the observed second-

order rate of equation 3 changes many orders of magnitude as the weight percentage of sulphuric acid changes, for example k_2 increases typically by a factor of 10^9-10^{12} between 50 and 80 wt. % H_2SO_4. Furthermore, it has long been noted that the rates of nitration of different compounds unexpectedly showed a maximum at approximately 90 wt % H_2SO_4 and then a gentle decrease in the 90-98 wt % H_2SO_4 range, see nitrobenzene in fig. 2.

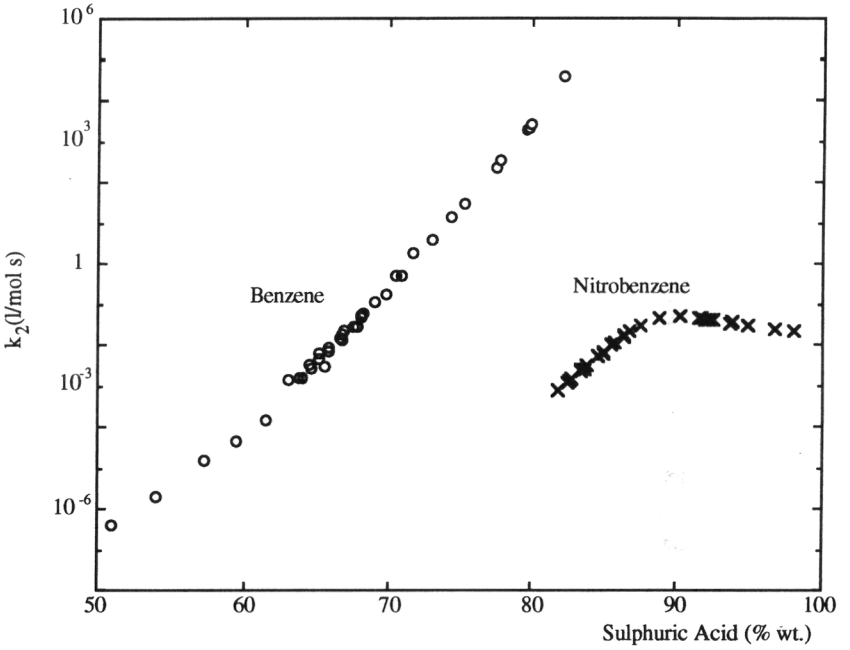

Figure 2. Observed second order rate constants for the nitration of benzene and nitrobenzene in sulphuric acid at 298.2 K. Experimental data from Deno and Stein (1956), Coombes *et al.* (1968), Marziano *et al.* (1977) and Marziano *et al.* (1984).

In order to obtain the reaction rate constant k'_2, by comparing Eqs. (2) and (3), and to explain the dependence of nitration rates on the sulphuric acid concentration, it is necessary to know the mechanism of the formation of NO_2^+. Correlations of nitration rates with different acidity functions H_0, H_R and M_c have been used to get information on the reaction mechanism as well as acidity dependence of reagents, see Schofield (1980) and Marziano *et al.* (1980). In this paper two of these kinetic formulations will be developed from homogeneous nitration data and then used to predict the reaction rate constants under industrial conditions.

2.1. Determination of k'_2 using the H_R acidity function

Field and Strachan (1982) described the formation mechanism of the nitronium ion as:

$$HNO_3 \cdot H_2O + HA \overset{K}{\rightleftarrows} NO_2^+ + 2H_2O + A^- \qquad (4)$$

HA being any strong acid, in this case sulphuric or nitric acid. Equation (4) takes into account the experimental fact that two water molecules are needed to hydrate the nitronium ion, see Moodie *et al.* (1979). The role of the second water molecule in the hydration step is that of a general-base catalyst.

The equilibrium constant K in eq. 4 is expressed as:

$$K = \frac{a_{NO_2^+} \cdot a_{H_2O}^2 \cdot a_{A^-}}{a_{HNO_3 \cdot H_2O} \cdot a_{HA}} \qquad (5)$$

For the acid compositions employed in industrial mononitrations, the concentration of the nitronium ion is so small that the activity of the nitronium ion equals its concentration. Hence:

$$C_{NO_2^+} \cong a_{NO_2^+} = \frac{K \cdot C_{HNO_3 \cdot H_2O}^{L2} \cdot \gamma_{HNO_3 \cdot H_2O} \cdot a_{HA}}{a_{H_2O}^2 \cdot a_{A^-}} \qquad (6)$$

Furthermore, if we assume the concentration of the aromatic species in the acid phase to be small, the activity coefficients are equal to one and it is possible to obtain:

$$k_2 = \frac{r}{C_{HNO_3}^{L2} \cdot C_{ArH}^{L2}} = k_2' \cdot K \cdot \gamma_{HNO_3 \cdot H_2O} \frac{a_{HA}}{a_{H_2O}^2 \cdot a_{A^-}} \qquad (7)$$

by introducing eq. 6 into eq. 2 and comparing this with eq. 3. If we now take logarithms, we will obtain:

$$\log k_2 = \log k'_2 + \log K + \log \gamma_{HNO_3 \cdot H_2O} + \log \frac{a_{HA}}{a_{H_2O}^2 \cdot a_{A^-}} \qquad (8)$$

Further holds:

$$\log \frac{a_{HA}}{a_{H_2O}^2 \cdot a_{A^-}} = -(H_R + \log a_{H_2O}) \qquad (9)$$

where H_R is the acidity function, see Rochester (1970). Hence:

$$\log k_2 = \log k_2' + \log K + \log \gamma_{HNO_3 \cdot H_2O} - (H_R + \log a_{H_2O}) \qquad (10)$$

In the homogeneous nitration experiments - the concentration of nitric acid is low - the activity coefficient can be approximated to be equal to 1; hence the plot of log k_2 versus -(H_R +log a_{H_2O}) should give a straigth line with a slope 1 and intercept log(k'_2·K), see Hoggett *et al.* (1971).

Consequently, to obtain k'_2 from homogeneous nitration rate experiments, it is necessary to calculate:

a/ the Acidity function , H_R: The direct determination of the nitronium ion concentration is not possible for the mixed acid commonly used for mononitrations. To overcome this problem, the similarity of behaviour of triarylcarbinols (ROH) or their derivates in sulphuric acid with that of nitric acid has been extensively used:

$$ROH + HA \rightleftarrows R^+ + H_2O + A^- \qquad (11)$$

$$HNO_3 + HA \rightleftarrows NO_2^+ + H_2O + A^- \qquad (12)$$

The measurement of the ionisation ratios C_{R^+}/C_{ROH} by indicators undergoing ionisation according to eq. (11) has become the basis of an acidity function , see Lowen *et al.* (1950), defined as:

$$H_R = -pK_{ROH} - \log \frac{C_{R^+}}{C_{ROH}} \tag{13}$$

Rearrangement of eq. 13 leads to:

$$H_R = -\log \frac{a_{HA}}{a_{H_2O} \cdot a_{A^-}} \tag{14}$$

It follows that H_R approaches the pH at low ionic strengths and becomes identical at infinite dilution.

Experimental data from Cook *et al.* (1975) showed H_R to be proportional to 1/T whereas Kanhere and Chandalia (1981) correlated H_R to be a linear function of the sulphuric acid and nitric acid concentrations. Following these works the acidity function has been correlated by us as:

$$H_R = -(5.046 \cdot C_{H_2SO_4} + 3.268 \cdot C_{HNO_3}) \cdot \left(-0.214 + \frac{124.65}{T}\right) \tag{15}$$

In Figure 3 the comparison between the experimental and correlated data for different mixed acids compositions is shown, whereas in Fig. 4 the temperature dependence is illustrated.

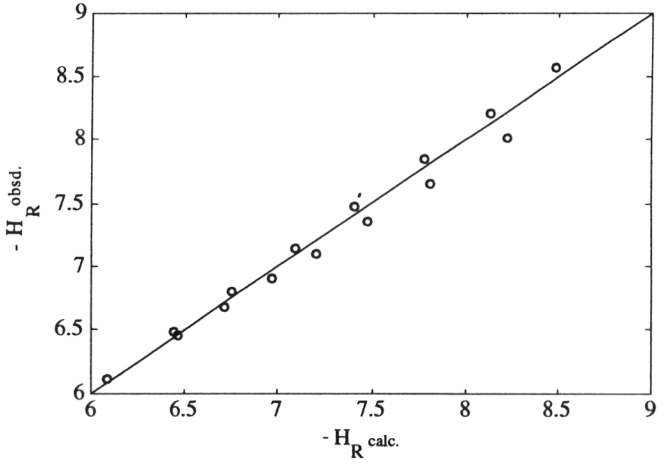

Figure 3. Parity plot of H_R values measured by Kanhere and Chandalia, (1981) and calculated according to Eq. 15, for different mixed acid compositions at 308.2 K.

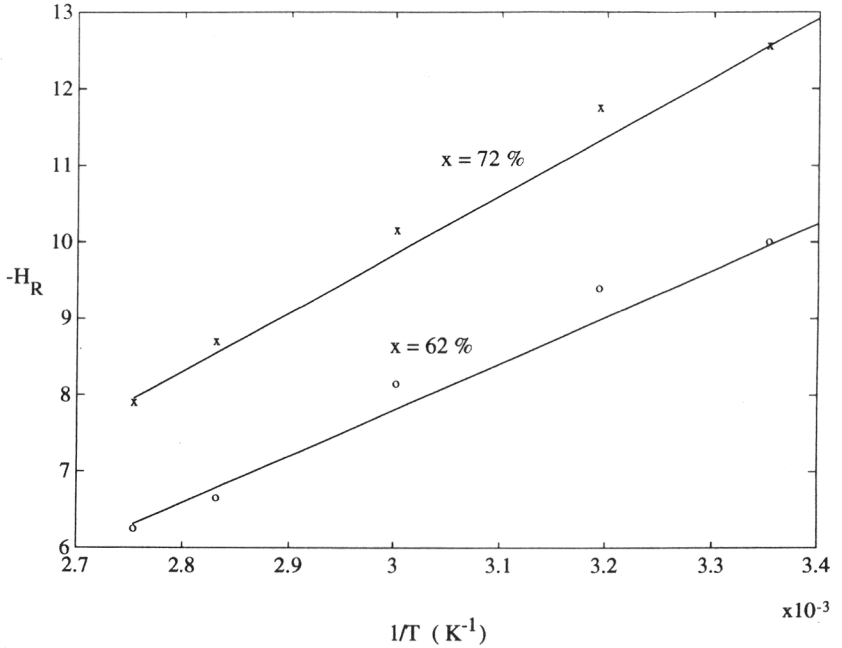

Figure 4. $-H_R$ values measured by Cook *et al.* (1975) and correlation curves according to Eq. 15 for sulphuric acid of 62 (o) and 72 (x) wt. % as a function of the inverse of temperature.

b/ activity coefficients for the mixed acid: The multicomponent Wilson equation, using optimum binary Wilson parameters, was applied to predict the activity coefficients, see Appendix 1

c/ the Equilibrium constant K for the formation of the nitronium ion: In the nitration of 1-3-Bis(trifluoromethyl)benzene, Miller *et al.* (1964) found a certain value for K at 298.2 K. Using this value, the free energy was obtained, being ΔG=45.37 kJ/mol, see Zaldívar *et al.* (1992a). However, it is well-known the linear relationship between log k_2 and (H_R+log a_{H_2O}) fails if wide acidity ranges are examined, for example, for halogenobenzenes when a range of 54-77 % wt. H_2SO_4 is considered, see Marziano *et al.* (1977). To overcome this problem, and as k'_2 should be the true rate constant and not a function of the composition of the medium, ΔG was assumed to be a function of the sulphuric acid strength and independent of the aromatic compound being nitrated. With these assumptions, it was possible to obtain - by a non-linear least squares optimisation of more than 20 different compounds with x= 45-82 % and at different temperatures - the following empirical correlation for the free energy:

$$\Delta G = 1.9188 \cdot 10^4 + 9.85014 \cdot 10^2 \cdot x - 10.5177 \cdot x^2 \qquad (16)$$

where x is the sulphuric acid strength, expressed as weight percentage of sulphuric acid in the total mass of sulphuric acid plus water; x approximately equals the weight percent of sulphuric acid in the case of homogeneous nitration experiments. The starting values for the correlation were the data from Miller *et al.* (1964). In this case, as K is not an experimental value, it is not possible to establish whether the "true" value of K or cK and $c^{-1}k'_2$ have been found, but for the purposes of this work this is not important, since they will be always used as a product in eq. (10).

Figures 5 to 7 show the comparison between experimental and calculated values for k_2 at 298.2 K as a function of the sulphuric acid strength. It can be seen that at low and medium sulphuric acid concentrations up to 85%, eq. (10) produces accurate results. At high sulphuric acid concentrations, see fig. 7, the results are poor. Different explanations have been proposed in literature for this behaviour, see Schofield (1980), amongst them that at these concentrations the activity coefficient of nitronium ion can no more be equated to the concentration, see eq. 6, and that to interpret correctly the experimental results, activity functions instead of concentrations should be introduced in the kinetic formulations.

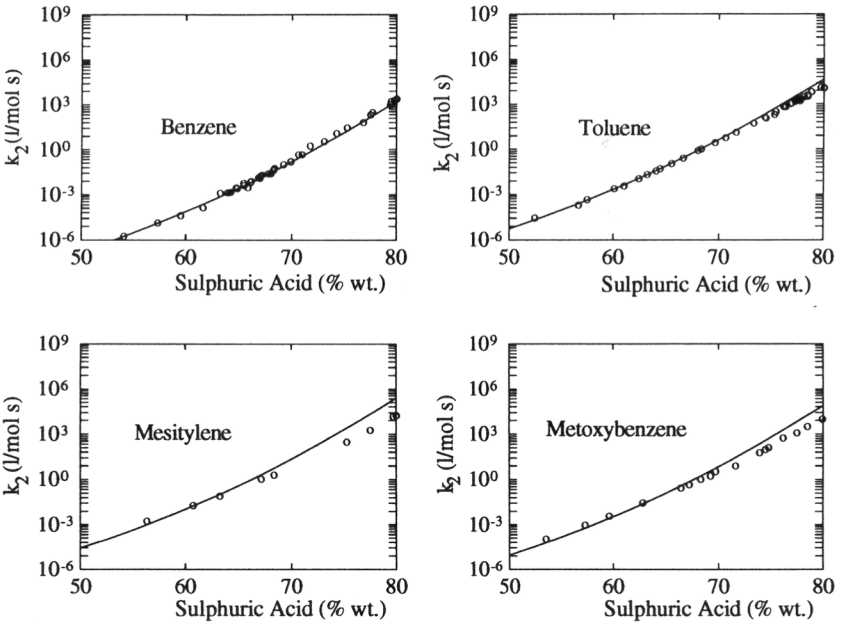

Figure 5. Experimental (o) and calculated (-) second-order nitration rate constants for benzene, toluene, mesitylene and metoxybenzene at 298.2 K. Experimental data from Deno and Stein (1956), Coombes *et al.* (1968), Cox and Strachan (1972a), Barnett *et al.* (1975), Moodie *et al.* (1979), and Marziano *et al.* (1977). Calculation with Eq. 10.

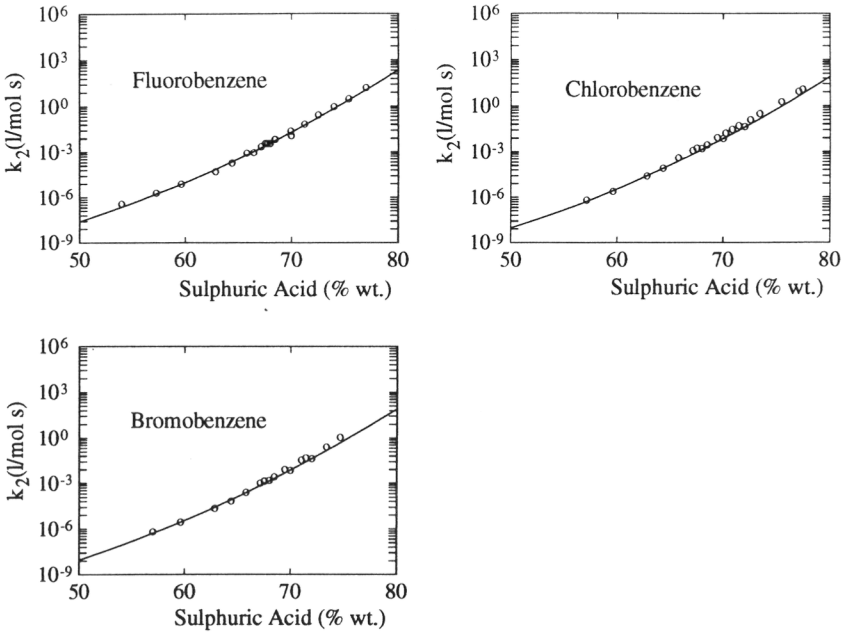

Figure 6. Experimental (o) versus calculated (-) second-order nitration rate constants for halogenobenzenes at 298.2 K. Experimental data from Deno and Stein (1956), Coombes *et al.* (1970), and Marziano *et al.* (1977). Calculation with Eq. 10.

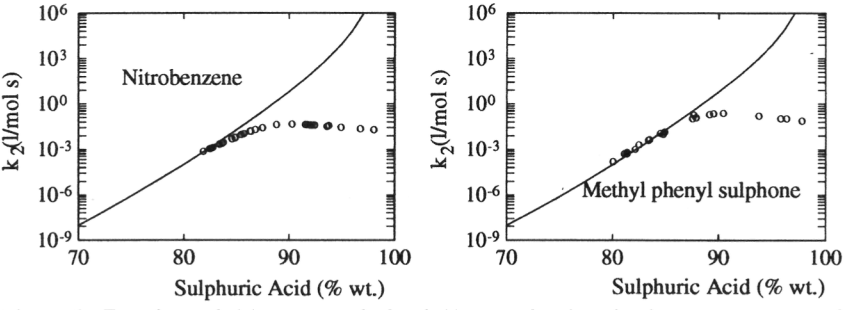

Figure 7. Experimental (o) versus calculated (-) second-order nitration rate constants for nitrobenzene and Methyl phenyl sulphone at 298.2 K. Experimental data from Marziano *et al.* (1984). Calculation with Eq. 10.

Using the previous empirical correlations and experimental data from homogeneous nitration experiments at different temperatures, it is possible to obtain k'_2 for each aromatic compound. The frequency factor and the activation energy are given in Table I for some aromatic compounds, see Appendix 2 for the derivation.

Table I. Frequency factor and activation energy for the reaction rate constant k'_2.

Compound	ln A	$(Ea/R)\cdot10^{-3}$
Benzene	51.456	2.03
Toluene	62.362	22.83
Chlorobenzene	59.451	23.16

2.2. Determination of k'_2 using the M_c Activity Coefficient Function

To solve the problems and shortcomings of the above formulation, Marziano and co-workers (1977, 1980, 1984) developed a new method to describe the second-order nitration rates observed in homogeneous experiments. This method takes into account the effective concentration of solutes and changes in the $\gamma_{ArH}\cdot\gamma_{NO_2^+}/\gamma^{\ddagger}$ ratio with acidity, using the M_c function to be discussed in the following. With this procedure, they were able to obtain a correct description of rate profiles for acid concentrations below and above 90 wt. % of sulphuric acid.

It is well-known that two different equilibria for nitric acid coexist simultaneously in aqueous sulphuric acid, being:

$$HNO_3 \rightleftarrows H^+ + NO_3^- \tag{17}$$

$$HNO_3 + H^+ \leftrightarrows NO_2^+ + H_2O \tag{18}$$

The corresponding equilibrium constants can be written as:

$$K_{HNO_3} = \frac{a_{NO_3^-}\cdot a_{H^+}}{a_{HNO_3}} = \frac{C_{NO_3^-}\cdot C_{H^+}}{C_{HNO_3}}\,\frac{\gamma_{NO_3^-}\cdot\gamma_{H^+}}{\gamma_{HNO_3}} \tag{19}$$

for the nitric acid dissociation and:

$$K_{NO_2^+} = \frac{a_{HNO_3}\cdot a_{H^+}}{a_{NO_2^+}\cdot a_{H_2O}} = \frac{C_{HNO_3}\cdot C_{H^+}}{C_{NO_2^+}\cdot C_{H_2O}}\,\frac{\gamma_{HNO_3}\cdot\gamma_{H^+}}{\gamma_{NO_2^+}\cdot\gamma_{H_2O}} \tag{20}$$

for the formation of the nitronium ion. The equilibria of Eqs. 17 and 18 have been experimentally studied using various spectroscopic techniques, amongst others Raman and UV spectroscopy, see Deno *et al.* (1960), Marziano *et al.* (1978), and Sampoli *et al.* (1985) and ^{14}N NMR, see Ross *et al.* (1983), in a wide acidity range from 1 to 98 wt. % sulphuric acid. From these experiments the evaluated values at 298.2 K were $K_{HNO_3} = 284.75$ and $K_{NO_2^+} = 1.47523\cdot10^{17}$, see Marziano *et al.* (1991).

Figure 8 shows how the equilibria switch from the nitric acid dissociation to the nitronium ion formation as the sulphuric acid wt. % increases. The point of a 50 % formation of nitronium ion at 298.2 K occurs at about 88 % wt. H_2SO_4 and at acidities greater than 93 % wt. H_2SO_4 the nitronium ion is practically the only species.

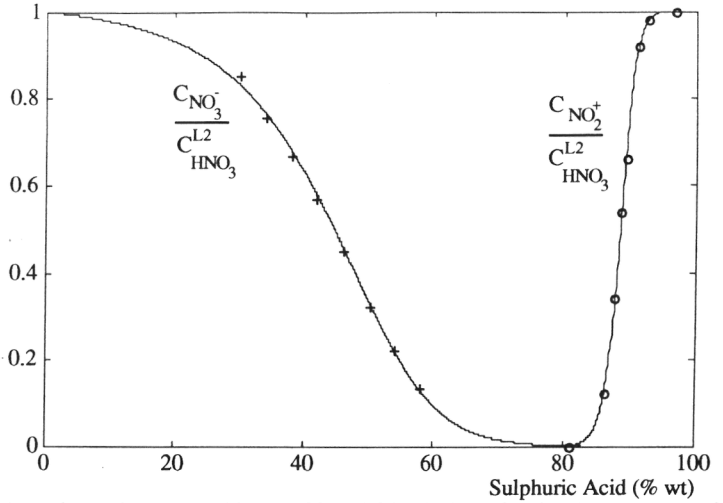

Figure 8. Experimental versus with Eqs. 23 and 24 calculated fractional conversion of nitric acid in sulphuric acid of varying strength at 298.2 K. Experimental data from Deno *et al.* (1961), '+'; and Ross *et al.* (1983), 'o'.

Following the work of Marziano and coworkers, it is possible to use the empirical activity coefficient or M_c function, see Marziano *et al.* (1973, 1981), also called the excess acidity function, defined formally as:

$$M_c = \log \frac{\prod \text{activity coefficients of reactant s}}{\prod \text{activity coefficients of products}} \tag{21}$$

to evaluate Eqs. 19 and 20. The M_c procedure is based on the following empirical linear relationship in concentrated acid solutions for the protonation equilibria of two generic basic indicators, i and j:

$$-\log\left(\frac{\gamma_{B_i}\cdot\gamma_{A_i}}{\gamma_{C_i}}\right) = -n_{ij}\log\left(\frac{\gamma_{B_j}\cdot\gamma_{A_j}}{\gamma_{C_j}}\right) \tag{22}$$

where B is base, A acid, C conjugated acid and n_{ij} a constant dependent on the two indicators. This empirical equation shows that the ratio of activity coeficients of base i are multiples of those of base j. Therefore, substituting eq. 21 into eq. 19 and 20 and using the values obtained by Sampoli *et al.* (1985) for n_{HNO_3} and $n_{NO_2^+}$, the equations read:

$$K_{HNO_3} = \frac{C_{NO_3^-}\cdot C_{H^+}}{C_{HNO_3}}\ 10^{-0.571\cdot M_c} \tag{23}$$

$$K_{NO_2^+} = \frac{C_{HNO_3}\cdot C_{H^+}}{C_{NO_2^+}\cdot C_{H_2O}}\ 10^{-2.542\cdot M_c} \tag{24}$$

Furthermore, combining eq. (2) and eq. (3) yields:

$$k_2' \cdot C_{NO_2^+}^{L2} \frac{\gamma_{ArH} \cdot \gamma_{NO_2^+}}{\gamma^{\ddagger}} = k_2 \cdot C_{HNO_3}^{L2} \qquad (25)$$

and assuming the M_c function is also able to describe the ratio of the activity coefficients of the nitration rate process, see Marziano *et al.* (1984), we obtain:

$$k_2' \cdot C_{NO_2^+}^{L2} \cdot 10^{-n \cdot M_c} = k_2 \cdot C_{HNO_3}^{L2} \qquad (26)$$

As the total concentration of nitric acid $C_{HNO_3}^{L2}$ can be expressed as $C_{HNO_3}^{L2} = C_{NO_3^-} + C_{HNO_3} + C_{NO_2^+}$, eq. 22 leads to:

$$k_2' \cdot 10^{-n \cdot M_c} = k_2 \left(\frac{C_{NO_3^-}}{C_{NO_2^+}} + \frac{C_{HNO_3}}{C_{NO_2^+}} + 1 \right) \qquad (27)$$

Using eq. 24 and eq. 25, it is possible to obtain:

$$k_2' \cdot 10^{-n \cdot M_c} = k_2 \left(\frac{K_{HNO_3}}{C_{H^+} \cdot 10^{-0.571 \cdot M_c}} + 1 + \frac{C_{H^+} \cdot 10^{-2.542 \cdot M_c}}{C_{H_2O} \cdot K_{NO_2^+}} \right) \frac{C_{H_2O} \cdot K_{NO_2^+}}{C_{H^+} \cdot 10^{-2.542 \cdot M_c}} \qquad (28)$$

In consequence, plotting the logarithm of the right-hand side of eq. 28 versus Mc should give a straight line with a slope equal to n and an intercept equal to k'_2 , see Marziano *et al.* (1984). Hence, in order to obtain the values of k'_2 and n, which will be specific for each aromatic compound, it is necessary to calculate:

a/ the M_c function: The M_c function at 298.2 K was correlated by Marziano *et al.* (1981) as a polynomial expansion:

$$\begin{aligned} -M_c = {} & 0.2264 \cdot C_{H_2SO_4} + 0.0216 \cdot C_{H_2SO_4}^2 - 0.1394 \cdot 10^{-2} \cdot C_{H_2SO_4}^3 + \\ & 0.2134 \cdot 10^{-3} \cdot C_{H_2SO_4}^4 - 0.4274 \cdot 10^{-4} \cdot C_{H_2SO_4}^5 + 0.3078 \cdot 10^{-5} \cdot C_{H_2SO_4}^6 + \\ & 0.6355 \cdot 10^{-7} \cdot C_{H_2SO_4}^7 - 0.1434 \cdot 10^{-7} \cdot C_{H_2SO_4}^8 + 0.3930 \cdot 10^{-9} \cdot C_{H_2SO_4}^9 \end{aligned} \qquad (29)$$

This function can, in principle, be extended to temperatures other than 298.2 K, according to Cox *et al.* (1979), by:

$$M_c(T) = \frac{298.2 \cdot M_c(298.2)}{T} \qquad (30)$$

b/ the Proton Concentration: The experimental data from Robertson and Dunford (1964) for the proton concentration in aqueous sulphuric acid in the range of 1 to 99 wt. % and at 298.2 K, were correlated according to the following function:

$$\begin{aligned} C_{H^+} = {} & -1.1757 \cdot 10^{-2} + 1.2406 \cdot C_{H_2SO_4} + 9.4286 \cdot 10^{-2} \cdot C_{H_2SO_4}^2 - \\ & 2.5102 \cdot 10^{-2} \cdot C_{H_2SO_4}^3 + 2.171 \cdot 10^{-3} \cdot C_{H_2SO_4}^4 - 6.917 \cdot 10^{-5} \cdot C_{H_2SO_4}^5 \end{aligned} \qquad (31)$$

Furthermore, it was assumed as a first approximation, that this proton concentration would not change appreciably with temperature (Marziano, private communication).

c/ the equilibrium constants $K_{NO_2^+}$ and K_{HNO_3} as a function of temperature: It has been assumed for the nitric acid dissociation that:

$$K_{HNO_3} = e^{\frac{-\Delta G_{HNO_3}}{R \cdot T}} \qquad (32)$$

where ΔG_{HNO_3} was calculated from data at 298.2 K. Ross et al. (1983) using ^{14}N NMR studied the equilibrium eq. 18 for temperatures between 287.36 and 316.16 K. Using their data, it was possible to correlate the formation of the nitronium ion constant $K_{NO_2^+}$ as:

$$K_{NO_2^+} = e^{\left(\frac{1.360 \cdot 10^4}{T} - 5.935\right)} \qquad (33)$$

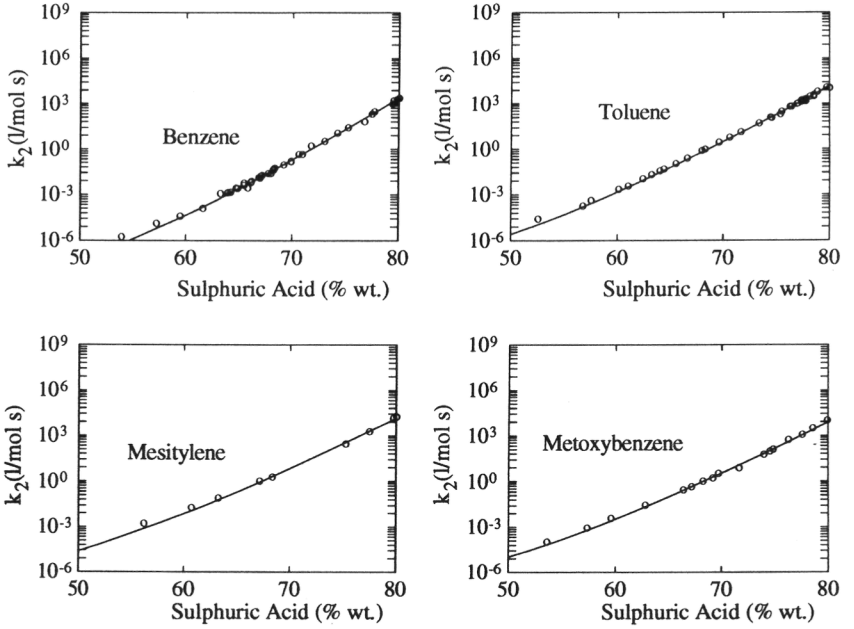

Figure 9. Experimental (o) versus calculated (-) second-order nitration rate constants for benzene, toluene, mesitylene and metoxybenzene at 298.2 K, using Eq. 28.

Figures 9 from 11 show the comparison between predicted and calculated values for log k_2 at 298.2 K as a function of sulphuric acid strength. These figures show that the correlation for calculating the observed second-order rate constants produces accurate results, even at high sulphuric acid concentrations, i.e. in the case for nitrobenzene and methyl phenyl sulphone.

Using the empirical correlations obtained above and experimental data from homogeneous nitration experiments at different temperatures, it is possible to obtain k'_2 for each aromatic

compound. The frequency factor and the activation energy are given in Table II for different aromatic compounds, see Appendix 3 for the derivation.

Table II. Frequency factor and activation energy, for the reaction rate constant k'_2, and n.

Compound	ln A	$(Ea/R)\cdot10^{-3}$	n
Benzene	25.074	4.033	0.318
Toluene	32.264	4.989	0.140
Chlorobenzene	28.852	6.003	0.389

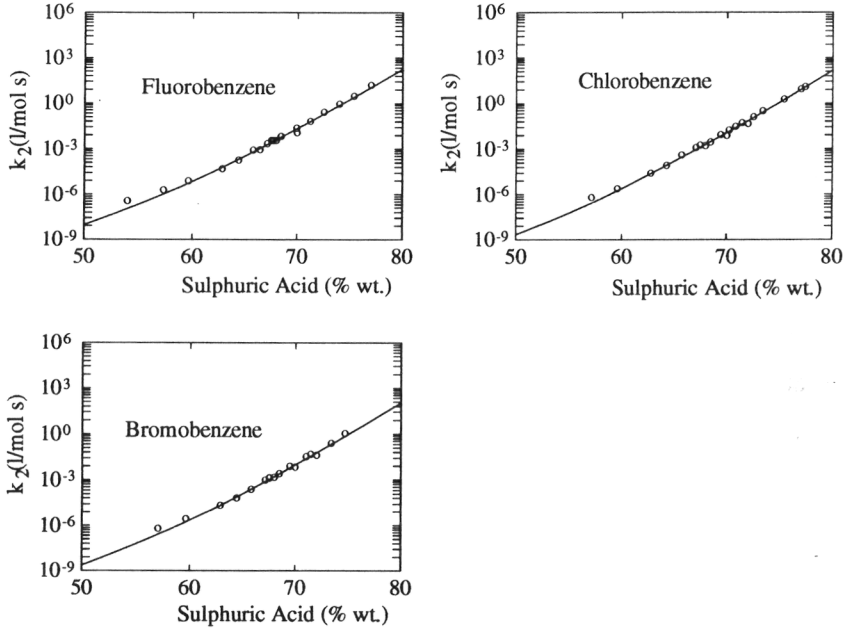

Figure 10. Experimental (o) versus calculated (-) second-order nitration rate constants for halogenobenzenes at 298.2 K, using Eq. 28.

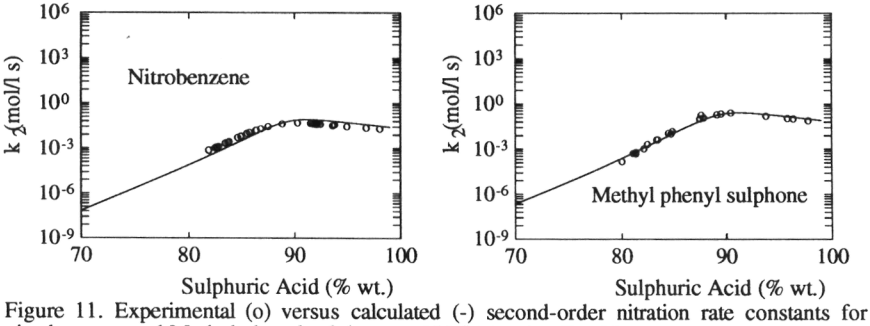

Figure 11. Experimental (o) versus calculated (-) second-order nitration rate constants for nitrobenzene and Methyl phenyl sulphone at 298.2 K, using Eq. 28.

3. SOLUBILITY OF AROMATIC COMPOUNDS IN MIXED ACID: MEASUREMENT AND PREDICTION

An important parameter in the derivation of an overall reaction rate expression is the solubility of the aromatic compounds in mixed acid, since it determines the maximum possible concentration in the reaction phase. Cerfontain (1965) showed that the solubility of aromatic compounds in aqueous sulphuric acid can be correlated by:

$$m_{ArH} = \frac{C_{ArH}^{L2}}{C_{ArH}^{L1}} = e^{\frac{-\Delta G_{ArH}}{R \cdot T}} \qquad (34)$$

where ΔG_{ArH} is a function of the sulphuric acid strength, the difference in internal pressure of the two immiscible solvents and the molar volume of the aromatic compound. It was found by Ismail (1973), that in industrial mixed acids also the effect of the nitric acid concentration on the total solubility has to be taken into account. Therefore, following the work of Cerfontain ΔG_{ArH} was empirically correlated as:

$$\Delta G_{ArH} = c_1 \cdot f(x_S) \cdot f(x_N) + c_2 - c_3 \cdot T \qquad (35)$$

where c_1, c_2, and c_3 are constants, to be determined for each individual aromatic compound, and $f(x_S)$ and $f(x_N)$ are polynomial functions of the sulphuric acid and nitric acid molar fractions respectively.

$$f(x_S) = \sum_i d_i \cdot x_S^{i-1} \qquad (36)$$

$$f(x_N) = \sum_i b_i \cdot x_N^{i-1} \qquad (37)$$

The constants of eq. 35 for benzene, toluene and chlorobenzene are given in Table III, whereas the coefficients of the polynomials $f(x_S)$ and $f(x_N)$, Eqs. 36 and 37, are given in Tables IV and V. Figure 12 shows a comparison between experimental and calculated distribution coefficients for chlorobenzene at 298.2 K in aqueous sulphuric acid. It can be seen that benzene, toluene and chlorobenzene have very low distribution coefficients of 2 to $4 \cdot 10^{-4}$ in the range of interest for mononitration between 60-80 % wt H_2SO_4; this will simplify the derivation of the overall rate expression.

Table III. Constants for the calculation of the distribution coefficient of aromatic compounds. Experimental data from Deno and Perizzolo (1957), Cerfontain (1965), Cerfontain and Telder (1965), Ismail (1973) and Chapman and Strachan (1976).

Compound	c_1	$c_2 \cdot 10^3$	c_3
Benzene	57.087	-1.382	-5.198
Toluene	44.359	14.576	28.638
Chlorobenzene	41.788	4.170	-15.414

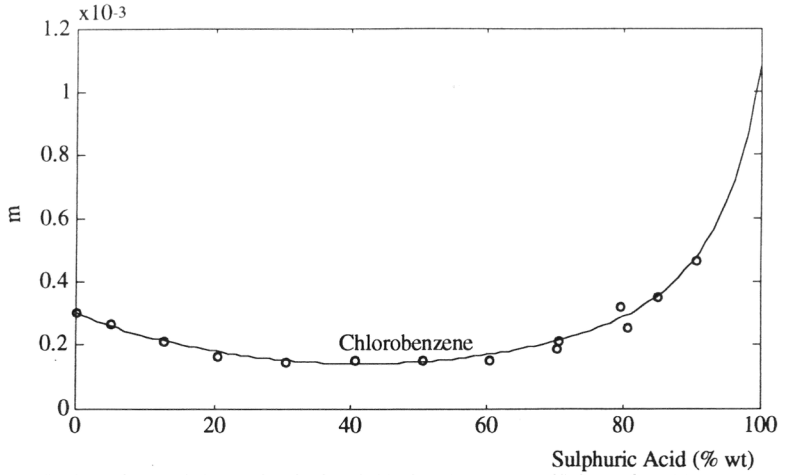

Figure 12. Experimental (o) and calculated (-) distribution coefficients for chlorobenzene in sulphuric acid solutions at 298.2 K based on Eqs. 34 and 35. Experimental data from Deno and Perizzolo (1957) and Chapman and Strachan (1976).

Table IV. Constants for the calculation of Eq. 36.

Compound	d_1	d_2	$d_3 \cdot 10^{-2}$	$d_4 \cdot 10^{-3}$	$d_5 \cdot 10^{-5}$	$d_6 \cdot 10^{-7}$	$d_7 \cdot 10^{-9}$
Benzene	167.001	6.0582	-44.556	13.4011	-13.821	-5.9687	12.8762
Toluene	172.399	3.4795	-8.7417	0.1209	0.1658	3.9341	-6.4481
Chlorobenzene	171.868	3.1632	-9.5261	-0.9216	2.6910	4.5063	-7.6594

Table V. Constants for the calculation of Eq. 37.

b_1	b_2	b_3
1.6042	-4.990	$2.23 \cdot 10^{-3}$

In order to take into account the amount of nitric acid present in the organic phase and, therefore, not available to form nitronium ion, experimental data from Barduhm and Kobe (1956), Gilles (1970), Sohrabi (1972) and Ismail (1973) were used to derive a similar expression as eq. (35) also accounting for the amount of conversion in the organic phase.

4. OVERALL CONVERSION RATES FOR SLOW LIQUID-LIQUID REACTIONS

It is well-known that in heterogeneous liquid-liquid reactions mass transport can be increased if the substance transported into the other phase reacts there chemically. Viceversa, chemical reaction can be slowed down by a mass transfer resistance, so that the conversion rate is lower than the chemical reaction rate. If the rate of chemical reaction is slow with respect to the rate of

mass transfer, the rate of mass transfer is not enhanced by reaction and the reaction mainly proceeds in the bulk of the reaction phase. For such situations, we must check that the consumption by reaction in the thin boundary layer is negligible. This assumption is justified if Ha < 0.3 holds, see Westerterp *et al.* (1984), where the Hatta number Ha is defined as:

$$Ha = \frac{\sqrt{k_2 \cdot D_{ArH} \cdot C_{HNO_3}^{L2}}}{k_{L2}} \qquad (38)$$

and D_{ArH} is the diffusivity of the aromatic compound in the acid phase.

Furthermore, as the solubility of the aromatic compounds in the acid phase is low and the mass transfer coefficients, k_{L1} and k_{L2} being of the same order of magnitude, also $k_{L1}/k_{L2} \cdot m >> 1$, so it can be assumed $C_{ArH}^{i1} \approx C_{ArH}^{L1}$. The concentration drop from C_{ArH}^{i2} to C_{ArH}^{L2} is relatively more important. Hence, the conditions under which the concentration drop of the aromatic compound transferred over the boundary layer in phase L2 is more than e.g. 5%, must be checked. If this is the case, the simple approximation $C_{ArH}^{i2} \approx C_{ArH}^{L2}$ starts to lead to inaccuracies, see Steensma and Westerterp (1988). To check this approximation is possible to compare the rate of mass transfer with the chemical reaction:

$$J_{ArH} \cdot a \cdot V = k_{L2} (C_{ArH}^{i2} - C_{ArH}^{L2}) a \cdot V \qquad (39)$$

$$J_{ArH} \cdot a \cdot V = \varepsilon_{L2} \cdot k_2 \cdot C_{ArH}^{i2} \cdot C_{HNO_3}^{L2} \qquad (40)$$

where ε_{L2} refers to the volumetric fraction acid phase in which the reaction takes place and a is the interfacial area per unit volume.

The combination of both equations gives:

$$\frac{\varepsilon_{L2} \cdot k_2 \cdot C_{HNO_3}^{L2}}{k_{L2} \cdot a} = 1 - \frac{C_{ArH}^{L2}}{C_{ArH}^{i2}} \qquad (41)$$

Hence, in the case $C_{ArH}^{i2} \approx C_{ArH}^{L2}$ it must be checked that $k_{L2} \cdot a >> \varepsilon_{L2} \cdot k_2 \cdot C_{HNO_3}^{L2}$.

For the case where the transport of the aromatic compound in the reaction phase is not chemically enhanced and the concentration drop in the reaction phase is relatively small, it is possible to derive an overall reaction rate expression as, see Steensma and Westerterp (1988):

$$R = \varepsilon_{L2} \cdot k_2 \cdot C_{ArH}^{L2} \cdot C_{HNO_3}^{L2} \qquad (42)$$

In order to check the validity of these assumptions it is necessary to calculate, by means of empirical correlations, the diffusion and mass transfer coefficients. Furthermore the interfacial area has to be obtained.

4.1. The Diffusion Coefficients

Despite different available theoretical treatments for the description of diffusion in liquids, there are hardly any satisfactory methods to predict the diffusion coefficients in multicomponent mixtures. Therefore, prediction procedures must be applied only when experimental data are not available. Such procedures can be divided in those suitable for nonelectrolytes and those suitable for electrolytes.

For the diffusitivity of aromatic compounds in mixed acid, as suggested by Chapman and Strachan (1976), a modified version of the widely used correlation, recommended by Perkins and Geankoplis (1969) to estimate the multicomponent diffusion coefficient in liquid mixtures, can be used:

$$D = \frac{F \cdot T}{\mu^{0.8}} \tag{43}$$

where F is given by:

$$F = \frac{4.67 \cdot 10^{-6} \cdot (\phi M)^{0.5}}{V_b^{0.6}} \tag{44}$$

and V_b in l/mol is the total molal volume of the aromatic compound at its normal boiling point and ϕM is defined according to Cox and Strachan (1972) as:

$$\phi M = 2.6 \cdot x_W \cdot M_W + 2.0 \cdot x_S \cdot M_S + 1.05 \cdot x_N \cdot M_N \tag{45}$$

where x, and M are the mole fraction and molecular weight respectively.

Values of D for toluene and benzene were experimentally determined by Hanson and Ismail (1976) using the laminar-jet technique. Figure 13 shows the comparison between experimental and calculated diffusivities for toluene and benzene, using Eqs. 43-45.

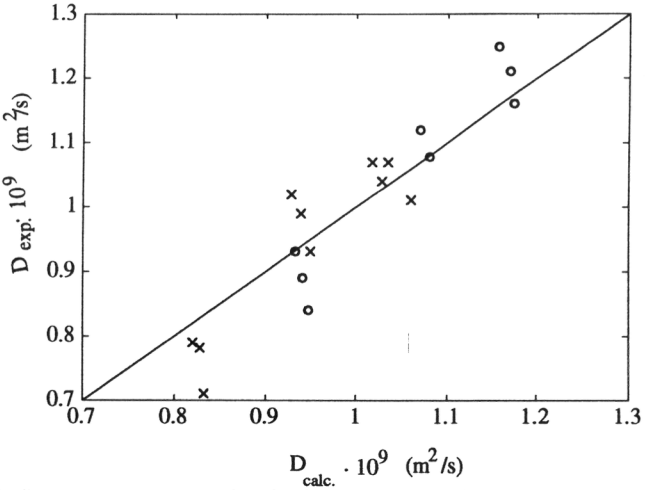

Figure 13. Pariry plot of experimental and calculated diffusivities for toluene (x) and benzene (o) at 303.2 K, for different mixed acid compositions. Experimental data from Hanson and Ismail (1976).

4.2. Mass transfer coefficient

Unfortunately, there is only one experimental value in literature for the mass transfer coefficient k_{L2} equal to $1.03 \cdot 10^{-5}$ m/s. This value was obtained by Chapman *et al.* (1974) in a series of toluene nitration experiments using acid strengths between 76 and 79 %. In these experiments, the acid phase was the continuous one. This value is in agreement with typical values found in

liquid-liquid systems, e.g. Fernandes and Sharma (1967) found values between $1.13\text{-}1.6\cdot10^{-5}$ m/s for the system n-hexylacetate and 1M NaOH solution. The following empirical correlation developed by Calderbank and Moo-Young (1961) and experimentally validated in a wide range of operating conditions, see Uhl and Gray (1967), may be used to determine the mass transfer coefficient in the continuous phase k_{L2} in liquid-liquid dispersion systems, see De Santiago and Trambouze (1971):

$$k_{L2} = 0.13 \left(\frac{P \cdot \mu_c}{V_d \cdot \rho_c^2} \right)^{\frac{1}{4}} \left(\frac{\mu_c}{\rho_c \cdot D_{ArH}} \right)^{-\frac{2}{3}} \qquad (46)$$

where P refers to the power dissipated by the stirrer,

$$P = \phi \cdot \rho_m \cdot n_a^3 \cdot D_a^5 \qquad (47)$$

and ϕ may be considered as a constant and here $\phi = 2.2$, see Bourne et al. (1981) and Zaldívar *et al.* (1990).

Using the correlation eq. 44, and the experimental data from Chapman *et al.* (1974), the value obtained for k_{L2} is $1.1\cdot10^{-5}$ m/s - see Appendices 4 and 5 for a calculation of the physical and transport properties - which is in agreement with the reported literature experiments.

5. ISOMER DISTRIBUTION

Another aspect to consider in the mononitration of toluene and chlorobenzene is the isomer distribution. The relative reactivities of the ortho, meta and para carbon atoms should be proportional to the electron availability at these sites and the relative probability of collision with a given nitronium ion. At the same time the reaction rate measurements only consider the aromatic compound decay. Therefore the overall conversion rate obtained was splitted into partial rates for each isomer. The distribution of isomers depends on temperature and on the sulphuric acid strength.

The isomer distribution after reaction completion in the nitration of toluene was found to be 57.0-61.0, 3.4-4.2, and 34.0-38.0 molar % for ortho-, meta- and para-nitrotoluene, respectively , depending on reaction conditions, see Molga *et al.* (1993). A rather weak dependence, still within the experimental error range, was observed for the selectivity ratios ortho/para on the reactor temperature. A temperature rise from 15° C to 45° C changes the values of this ratio at the end of the reaction from 1.69 to 1.76, which is in whithin the experimental error. Also an influence of the sulphuric acid strength was observed and it was correlated in the range of 60-80 wt % as:

$$\frac{\text{o-MNT}}{\text{p-MNT}} = 3.246 - 0.022 \cdot x \qquad (48)$$

Similar dependences have been found by Harris (1976) and Barnet *et al.* (1975). They obtained a value of - 0.021 for the slope in eq. 46. The percentage of m-MNT was considered to be constant at 4%.

In the nitration of chlorobenzene the data from Coombes *et al.* (1970) in the range of 68-74 wt % of sulphuric acid strength were used to obtain the isomer distribution in molar % as:

$$o\text{-MNC} = 1.22+0.466 \cdot x \quad (49)$$

$$m\text{-MNC} = 0.89-1.36 \cdot 10^{-3} \cdot x \quad (50)$$

$$p\text{-MNC} = 97.89-0.467 \cdot x \quad (51)$$

6. EXPERIMENTAL STUDY. MODEL VERIFICATION WITH REACTION CALORIMETRY

The mathematical model for the nitration rates as described above was developed using data from homogeneous experiments with low nitric acid concentrations between 10^{-4} and 10^{-2} mol/l. In order to validate this model also under heterogeneous conditions, a series of experiments were carried out in a reaction calorimeter RC1 of Mettler. This apparatus provides an accurate measurement of the heat removal from the reactor, which through a heat balance is used to deduce the rate of heat generation in a certain reaction mass and hence the rate of reaction. The precision of this calorimetric method depends on the correct representation of all the secondary heat effects like heat losses, stirring power supply, heat taken up by reactor wall and dilution heat, see Hernández *et al.* (1993). In this particular case, the heat of dilution, which cannot be neglected as part of the total heat generated during the nitration, was evaluated using a model developed in previous work, see Zaldívar *et al.* (1992b).

Table VI. Isothermal nitration experiments in the kinetic regime: initial and operating conditions.

Compound	Temperature (K)	x (% wt)	Na (s^{-1})	Feeding time	$Ha_{calc.}$ (max.)
Benzene	298.2	62.0	6.67	Batch	0.2
Toluene	308.2	61.4	6.67	Batch	0.03
Chlorobenzene	328.2	62.0	6.67	Batch	0.2

The experiments in the reaction calorimeter were carried out in such a way so as to assure the overall conversion rate is always controlled by chemical reaction. This is accomplished by using sulphuric acid of a low strength, between 60-62 wt. %, for industrial aromatic mononitrations. The operating conditions are summarised in Table VI where the maximum Hatta number calculated is also included. The calculated diffusitivity coefficients as well as the mass transfer coefficient discussed above were used to check the validity of the assumptions that $Ha < 0.3$ and $k_{L2} \cdot a >> \varepsilon_{L2} \cdot k_2 \cdot C_{HNO_3}^{L2}$ during the reaction and that the reaction rate expression eq. 42 is correct under the experimental conditions. In a typical case $k_{L2} \approx 10^{-5}$ (m/s), $a \approx 4 \cdot 10^3 (m^2/m^3)$, see Zaldívar *et al.* (1995), $D_{ArH} \approx 10^{-9}$ (m^2/s), $\varepsilon_{L2} \approx 0.8$, $C_{HNO_3}^{L2} \approx$ 2 M and $k_2 \approx 10^{-4}$ (l/mol·s), so the assumptions are valid.

Selectivity and yields were determined directly from the concentration measurements by Gas Chromatography, see Molga *et al.* (1993), whereas the reaction rate was estimated independently from calorimetric measurements, see Hernández *et al.* (1993).

Figures 14-17 show experimental results and simulations using the H_R and the M_C acidity functions. Figure 14 shows the concentration profiles during the nitration of benzene. In this experiment 195 g of benzene were added batchwise to 868 g of mixed acid with a H_2SO_4 strength of 62.0 wt. %. The reactor temperature set-point was 298.2 K and the stirrer speed was 6.67 s^{-1}. Figures 15 and 16 show the concentration profiles, obtained by GC, and the overall conversion rates, obtained by calorimetric measurements, for the nitration of toluene. As can be seen the agreement between these two independent measurements is satisfactory. The nitration of toluene was carried out at 308.2 K and the stirrer speed was 6.67 s^{-1}. The procedure was identical to the one described above for benzene, i.e. 184 g of toluene were added batchwise to 1870 g of mixed acid with a H_2SO_4 strength of 61.4 wt. %. Figure 17 shows the concentration profiles during a nitration of chlorobenzene which was carried out at 328.2 K and a stirrer speed of 6.67 s^{-1}. In this experiment 281 g of chlorobenzene were added batchwise to 851 g of mixed acid with a H_2SO_4 strength of 62.0 wt. %.

The concentration profiles show the behaviour is not such of a typical second order reaction since the rate of consumption decreases more rapidly; this is due to the fact that the concentration of the nitronium ion decreases as water is produced. The differences between the experimental and simulated conversion rates at the beginning of the toluene nitration experiment are due to the slow conversion rates measured. Under such conditions small errors in the evaluation of the heat capacity become important, since the reactor temperature is not stabilised and its derivative is not zero.

From comparisons between model and experimental results it can be concluded that it is possible to extrapolate to heterogenous reactions in the kinetic regime of a slow liquid-liquid reaction using data from homogeneous nitration experiments; it is also possible to interpret the dynamic behaviour of discontinuous nitration processes in such conditions.

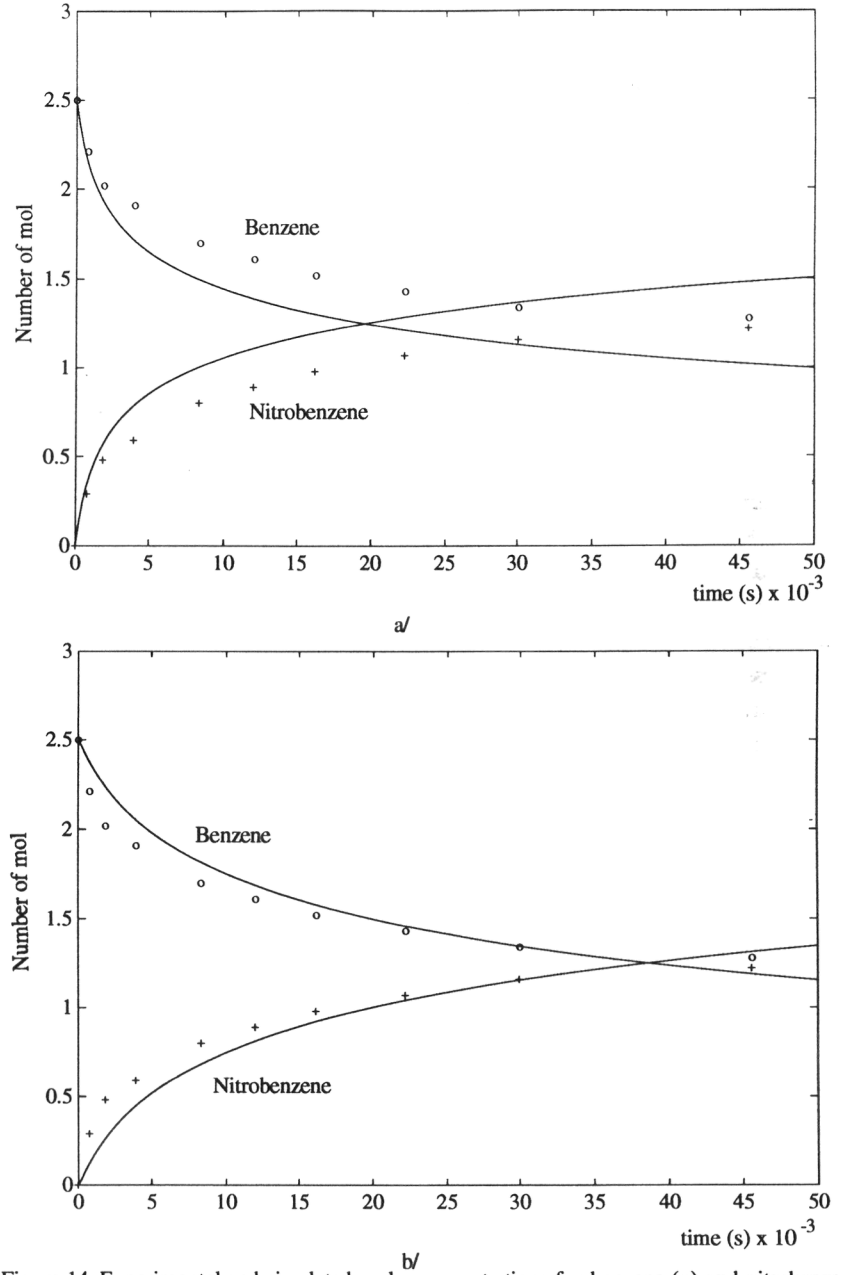

Figure 14. Experimental and simulated molar concentrations for benzene (o) and nitrobenzene (+) as a function of time during a batch nitration: a/ using the H_R function; b/ using the M_C function.

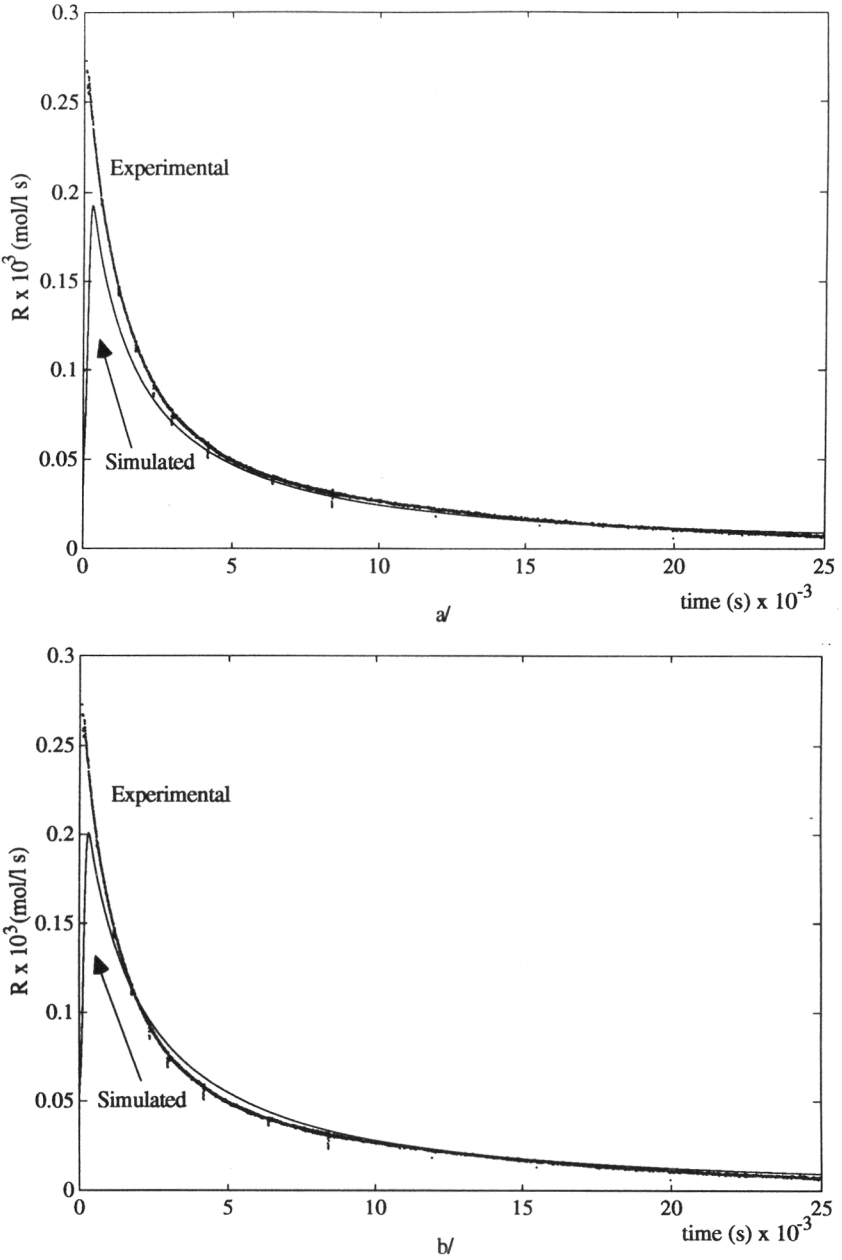

Figure 15. Experimental and simulated reaction rate for batch toluene mononitration: a/using the H_R function; b/ using the M_C function.

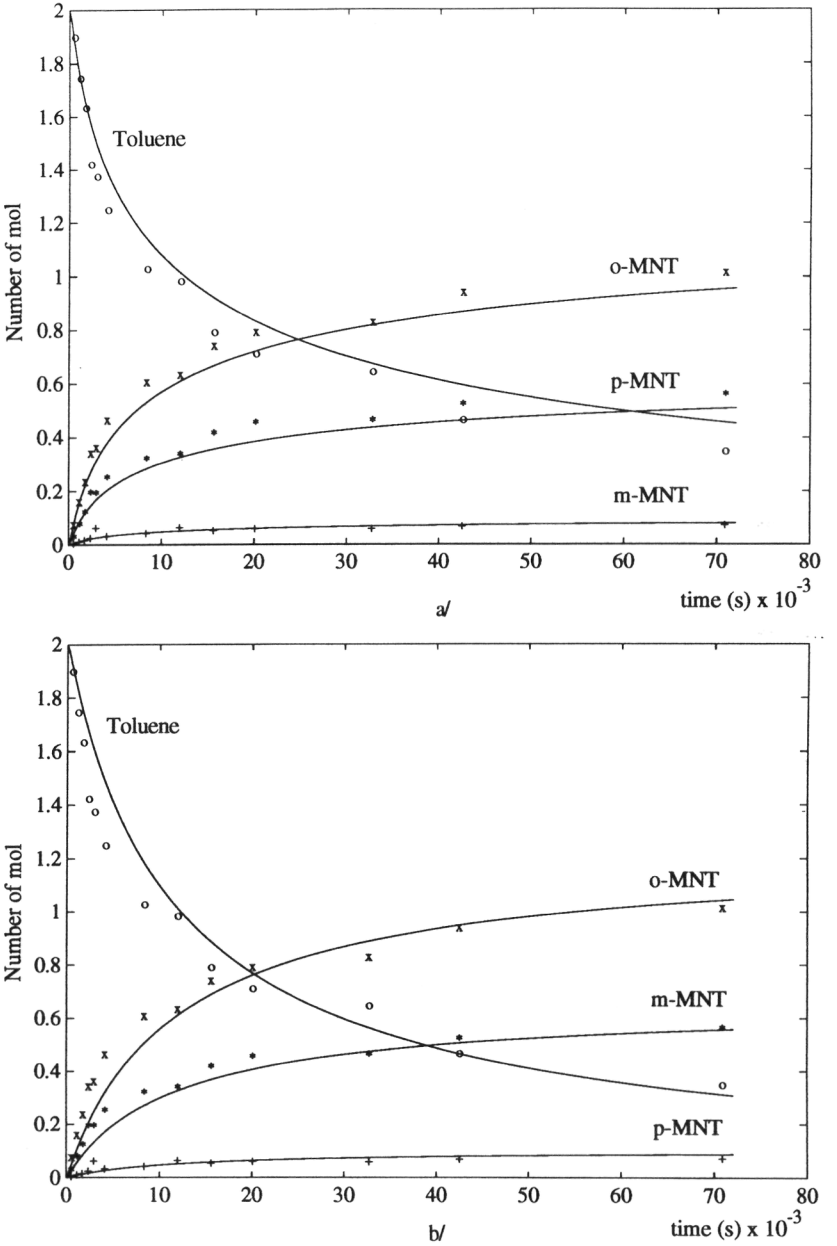

Figure 16. Experimental and simulated molar concentrations for (o) toluene, (x) o-nitrotoluene (o-MNT), (+) m-nitrotoluene (m-MNT), and (*) p-nitrotoluene (p-MNT) as a function of time for a batch nitration: a/ using the H_R function; b/ using the M_C function.

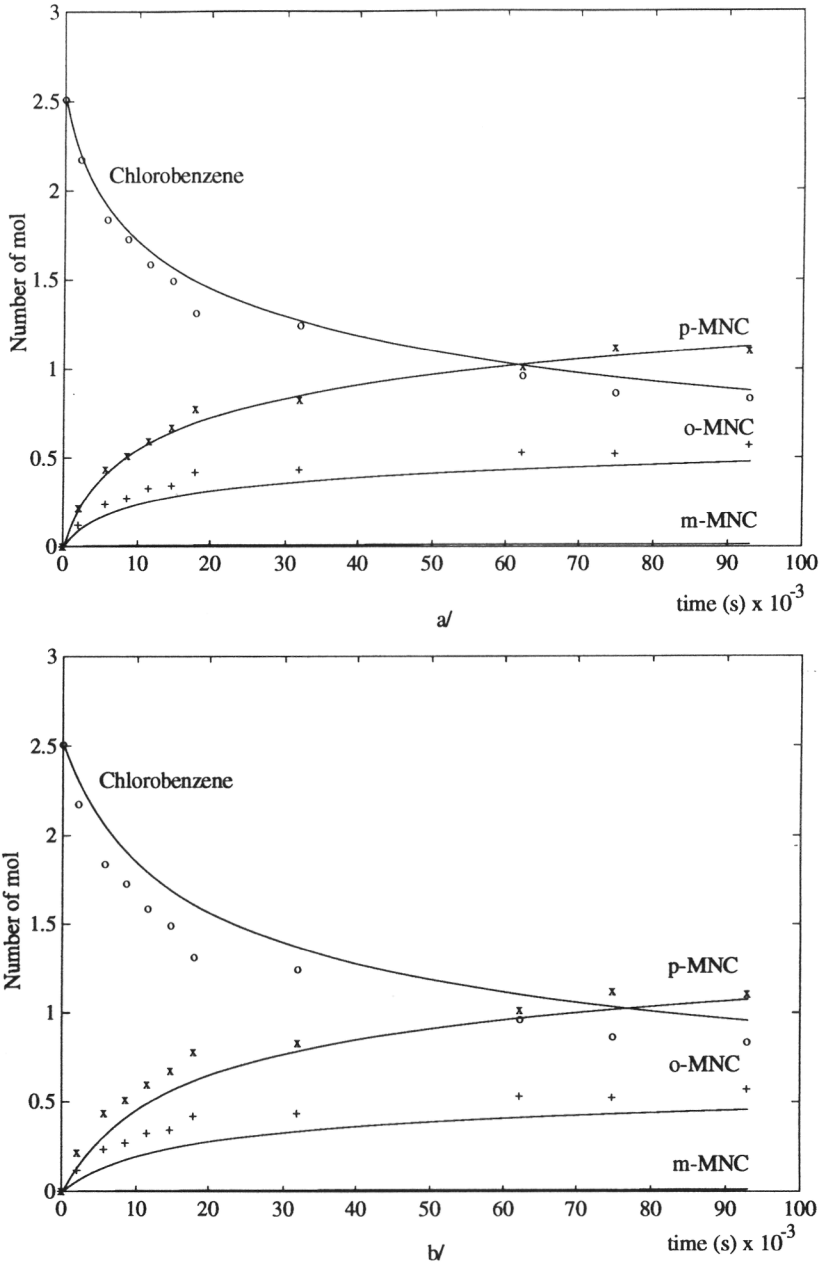

Figure 17. Experimental and simulated molar concentrations for chlorobenzene (o), ortho-chloronotrobenzene, o-MNC(+) and p-nitrochlorobenzene, p-MNC (x) and m-MNC as a function of time during a batch nitration: a/ using the H_R function; b/ using the M_C function.

7. DISCUSSION AND CONCLUSIONS

The main objective of this paper was to analyse the possibility of extrapolating experimental data obtained from homogeneous nitration experiments - with nitric acid concentrations between 10^{-4} and 10^{-2} and a temperature of 298.2 K- to discontinuous heterogeneous nitrations under conditions of high nitric acid concentrations and temperatures other than 298.2 K. Under such conditions, the composition of the acid phase is different from that used in the mechanistic studies analysed so far and the nitration rates available from the latter are not immediately relevant to the former. Furthermore, in discontinuous nitrations the process is even more complex because the two phases change in composition as the reaction proceeds and therefore all the relevant parameters like reaction rate constant, acidity of the acid phase, diffusivity of aromatic compounds, mass transfer coefficient, interfacial area, interfacial tension and physical and transport properties change. For these reasons, the first necessary step was to validate the model in the kinetic regime - in which mass transfer resistance does not have an influence on the overall conversion rate - where the only important parameters are the reaction rate constant and the solubility of the aromatic compound in the mixed acid.

From the comparisons between model and experimental results it can be concluded it is possible to extrapolate data from homogeneous nitration experiments and to interpret the dynamic behaviour of discontinuous nitration processes in the kinetic regime of slow liquid-liquid reactions. The H_R function produces acceptable results in the acidity range studied of 60 to 62 % wt. sulphuric acid; it is clear from fig. 6 that at high acidity values the results become inaccurate, see Marziano *et al.* (1977). This is the case for deactivated aromatic rings, e.g. in di- and trinitrations, for which it is necessary to work between 80-100 % wt. sulphuric acid strength to obtain significant conversion rates. This may be corrected by adjusting K in eq. 10 to take into account such behaviour, but always the necesity remains of introducing monohydrated nitric acid for the determination of the reaction rates, even in the regions where practically no water is present.

Even though we are able to calculate correctly the reaction rate constant in a wide acidity range with the M_c function, for the determination of the kinetic function it still is difficult to extent these results to temperatures other than 298.2 K since less experimental data are available when compared to the H_R function. In particular, more data on the temperature dependence of the dissociation constant of nitric acid and the formation of nitronium ion are required, as well as the temperature variation of the M_c function. Despite this, the results are acceptable within the range of temperatures studied of 298.2 to 328.2 K. Future work will be dedicated to the acquisition of the temperature dependence data to apply the M_c function.

In a second part of this work the determination of the effective interfacial area and the mass transfer controlled region will be evaluated.

NOTATION

a	activity (mol/l) or interfacial area (m^2/m^3)
C	concentration (mol/l)
d_{32}	droplets Sauter mean diameter (m)
D	stirrer diameter (m)
D_{ArH}	diffusivity of aromatic compound (m^2/s)
Ha	Hatta number
H_R	acidity function
H_0	Hammett's acidity function
J_{ArH}	mass transfer rate ($mol/m^2 \cdot s$)
k_2'	reaction rate constant related to mechanism, see text (l/mol·s)
k_2	measured 2nd order rate constant (l/mol·s)
k_{L2}	mass transfer coefficient (m/s)
K	equilibrium constant,
m	distribution coefficient
M	molecular weight (g/mol)
M_c	empirical activity coefficient
MNT	mono-nitro-toluene
MNC	mono-nitro-chlorobenzene
n	stirrer speed (s^{-1})
P	power dissipated by the stirrer (W)
R	overall conversion rate based on the total reaction volume (mol/l·s)
r	reaction rate in the acid phase (mol/l·s)
T	temperature (K)
V	volume (l)
We	Weber number,
x	sulphuric acid strength, or molar fraction

Greek letters

ρ	density (kg/m^3)
μ	viscosity (kg/m·s)
γ	activity coefficient

Subscripts and superscripts

a	stirrer
ArH	Aromatic compound
L1	organic phase
L2	acid(aqueous) phase
i1	organic interphase
i2	acid(aqueous) interphase
c	continuous phase
d	dispersed phase
m	reacting mixture
e	heat transfer fluid
S	Sulphuric acid
N	Nitric acid
W	Water
‡	activated transition intermediate

REFERENCES

Albright, L.F. and C. Hanson (eds), 1976, *Industrial and Laboratory Nitrations*, ACS Symposium Series n 22, Washington DC.

Al-Khudhairy, D. and J.M. Zaldívar, 1989, Activity coefficients in HNO_3-H_2SO_4-H_2O mixtures, *Technical Note I.89.90*, Joint Research Centre- Ispra Site, Italy.

Barton, J.A. and P.F. Nolan, 1984, Runaway reactions in batch reactors, *The Protection of Exothermic Reactors and Pressurised Storage Vessels*, IChemE Symposium Series 85, 13-21.

Barduhm A.J. and K.A. Kobe, 1956, Toluene nitration kinetics, *Ind. Engng. Chem.* **48**, 1305-1315.

Barnet, J.W., R.B. Moodie, K. Schofield and J.B. Weston, 1975, Electrophilic aromatic substitution. Part XIII. Kinetics, isomer yields and the consequences of ipso-attack in the nitration of toluene and polymethylbenzenes in aqueous sulphuric acid, and their significance for the mechanism of aromatic nitration, *J.C.S. Perkin II*, 648-654.

Bosen, A. and H. Engels, 1988, Description of the phase equilibrium of sulfuric acid with the NRTL equation and a solvatation model in a wide concentration and temperature range, *Fluid Phase Equilibria* **43**, 213-230.

Bourne, J.R., M. Buerli and W. Regenass, 1981, Heat transfer and power measurements in stirred tanks using heat flow calorimetry, *Chem. Eng. Sci.* **36**, 347-354.

Calderbank P.H. and M.B. Moo Young, 1961, The continuous phase heat and mass-transfer properties of dispersions, *Chem. Eng. Sci.* **16**, 39-54.

Calderbank P.H., 1967, Mass Transfer in V.W. Uhl, J.B. Gray (eds), *Mixing Theory and Practice*, Academic Press, New York.

Chapman, J.W., P.R. Cox and A.N. Strachan , 1974, Two phase nitration of toluene III, *Chem. Eng. Sci.* **29**, 1247-1251.

Chapman, J.W. and A.N. Strachan , 1976, Two phase nitration of chlorobenzene in 79.8% sulfuric acid, *Industrial and Laboratory Nitrations*, Albright, L.F. and C. Hanson (eds), ACS Symposium Series n 22, Washington DC, 219-223.

Cook, M.J., A.R. Johnson, A.R. Katritzky, and T.W. Toone, 1975, Temperature variation of the H_R acidity function in aqueous sulfuric acid, *J.A.C.S.* **97**,760-764.

Coombes, R.G., R.B. Moodie, and K. Schofield, 1968, Electrophilic aromatic substitution. Part I. The nitration of some reactive aromatic compounds in concentrated sulphuric and perchloric acids, *J. Chem. Soc. B*, 800-804.

Coombes, R.G., D.H.G. Crout, J.G. Hoggett, R.B. Moodie and K. Schofield, 1970, Electrophilic aromatic substitution. Part VI. Kinetics and mechanism of nitration of halogenobenzenes, *J. Chem. Soc. B*, 347-357.

Cox, P.R. and A.N. Strachan, 1972a, Two phase nitration of toluene-I, *Chem. Eng. Sci.* **27**, 457-463.

Cox, P.R. and A.N. Strachan , 1972b, Two-phase nitration of toluene, Part II, *Chem. Eng. J.* **4**, 253-261.

Cox, R.A., M.F. Goldman and K. Yates, 1979, The hydrolyses of some sterically crowed benzoate esters in sulfuric acid. The excess acidity method at different temperatures, *Can. J. Chem.* **57**, 2960-2966.

Deno, N.C. and C. Perizzolo, 1957, The application of activity coefficient data to the relations between kinetics and acidity functions, *J.A.C.S.* **79**, 1345-1348.

Deno, N.C. and R. Stein, 1956, Carbonium ions.III. Aromatic nitration and the C_0 acidity function, *J.A.C.S.* **78**, 578-581.

Deno, N.C., H.J. Peterson and E. Sacher, 1961, Nitric acid equilibria in water-sulphuric acid, *J. Phys. Chem.* **65**, 199-201.

De Santiago, M. and P. Trambouze, 1971, Applicabilité de la méthode chimique de measure de l'aire interfaciale, *Chem. Eng. Sci.* **26**, 1803-1815.

Fénéant , S. and J. Chédin, 1956, Dosages par effet Raman et équilibres de formation de l'ion NO_2^+ dan les mélanges binaries HNO_3-H_2SO_4, *Compt. Rendus* **243**, 141-144.

Fernandes, J.B., and M.M. Sharma, 1967, Effective interfacial area in agitated liquid-liquid contactors, *Chem. Eng. Sci.* **22**, 1267-1282.

Field, J.P., and A.N. Strachan, 1982, Dependence of the rate constant and activation energy of aromatic nitration on mixed acid composition, *Ind. Eng. Chem. Prod. Res. Dev.* **21**, 352-355.

Giauque, W.F., E.W. Hornung, J.E. Kunzler and T.R. Rubin, 1960, The thermodynamic properties of aqueous solutions and hydrates from 15 to 300 K, *J. A. C. S.* **82**, 62-70.

Giles, J. W., 1970, PhD Thesis, University of Bradford, UK.

Guarise, G.B., 1966, Attività nel sistema HNO_3-H_2SO_4-H_2O, *La Chimica e L'industria* **48** (12), 1316- 1322.

Hàla, E. I. Wichterle, J. Polàk and T. Boublik, 1968, *Vapour-Liquid Equilibrium Data at Normal Pressures*, Pergamon Press, London.

Hanson, C. and H.A.M. Ismail, 1976, Diffusion of benzene and toluene into aqueous nitric acid-sulphuric acid mixtures, *J. appl. Chem. Biotechnol.* 26, 111-116.

Harris, G.F.P., 1976, Isomer control in the mononitration of toluene, 1976, *Industrial and Laboratory Nitrations*, Albright, L.F. and C. Hanson (eds), ACS Symposium Series n 22, Washington DC, 300-312.

Hernández, H. and J.M. Zaldívar, 1990, The JRC FIRES Project for investigations on runaway reactions, *Eurotherm Seminar n 14*, Proceedings of Heat Transfer and Major Technological Hazards, 13, 1-10.

Hernández, H., J.M. Zaldívar and C. Barcons, 1993, Development of a mathematical model and a numerical simulator for the analysis and optimization of batch reactors, *Computer Chem. Engng.* **17S**, 45-50.

Hoggett, J.G., R.B. Moodie, J.R. Penton and K. Schofield, 1971, *Nitration and Aromatic Reactivity*, Cambridge University Press, Cambridge.

Ingold, C.K., 1953, *Structure and Mechanism in Organic Chemistry*, ch. 6, Bell, London.

Ismail H.A.M. , 1973, PhD Thesis, University of Bradford, UK.

Kanhere J.M. and S.B. Chandalia, 1981, Kinetics of nitration of aromatic compounds with mixed acid: Reinterpretation of published data, *Ind. Eng. Chem. Process Des. Dev.* **20**, 404-407.

Marziano, N.C., G.M. Cimino and R.C. Passerini, 1973, The M_c activity coefficient function for acid-base equilibria. Part I. New methods for estimating pKa values for weak bases, *J. C. S. Perkin II*, 1915-1922.

Marziano, N.C., A. Zingales and V. Ferlito, 1977, A reinvestigation of nitration in aqueous sulfuric acid of benzene and halogenobenzenes, *J. Org. Chem.* **42**, 2511-2513.

Marziano N.C., P.G. Traverso, A. de Santis and M. Sampoli, 1978, Determination of the basicity of nitric acid in concentrated sulphuric acid by Raman and Ultraviolet spectroscopy, *J. Chem. Soc. Chem. Comm.* **20**, 873-874.

Marziano, N.C., P.G. Traverso and G.G. Cimino, 1980, Thermodynamic nitration rates of aromatic compounds. Part 1. The nitration of benzene and some benzene derivatives in aqueous sulphuric and perchloric acids. A comparison of the results referred to water as standard state, *J. C. S. Perkin II*, 574-578.

Marziano, N.C., A. Tomasin, and P.G. Traverso, 1981, The M_c activity coefficient function for acid-base equilibria. Part 5. The Mc activity coefficient for reliable estimate of thermodynamic values, *J. C. S. Perkin II*, 1070-1075.

Marziano, N.C., M. Sampoli, F. Pinna and A. Passerini, 1984, Thermodynamic nitration rates of aromatic compounds. Part 2. Linear description of rate profiles for the nitration of aromatic compouns in the range 40-98 wt % sulphuric acid, *J. C. S. Perkin II*, 1163-1166.

Marziano, N.C., C. Tortato and M. Sampoli, 1991, Thermodynamic nitration rates of aromatic compounds. Part 3. Nitration of aromatic compounds in concentrated aqueous trifluoromethanesulphonic Acid, *J. Chem. Soc. Perkin Trans.* **2**, 423-429.

Miller, R.C., D.S. Noyce and T. Vermeulen, 1964, The kinetics of aromatic nitration, *Industrial and Engineering Chemistry* **56** (6), 43-53.

Moodie, R.B., K. Schofield and P. Taylor, 1979, Electrophilic aromatic substitution. Part 21. Rate constants for formation of nitronium ion in aqueous sulphuric, perchloric, and methane-sulphonic acids, J.C.S. Perkin II, 133-136.

Molga, E.J., C. Barcons and J.M. Zaldívar, 1993, Mononitration of toluene and quantitative determination of the isomer distribution by Gas Chromatography, *Afinidad* **50**, 15-20.

Olah, G.A., R. Malhotra and S.C. Narang, 1989, *Nitration: methods and mechanisms*, VCH Publishers, New York.

Perkins L.R. and C.J. Geankoplis, 1969, , Molecula diffusion in a ternary liquid system with the diffusing component dilute . *Chem. Eng. Sci.* **24**,1035-1042.

Reisen, R. and B. Grob, 1985, Reaction calorimetry in chemical process development, *Swiss Chem.* **7**, 39-43.

Robertson, E.B., and H.B. Dunford, 1964, The state of the proton in aqueous sulfuric acid, J. A. C. S., 86, 5080-5089.

Rochester, C.H., 1970, *Acidity Functions*, Academic Press, London.

Ross D.S., K.F. Kuhlmann and R. Malhotra, 1983, Studies in aromatic nitration.2. ^{14}N NMR Study of the nitric acid/nitronium ion equilibrium in aqueous sulphuric acid, *J. A. C. S.* **105**, 4299-4302.

Sampoli, M., A. De Santis and N.C. Marziano, 1985, On the relationship between the dissociation of indicators in non-ideal acid solution and the dissociation of the acid itself, *J. Chem. Soc., Chem. Commun.*, 110-111.

Sampoli, M., A. De Santis, N.C. Marziano, F. Pinna and A. Zingales, 1985, Equilibria of nitric acid in sulfuric and perchloric acid at 25° C by Raman and UV spectroscopy, *The Journal of Physical Chemistry* **89**, 2864-2869.

Schofield, K., 1980, *Aromatic Nitration*, Cambridge University Press, Cambridge.

Sheats, G.F. and A.N. Strachan, 1978, Rates and activation energies of nitronium ion formation and reaction in the nitration of toluene in ~78% sulphuric acid, *Can. J. Chem.* **56**, 1280 -1283.

Singh, J., 1989, PHI-TEC: Enhanced vent sizing calorimeter, *in International Symposium on Runaway Reactions*, AIChE, New York, 313-330.

Sohrabi, M., 1972, PhD Thesis, University of Bradford, UK.

Steensma, M., and K.R. Westerterp, 1988, Thermally safe operation of a cooled semi-batch reactor. Slow liquid-liquid reactions, *Chem. Eng. Sci.* **43**, 8, 2125-2130.

Traverso, P.G., N.C. Marziano and R.C. Passerini, 1977, The M_c activity coefficient function for acid-base equilibria. Part 4. Limitations of empirical relationships involving observed nitration rates and acidity functions, *J. C. S. Perkin II*, 845-847.

Uhl, V.W. and Gray (eds.), 1967, *Mixing: Theory and Practice*, vol. II, Academic Press.

Van Velzen, D., R. Lopes and H. Langenkamp, 1972, Liquid viscosity and chemical constitution of organic compounds: A new correlation and a compilation of literature data, *EUR 4735e*, Joint Research Centre- Ispra Site, Italy.

Westerterp, K.R., W.P.M. van Swaaij, and A.A.C.M. Beenackers, 1984, *Chemical Reactor Design and Operation*, J. Wiley & Sons, Chichester.

Zaldívar, J.M., H. Hernández and C. Barcons, 1990, Development of a numerical simulator for a reaction calorimeter. FISIM, RC1 version, *TN n° I.90.109*, Joint Research Centre - Ispra Site, Italy.

Zaldívar, J.M., C. Barcons, H. Hernández, E. Molga and T.J. Snee, 1992a, Modelling and optimization of semibatch toluene mononitration with mixed acid from performance and safety viewpoints, *Chem. Eng. Sci.* **47**, 2517-2522.

Zaldívar, J.M., H. Hernández, C. Barcons and R. Nomen, 1992b, Heat effects due to dilution during aromatic nitrations by mixed acid in batch conditions, *J. of Thermal Analysis* **38**, 2575-2582.

Zaldívar, J. M., E. Molga , M. A. Alós, H. Hernández and K. R. Westerterp, Aromatic nitrations by mixed acid. Fast liquid-liquid reactions, 'submited for publication' (1995).

Appendix 1. Activity Coefficients in HNO_3-H_2SO_4-H_2O mixtures.

In recent years considerable attention has been paid to activity coefficients in aqueous mixtures of electrolytes, see a.o. Liu and Grén (1991), Kumar and Patwardhan (1992). Unfortunately, this is still an open area of research and data required for such correlations be applied for the mixed acid system are not available at the moment. As a consequence, a compromise has to be made to avoid unnecessary and complex calculations, in using the Wilson method, see Al-Khudhairy and Zaldívar (1989).

An important characteristic of the Wilson equation is that no specific interaction parameters for ternary systems are required and that it uses only two temperature dependent terms to describe the binary system: this reduces the amount of experimental data to characterise a multi-component solution. The Wilson's expression for the liquid phase activity coefficient in a multicomponent system is:

$$\ln \gamma_k = 1 - \ln\left(\sum_{j=1}^{n} x_j \cdot \Lambda_{kj}\right) - \sum_{i=1}^{n} \frac{x_i \cdot \Lambda_{ik}}{\sum_{j=1}^{n} x_j \cdot \Lambda_{ij}} \qquad \textbf{(A1)}$$

where:

$$\Lambda_{ij} = \frac{v_j^L}{v_i^L} \exp\left[\frac{-(\lambda_{ij}-\lambda_{ii})}{R \cdot T}\right] \qquad \textbf{(A2)}$$

and v^L refers to the liquid molar volume. In general, it is assumed that $\Lambda_{ij} \neq \Lambda_{ji}$, $\Lambda_{ii}=\Lambda_{jj}=1$ and $\lambda_{ij}=\lambda_{ji}$.

The Wilson parameters Λ_{ij} for the binary systems HNO_3-H_2O, H_2SO_4-H_2O, and HNO_3-H_2SO_4 were calculated from a series of experimental isothermal and isobaric vapour-liquid equilibrium data points by means of the corrected Gauss-Newton non-linear least squares method in conjunction with either of the following objective functions O.F:

$$O.F = \sum_{i=1}^{n} \left(\frac{P_{exp.} - P_{calc.}}{P_{exp.}}\right)_i^2 \qquad \textbf{(A3)}$$

$$O.F = \sum_{i=1}^{n} (1 - y_{1,calc.} - y_{2,calc.})_i^2 \qquad \textbf{(A4)}$$

The calculation of the objective functions given in Eqs. A3 and A4 requires only the values of x and the total pressure at constant temperature or the values of y and temperature at constant total pressure. The values are listed in Table A1. The experimental data sets used were: isothermal data at 298.2 K from Hàla *et al.* (1968) for the nitric acid-water system and for the sulphuric acid-water system and further data from Bosen and Engels (1988). Vapour-liquid-equilibria data for the nitric acid-sulphuric acid system are extremly scarce due to the impossibility to obtain pure anhydrous sulphuric acid under normal conditions. A series of liquid activity

coefficients over a range of liquid compositions at 298.2 K in the binary mixture HNO_3-H_2SO_4 were found in Fénéant and Chédin (1956). The ternary system was checked against experimental data from Guarise (1966) showing that the calculated activity coefficients for nitric acid and water were in good agreement with the experimental values, see Al-Khudhairy and Zaldívar (1989). Future efforts should be directed towards the use of more realistic functions that correctly represent the complex behaviour of nitric acid, sulphuric and water mixtures.

Table A1. Wilson's energy constants (cal./g-mol) and parameters. P=1.bar.

Binary System	$\lambda_{12}-\lambda_{11}$	$\lambda_{21}-\lambda_{22}$	Λ_{12}	Λ_{21}	T (K)
HNO_3-H_2O	-1309.58	-971.42	3.8	12.38	298.2
H_2SO_4-H_2O	-3870.0	-1812.0	9.97	12.06	581.3
HNO_3-H_2SO_4	-1127.85	1127.85	8.56	0.117	298.2

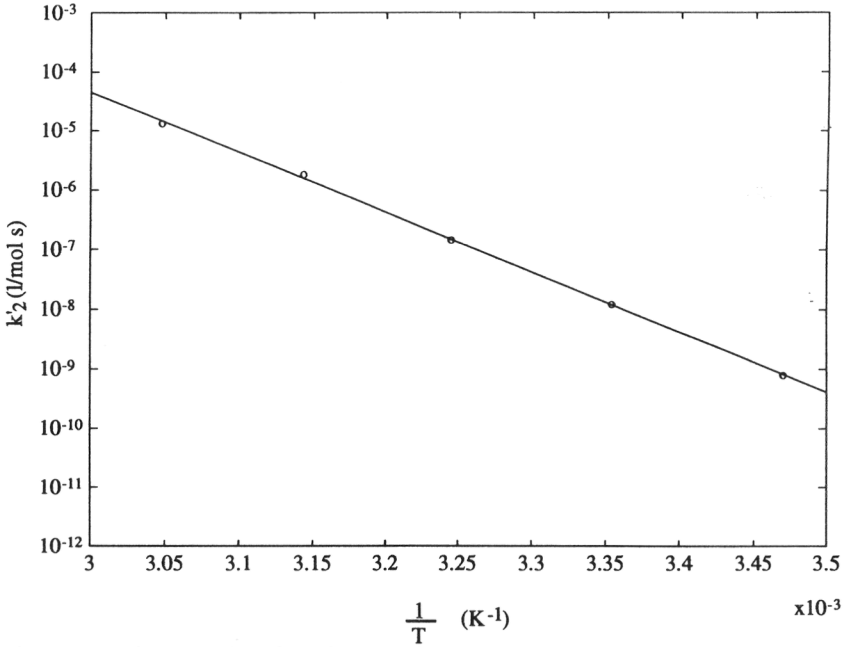

Figure A1. Arrhenius plot of k'_2 for chlorobenzene. Experimental data from Chapman and Strachan (1976). ln A = 59.451, Ea/R=23160.

Appendix 2. Calculation of the reaction rate constant k'_2 for chlorobenzene at different temperatures using the H_R function.

In order to derive the reaction rate constant k'_2 related to the mechanism described in this paper, it is necessary to assume this constant is independent of the acidity of the acid phase and only depends on the aromatic compound and the temperature:

$$\log k'_2 = \log k_2 - \log K - \log \gamma_{HNO_3 \cdot H_2O} + (H_R + \log a_{H_2O}) \qquad \text{(A5)}$$

Table A2 and Figure A1 illustrate for chlorobenzene the calculation of k'_2 using experimental data at different temperatures.

Table A2. Calculation of the temperature dependence of k'_2 as a function of experimental data, for chlorobenzene.

T (K)	x	C_{HNO_3}	log k_2	$(H_R+\log a_{H_2O})$	log K	log $\gamma_{HNO_3 \cdot H_2O}$	log k'_2
288.2	79.45	0.019	2.111	-17.017	-5.630	-0.178	-9.099
298.2	79.45	0.019	2.408	-15.950	-5.441	-0.191	-7.910
308.2	79.45	0.019	2.657	-14.953	-5.264	-0.205	-6.826
318.2	79.45	0.019	2.971	-14.018	-5.099	-0.219	-5.729
328.2	79.45	0.019	3.086	-13.140	-4.943	-0.232	-4.878

Appendix 3. Calculation of the reaction rate constant k'_2 for toluene at different temperatures using the M_c function.

In order to derive the reaction rate constant k'_2 and n related to the mechanism described in this paper it is necessary to assume that k'_2 is independent of the acidity of the acid phase and only depends on the aromatic compound and the temperature:

$$\log k'_2 - n \cdot M_c = \log k_2 + \log\left(\frac{K_{HNO_3}}{C_{H^+} \cdot 10^{-0.571 \cdot M_c}} + \frac{C_{H^+} \cdot 10^{-2.542 \cdot M_c}}{a_{H_2O} \cdot K_{NO_2^+}} + 1 \right) + \log \frac{a_{H_2O} \cdot K_{NO_2^+}}{C_{H^+} \cdot 10^{-2.542 \cdot M_c}}$$

(A6)

Table A3 and Figure A2 illustrate for toluene the calculation of k'_2 using experimental data at different temperatures.

Table A3. Calculation of the temperature dependence of k'_2 as a function of experimental data, for toluene.

T (K)	x	C_{HNO_3}	log k_2	$n \cdot M_c$	log val_1+log val_2	log k'_2
288.2	70.2	0.013	3.2095	-0.7712	4.052	6.4904
293.2	70.2	0.013	3.3674	-0.7548	4.002	6.6148
298.2	70.2	0.013	3.5276	-0.7388	3.954	6.7430
303.2	70.2	0.013	3.7193	-0.7234	3.908	6.9039
308.2	70.2	0.013	3.8000	-0.7084	3.863	6.9550

For benzene the Arrhenius plot was calculated from E_a and A values reported by Coombes et al. (1968).

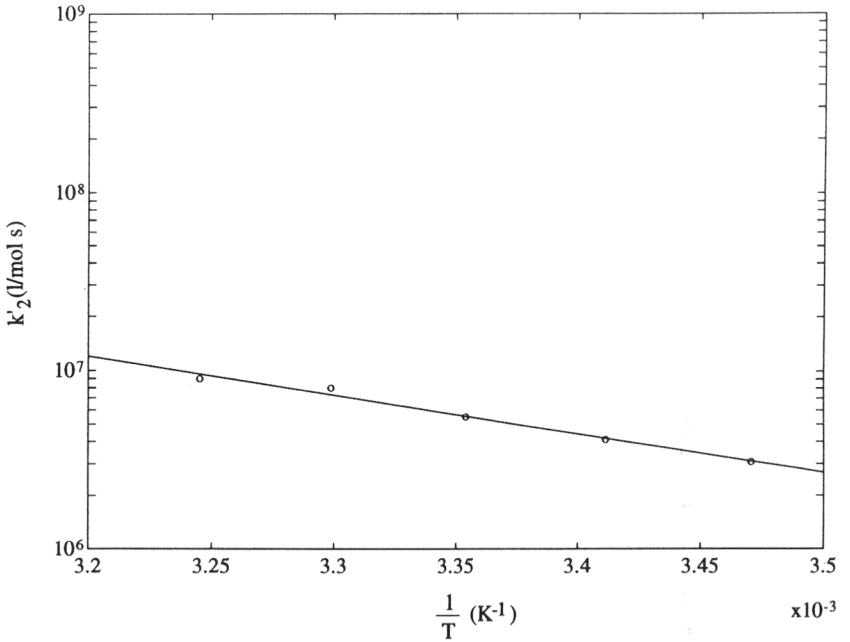

Figure A2. Arrhenius plot of k'_2 for toluene. Experimental data from Sheats and Strachan (1978). ln A = 32.264, E_a/R=4990.

Appendix 4. Physical and transport properties in HNO_3-H_2SO_4-H_2O mixtures.

The following correlations were employed to calculate the physical and transport properties for the mixed acid:

Volume: The volume of the mixed acid as a function of composition and temperature has been calculated with:

$$V = \sum_{i=1}^{3} n_i \cdot v_i^L \qquad \text{(A7)}$$

where v^L_i refers to the liquid molar volume of the i-th compound, that can be correlated by:

$$v_i^L = A \cdot B^{\left(1 - \frac{T}{C}\right)^{0.2857}} \qquad \text{(A8)}$$

where A, B and C are the constants given in Table A4, as obtained by fitting experimental data from Miller *et al.* (1964) and from Perry and Chilton (1984).

Table A4. Constants for the calculation of mixed acid volume.

Compound	A	B	C
H_2O	0.0458	0.3099	647.4
HNO_3	0.1187	0.2508	580.1
H_2SO_4	0.1910	0.2212	995.4

Viscosity: The expression of Van Velzen *et al.* (1972) was used for pure liquids:

$$\log \mu_i = B\left(\frac{1}{T} - \frac{1}{T_0}\right) \qquad \text{(A9)}$$

where B and T_0 are the constants as given in Table A5, and as obtained from experimental data in Perry and Chilton (1984).

Table A5. Constants for the calculation of mixed acid viscosity.

Compound	B	T_0
H_2O	80.239	139.78
HNO_3	843.16	147.16
H_2SO_4	1235.2	211.74

The total viscosity in terms of individual viscosities was calculated using:

$$\log \mu_T = \sum_{i=1}^{3} x_i \cdot \log \mu_i \qquad \text{(A10)}$$

where x_i refers the wt. % of the compound. The viscosity obtained by eq. A10 has been corrected by us using experimental data from Ismail and Hanson (1973) and Cox and Strachan (1972), to this end we used a second order polynomial expression:

$$\mu_{\text{mixed acid}} = 9.676 - 2.516 \cdot \mu_T + 0.315 \cdot \mu_T^2 \qquad \text{(A11)}$$

in this case the viscosity is expressed in cP.

Appendix 5. Physical and transport properties of the organic phase.

The following correlations were employed to calculate the physical and transport properties of the organic phase mixtures:

Volume : Equations A7 and A8 have been used for the calculation of the volume of the organic phase mixtures. The values for the constants A, B, and C are given in Table A6.

Viscosity : Equation A9 has been used for the calculation of the viscosity of the pure compounds in the organic phase. The values for the constants B and T_0 are given in Table A7. The viscosity of the organic phase itself has been calculated with eq. A10.

Table A6. Constants for the calculation of the organic phase volume.

Compound	A	B	C
Benzene	$2.560 \cdot 10^{-1}$	0.271	562.2
Nitrobenzene	$3.354 \cdot 10^{-1}$	0.251	712.0
Toluene	$3.195 \cdot 10^{-1}$	0.262	592.0
o-MNT	$3.976 \cdot 10^{-1}$	0.248	720.0
m-MNT	$3.976 \cdot 10^{-1}$	0.248	725.0
p-MNT	$3.976 \cdot 10^{-1}$	0.248	735.0
Chlorobenzene	$3.037 \cdot 10^{-1}$	0.271	632.4
o-MNC	$8.682 \cdot 10^{-3}$	0.0	805.9
m-MNC	$8.524 \cdot 10^{-3}$	0.0	789.7
p-MNC	$8.238 \cdot 10^{-3}$	0.0	799.8

Table A7. Constants for the calculation of the organic phase viscosity

Compound	B	T_0
Benzene	555.61	136.20
Nitrobenzene	735.54	174.88
Toluene	484.90	99.26
o-MNT	754.37	145.32
m-MNT	716.39	140.86
p-MNT	680.15	137.06
Chlorobenzene	497.81	103.93
o-MNC	691.38	179.27
m-MNC	691.38	179.27
p-MNC	691.38	179.27

CHAPTER 5

AROMATIC NITRATIONS BY MIXED ACID. FAST LIQUID-LIQUID REACTION REGIME

ABSTRACT

Aromatic nitrations by mixed acid have been selected as a specific case of a heterogeneous liquid-liquid reaction. An extensive experimental programme has been followed using adiabatic and heat flow calorimetry and pilot reactor experiments, supported by chemical analysis. A series of nitration experiments have been carried out to study the influence of different initial and operating conditions such as temperature, stirring speed, feed rate and sulphuric acid concentration. In parallel a mathematical model to predict the overall conversion rate has been developed. In this paper the mathematical modelling, implementation and experimental validation for mononitrations of benzene, toluene and chlorobenzene in the mass transfer controled regime of fast liquid-liquid reaction is presented and discussed.

Keywords.
Aromatic nitrations, fast liquid-liquid reactions, heterogeneous dispersions

1. INTRODUCTION

Despite the fact that aromatic nitrations in mixed acid were one of the earliest unit processes to be operated on a large scale - when the heavy organic chemical industry started its development by the end of last century - many questions remain to be answered, particularly in discontinuous reactors. The dynamic behaviour of aromatic nitrations in semibatch processes involve a considerable number of problems because in these heterogeneous liquid-liquid dispersions chemical reaction and mass transfer phenomena occur simultaneously. Furthermore, as the nitration proceeds, the acid phase composition varies and the observed second-order rate constant decreases appreciably, see Schofield (1980).

In previous work, see Zaldívar *et al.* (1995), the mechanistic aspects of homogeneous aromatic nitrations were studied to check their validity under heterogeneous conditions and with high nitric acid concentrations. To that end, the slow liquid-liquid reaction regime was chosen. In such a regime, i.e. low sulphuric acid strengths, the rate of mass transfer is not enhanced by reaction and the reactions proceed in the bulk of reaction phase, not in the boundary layer.

As we increase the sulphuric acid strength the nitration rate constant increases and the heterogeneous system enters into the fast regime. In this situation the rate of reaction is affected not only by the physical and chemical characteristics of the system, but also by the mechanical features of the equipment, see Westerterp *et al.* (1984). The former includes viscosities and densities of the phases, interfacial surface properties, diffusion coefficients, distribution coefficients of reagents and products between phases and chemical reaction constants. The latter include, for example, the type and diameter of the impeller, vessel geometry, the flow rate of each phase and the rotational speed of the impeller. Furthermore, dispersion phenomena such as coalescence and breakage of droplets, drop size distribution and phase inversion phenomena will affect the extent of conversion and the selectivity of the reactions, see Villermaux (1981).

To take into account such parameters experiments have been performed to characterise separately their influence, when possible. The interfacial area for our equipment was characterised using a similar non-reactive system, see Molga *et al.* (1994). Furthermore, nitration experiments of benzene, toluene and chlorobenzene in the fast regime were carried out to compare to the model predictions. The model employed, based on the effective interfacial area between the two liquids and the description of mass transfer with reaction using the film model is the most common approach. Theoretical model predictions are compared with experimental results and the effect of the different parameters is discussed. From the comparisons between model and experimental results it can be concluded it is possible to extrapolate data from homogeneous nitration experiments to heterogeneous systems and to interpret the dynamic behaviour of discontinuous nitration processes of benzene, toluene and chlorobenzene in different reaction regimes.

2. INTERFACIAL AREA MEASUREMENT AND ESTIMATION

The effective interfacial area is an important parameter which determines the efficiency and capacity of agitated liquid-liquid contactors; it is normally evaluated by the expression:

$$a = \frac{6 \cdot \varepsilon_d}{d_{32}} \qquad (1)$$

where ε_d is the fraction of dispersed phase and d_{32} is the Sauter mean diameter which can be computed as:

$$d_{32} = \frac{\sum_i n_i \cdot d_i^3}{\sum_i n_i \cdot d_i^2} \qquad (2)$$

where n_i is the number of droplets with a diameter d_i. The Sauter mean diameter cannot be evaluated through a simple analysis. Therefore, it is customary to evaluate the maximum stable diameter d_{max} encountered in the impeller zone of the vessel and multiply it by an empirical factor to obtain d_{32} , see Sprow (1967).

A liquid-liquid dispersion formed in an agitated vessel is characterised by a dynamic equilibrium between drop breakup and coalescence. The droplet size distribution and the interfacial area depend on the conditions of agitation and the physical properties of the system. The microscopic phenomena occurring in an agitated vessel are extremely complex. The exact mechanism of coalescence and breakage in systems of droplets is generally not very well understood, see e.g. Kumar *et al.* (1993). Drops are believed to be broken up in regions of high shear stress near the agitator blades or due to turbulent velocity and pressure variations along the surface of a single drop. On the other hand, coalescence occurs when drops collide and the collision happens to be "efficient", i.e. the amplitude of the fluctuation is high enough to overcome the resistance of the liquid film separating the drops.

A fairly extensive literature exist with regard to the average drop size obtained in dispersions. Semiempirical correlations are based on the local isotropy concept of Kolmogorov (1949) who proposed breakup of a drop occurs when the ratio of inertial stress to the elastic stress exceeds a critical value. Kolmogorov's expression for d_{max} is:

$$\frac{d_{max}}{D_a} = c_1 \cdot We^{-0.6} \qquad (3)$$

where We is the Weber number of the main flow, defined as:

$$We = \frac{\rho_c \cdot n_a^2 \cdot D_a^3}{\sigma} \qquad (4)$$

This expression cannot be used when the dispersed phase hold-up is larger than 0.05 or when the dispersed phase is viscous, because the deformation rate was neglected. To take into account these restrictions, various expressions to calculate d_{max} or d_{32} have been proposed,

see a.o. Coulaloglu and Tavlarides (1976) and Tavlarides and Stamatoudis (1981). The general form of the correlations is:

$$\frac{d_{32}}{D_a} = A \cdot f(\varepsilon_d)\, We^{-0.6} \qquad (5)$$

where $f(\varepsilon_d)$ normally reprersents a linear correlation of the volume fraction of dispersed phase:

$$f(\varepsilon_d) = 1 + B \cdot \varepsilon_d \qquad (6)$$

The constant B in eq. (6) can vary between 2.0 to 9.0 for dispersions where $\varepsilon_d < 0.2$, see Tavlarides and Stamatoudis (1981). In a recent study Brooks and Richmond (1994) showed that correlations of this type will become very inaccurate for $\varepsilon_d > 0.3$ and that the theoretical correlation developed by Delichatsios and Probstein (1976) should be used instead. In this case, the function of dispersed phase volumetric fraction $f(\varepsilon_d)$ is according to these authors:

$$f(\varepsilon_d) = \left(\frac{\ln(c_2 + c_3 \cdot \varepsilon_d)}{\ln c_2} \right)^{\frac{-3}{5}} \qquad (7)$$

where $c_2 = 0.011$ is a constant related to the cut-off velocity in the Gaussian probability function and c_3 is a constant proportional to the ratio of coalescence to break-up coefficients. c_3 allows for differences in collision efficiencies in different systems. The value of c_3 must be determined empirically and will differ from system to system; however, it should be of the order of 1.0.

The first objective of this work is to estimate the values of the interfacial area at similar conditions as during semibatch aromatic nitration experiments and to find a suitable correlation to predict the interfacial area for the bench-scale reactor, in which nitrations are carried out.

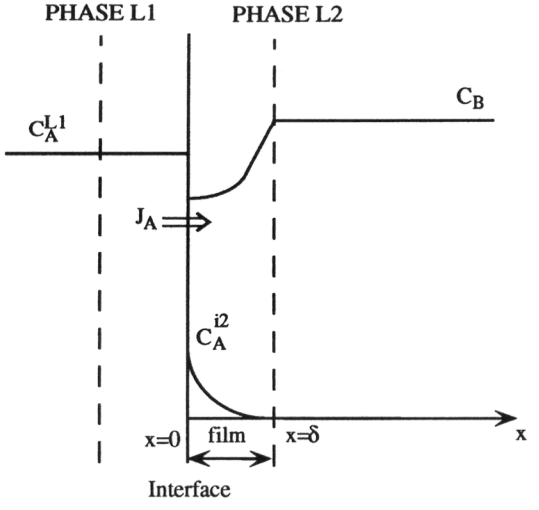

Figure 1. Concentrations profiles for chemically enhanced extraction

2.1. Determination by the chemical method. The theory

Numerous methods have been developed for the determination of the interfacial area. A few physical methods are employed such as optical techniques like light scattering or reflection and photographic or conductivity methods, see a. o. Calderbank (1958). In all these methods a local value of the interfacial area is determined.

Since its introduction the chemical method developed by Westerterp *et al.* (1963) has been widely used to determine the interfacial area in both gas-liquid and liquid-liquid systems. The application to liquid-liquid systems is based on a chemically enhanced extraction of reactant A from liquid phase L1 to liquid phase L2, in which an irreversible reaction takes place with reactant B which does not penetrate into phase L1, see fig.1.

The general equation for the molar flux of component A is - according to the Danckwerts penetration model - equal to:

$$J_A = \frac{k_{L2}\sqrt{1+Ha^2}\left(m\cdot C_A^{L1} - \frac{C_A^{L2}}{1+Ha^2}\right)}{1+\frac{m\cdot k_{L2}\sqrt{1+Ha^2}}{k_{L1}}} \qquad (8)$$

For a second order reaction the consumption rate of the component A is given as:

$$r = k_{1,1}\ C_B\ C_A^{L2} \qquad (9)$$

and the Hatta number is equal to:

$$Ha = \frac{\sqrt{k_{1,1}\cdot C_B\cdot D_A}}{k_{L2}} \qquad (10)$$

Equation (8) can be simplified at constant C_B over the film giving:

$$J_A = C_A^{i2}\sqrt{k\cdot D_A} = C_A^{L1}\cdot m\sqrt{k\cdot D_A} \qquad (11)$$

when the following conditions hold:

- The reaction is sufficiently fast to consume all A in the film, so that the concentration C_A in the bulk of phase L2 equals zero.
- The solubility of A in phase L2 is very low so mass transfer limitations in phase L1 can be neglected and the concentration of A at the interphase equals $C_A^{i2} = m\cdot C_A^{L1}$.
- Practically no depletion of component B is observed so $C_B \approx$ constant and the pseudo-first order reaction rate constant can be assumed to be $k = k_{1,1}\cdot C_B$.
- The reaction is so fast that holds:

$$Ha = \frac{\sqrt{k_{1,1}\cdot C_B\cdot D_A}}{k_{L2}} = \frac{\sqrt{k\cdot D_A}}{k_{L2}} > 3$$

Under the above listed conditions according to eq. (11) the extraction flux J_A is a unique function of the physico-chemical properties of the system and independent of the hydrodynamics conditions. Hence, the term $m\sqrt{(k\cdot D_A)}$ in eq. (11) can be determined separately in a liquid-liquid contactor with a well known interfacial area, e.g. in a stirred cell. Then the

effective interfacial area in any liquid-liquid stirred system can be determined if the same above mentioned conditions are valid in such a system.

In this work the extraction of diisobutylene (DIB) from a toluene solution into aqueous sulphuric acid has been chosen to measure the interfacial area, as recommended by Sankholkar and Sharma (1973), because the physico-chemical properties of the chosen system are supposed to be very similar to the toluene mononitration and other nitrations of aromatic compounds.

2.2. Experimental determination by the chemical method

As a small modification we used an isomer mixture containing 2,4,4-trimethyl-1-pentene DIB-1 and 2,4,4-trimethyl-2-pentene DIB-2 in our experiments instead of the pure DIB-2 isomer used by Sankholkar and Sharma (1973). A pure grade isomer mixture of DIB-1 and DIB-2 with a ratio of 3:1 supplied by Fluka was used in all experiments. Preliminary tests indicated that the specific extraction rate of DIB-2 from the isomer mixture is only around 6% higher compared to that measured for pure DIB-2 at the same conditions by Sankholkar and Sharma (1973). It has also been found that DIB-1 isomer reacts in a similar way as DIB-2 and the ratio of the characteristic terms $m_i\sqrt{(k_i \cdot D_i)}$ for DIB-1 and DIB-2, respectively, equals 0.703 for a 77 wt. % solution of sulphuric acid, so in all experiments the effective interfacial area could be determined following the concentration decrease of DIB-1 or DIB-2 separately as well as the total concentration of DIB in the organic phase.

Analysis of DIB in the organic phase was performed with a Carlo Erba Instruments GC 6000 Vega Series gas chromatograph equipped with 15m of a 0.3mm fused silica capillary column with the so called stationary phase SE 52. A Krüss Interfacial Tensiometer K8 was used to measure by the ring method the interfacial tension between the organic phase and the sulphuric acid solution. An average value of 18.75 mN/m was obtained at 308.2 K. Experiments were performed in a stirred cell and in a RC1 reactor calorimeter; the characteristics of the equipment are given in Table 1. All experiments were carried out under isothermal conditions at 308.2 K.

Table 1. Characteristics of the equipment.

Vessel	Diameter T (mm)	Height H (mm)	Volume V (l)	Agitator type	Impeller Diameter D_a (mm)	Impeller speed n_a (s^{-1})
Stirred cell SC	35	100	0.1	TBSP	30	1-2
Reactor RC1	115	200	2.0	FB45IP	59	6.6-13.3

TBSP - two-bladed straight paddle, unbaffled
FB45IP - four-bladed 45° inclined paddle, unbaffled

- *Determination of $m\sqrt{(k \cdot D_A)}$ in stirred cell measurements:*

The organic phase containing 7 mol % of a DIB isomer mixture in toluene was contacted in the stirred cell with a known interfacial area of $F_{sc} = 0.9 \cdot 10^{-3}$ m^2 with a 77 wt % aqueous solution

of sulphuric acid. To follow the concentration decrease of DIB in the organic phase in a reasonable time the volume of organic phase was always taken as small as 3.3 ml while the volume of sulphuric acid solution was 25 ml. Only the aqueous phase in the bottom part was continuously stirred to renew the interface without a pronounced vortex. The stirring rate was varied in the different experiments, samples of the organic phase with a volume of about 2 to 3 μl were taken and the concentration changes were followed by the chromatographic analysis of the organic phase composition.

Table 2. Values of $m\sqrt{(k \cdot D_A)}$ obtained in a stirred cell and in a RC1 reactor. T =308.2 K, 77 wt. % sulphuric acid, and 7 mol % DIB -isomer mixture 3 DIB-1 to 1 DIB-2- in toluene.

Run	Vessel	n_a (s^{-1})	$m\sqrt{(k \cdot D_A)} \cdot 10^9$ (m/s)
IFA_1	SC	0.93	12.6
IFA_2	SC	1.70	14.7
IFA_3	SC	1.33	12.1
IFA_4	SC	1.38	14.9
IFA_5	RC1	0.83	13.1
IFA_6	RC1	0.83	14.7

Average value taken for calculations, $m\sqrt{(k \cdot D_A)} = 13.51 \cdot 10^{-9}$ m/s

The mass balance for DIB in the organic phase can be written as follows:

$$V_o \frac{dC}{dt} = -F_{sc} \cdot C \cdot m\sqrt{k \cdot D_A} \qquad (12)$$

After integration of eq. (12) we can express the concentration of DIB in organic phase in relation to toluene as a function of time:

$$\ln \frac{C_A}{C_{To}} = \ln \frac{C_A^0}{C_{To}} - \frac{F_{sc}}{V_o} m\sqrt{k \cdot D_A}\, t \qquad (13)$$

Limitations of the assumed quasi-steady state and of the application of eq. (11) for interfacial area measurements are discussed in Appendix 1.

Typical plots as obtained from measurements in the stirred cell for DIB-1 and DIB-2 as well as for the isomer mixture are shown in fig.2. The straight line relationships indicate that the isomer mixture of DIB can be used for interfacial area measurements and that the $m\sqrt{(k \cdot D_A)}$ value determined for the total concentration of DIB is a weighted average of the individual values of $m\sqrt{(k \cdot D_A)}$ obtained for DIB-1 and DIB-2 isomers, respectively. The $m\sqrt{(k \cdot D_A)}$ values obtained from the measurements performed in the stirred cell are shown in Table 2. For control purposes two similar experiments were performed in the RC1 reactor as also listed in Table 2. We can conclude the $m\sqrt{(k \cdot D_A)}$ values do not depend on stirrer speed nor vessel geometry. This indicates that the assumption about the absence of mass transfer resistances in the organic phase holds, because of the low solubility of DIB in the aqueous phase. According to Sankholkar and Sharma (1973) the solubility of DIB in water is of order of 10^{-5} kmol/m^3 at 303.2 K.

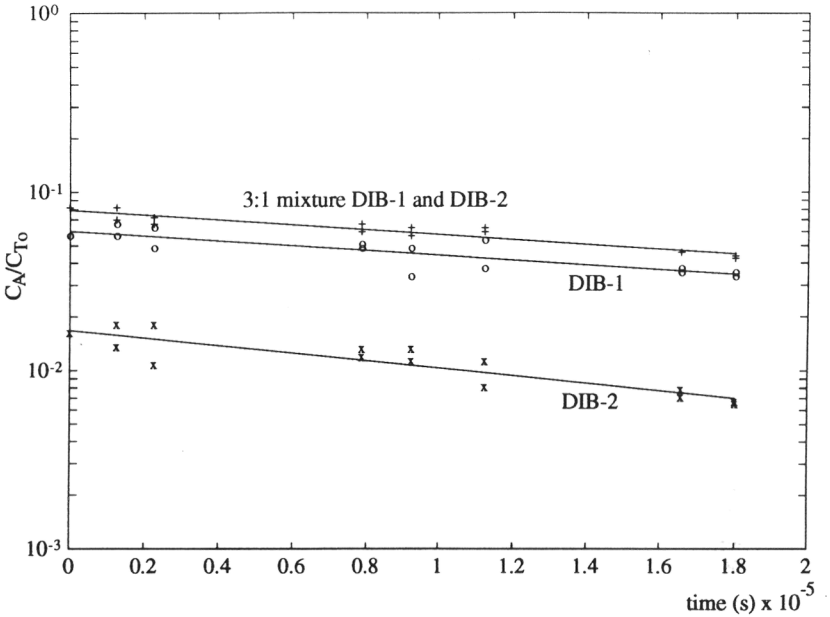

Figure 2. Individual and total concentrations of diisobutylenes vs. time measured during a stirred cell experiment.

- Interfacial area measurements in semibatch systems:

The purpose of this study was to check whether the correlations for droplets diameters as determined batchwise and at low dispersed phase volumetric fractions may be applied in semibatch reactors.

A series of experiments has been performed in a bench-scale RC1 reactor at three different agitator speeds. In each experiment two periods can be distinguished; the semibatch one while the acid phase is being added continuously to the reactor containing only organic phase at the start and after that the batch period, while the reaction continues in the dispersion after stopping the acid addition. The temperature of the reactor contents is kept constant during the experiments. Liquid samples of a volume of 1-2 ml are taken during both the semibatch and batch periods to follow the reaction progress.

In the batch period according to eq. 13 the slope K of a line plotted in the $\ln(C_A/C_{To})$ vs. time domain equals:

$$K = -\frac{F \cdot m\sqrt{k \cdot D_A}}{V_o} \qquad (14)$$

The effective interfacial area F in the vessel can be determined knowing the organic phase volume V_O as well as the previously determined value of $m\sqrt{(k \cdot D_A)}$. The interfacial area 'a'

related to the total volume V_m of the dispersion at the end of acid addition can be calculated as follows:

$$a = \frac{F}{V_m} = \frac{F}{V_o + V_a} \tag{15}$$

In the semibatch period the sulphuric acid solution of 77 % wt. is added continuously with a constant feed rate q_a into the reactor filled at the start with the organic phase, consisting of the isomer mixture of DIB and toluene, i.e. the conditions during semibatch nitrations were reproduced. The effective interfacial area as well as the mean droplet diameter can be determined as a function of the reaction time and volume fraction of the dispersed phase in the dispersion ε_d.

Assuming ideal mixing and absence of segregation, i.e. immediate homogenisation of the freshly added amount of acid solution, the mass balance of DIB in the organic phase can be written as:

$$V_o \frac{dC_A}{dt} = -F(t) \cdot J_A \tag{16}$$

where the specific extraction rate per unit of surface area J_A is expressed as in eq. (11). Also in this case the conditions for mass transfer with a fast pseudo-first order reaction are supposed to hold -see Appendix 1. Assuming additionally that the average droplet size equals the Sauter diameter, we can introduce:

$$F(t) = \frac{6 \cdot q_a \cdot t}{d_{32}(t)} \tag{17}$$

where t is the time measured as from the start of the acid addition.

Supposing that the organic continuous phase volume does not change and that the acid phase is fed at a constant rate, we obtain after integration:

$$\ln \frac{C_A}{C_{To}} = \ln \frac{C_A^0}{C_{To}} - \frac{6 \cdot q_a \cdot m \sqrt{k \cdot D_A}}{V_o} \int_0^t \frac{t}{d_{32}(t)} dt \tag{18}$$

Since the physico-chemical properties of the system and the stirrer speed can be assumed to be approximately constant during an experiment, the Weber number also will be constant. Furthermore, if d_{32} is given by:

$$d_{32} = A \cdot f(\varepsilon_d) \cdot We^{-0.6} \cdot D_a \tag{19}$$

we can calculate the constants for our system. Two types of correlations to estimate the interfacial area in semibatch system have been considered:

- A linear correlation, see eq. 6, which is based on the assumption that the linear correlation for d_{32}, as a function of the volume fraction of the dispersed phase as obtained in batch or in continuous flow systems, can be applied also in semibatch systems; only the values of constants A and B have to be fitted.

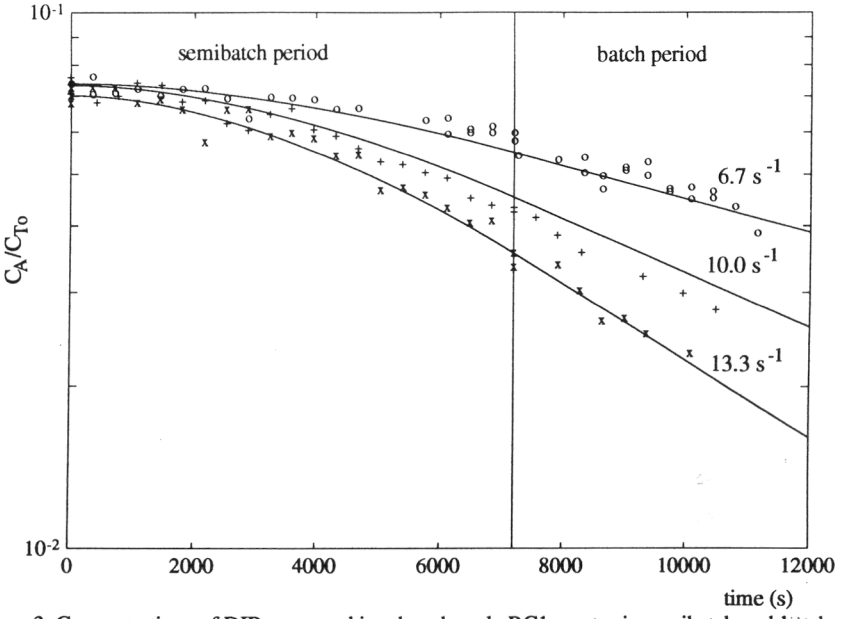

Figure 3. Concentrations of DIB measured in a bench scale RC1 reactor in semibatch and batch mode: experimental points and lines as calculated with Eqs. 18 and 20.

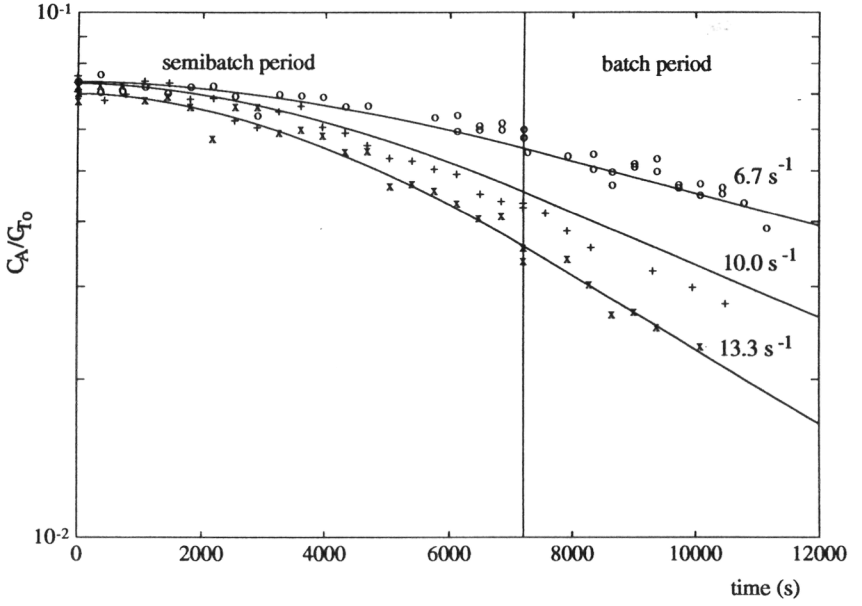

Figure 4. Concentrations of DIB measured in a bench scale RC1 reactor in semibatch and batch mode: experimental points and lines as calculated with Eqs. 18 and 21.

- The correlation of Delichatsios and Probstein, see eq. 7, in which A and c_3 have to be fitted.

For the first method, introducing eq. 19 into eq. 18, we obtain the following integral:

$$\int_0^t \frac{t}{d_{32}(t)}\,dt = \frac{1}{A\cdot Da\cdot We^{-0.6}} \int_0^t \frac{V_o\cdot t + q_a\cdot t^2}{V_o + q_a\,(1+B)\,t}\,dt \qquad (20)$$

which can be calculated analytically. The unknown constants A and B can be found with non-linear regression, fitting the analytical expression to the experimental data. Calculations indicated that, due to the form of eq. 20 and the scatter of the experimental data, the quality of the fit was independent of the value of B in the range of $1< B < 10$. Therefore, a value of B=2 was taken arbitrarily, in accordance to the correlation of Okufi *et al.* (1990); for A an optimal value of 0.3512 was obtained. The experimental and calculated values are shown in fig. 3.

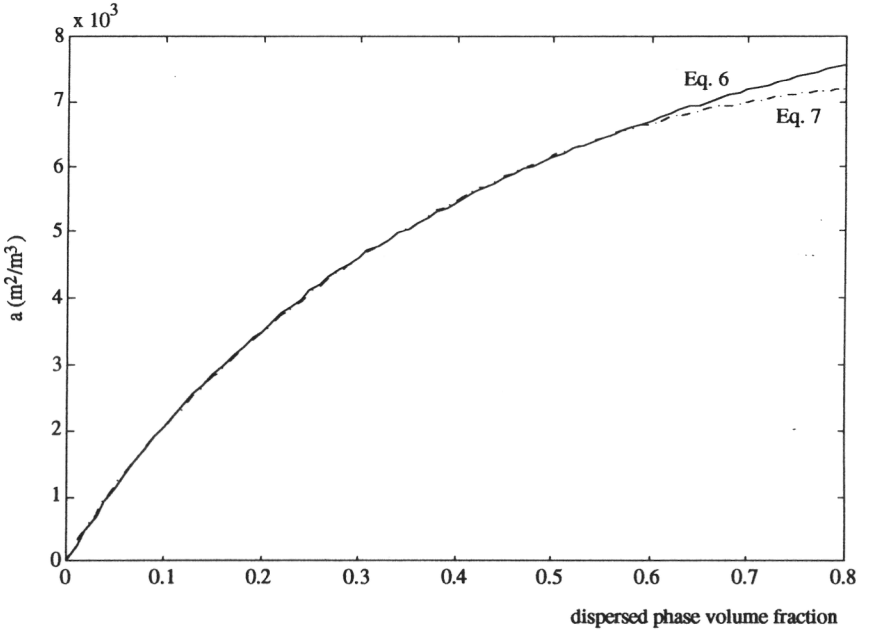

Figure 5. Calculated interfacial areas, Eq. 19, at 13.3 rps for the system DIB,Toluene-77 % wt sulphuric acid using fitted parameters for the linear correlation, Eq. 6, and that of Delichatsios and Probstein, Eq. 7.

In the second case, the integral expression is more complex, see eq. 21, and does not have an analytical solution. However, it can be solved numerically and the unknown constant can be fitted using non-linear regression techniques. The values obtained in this case were A=0.3029 and c_3=0.63563, see fig.4.

$$\int_0^t \frac{t}{d_{32}(t)}\,dt = \frac{1}{A\cdot Da\cdot We^{-0.6}\cdot \ln(c_3)^{\frac{3}{5}}} \int_0^t t\left[\ln\left(c_2+\frac{c_3\cdot q_a\cdot t}{V_o+q_a\cdot t}\right)\right]^{-\frac{3}{5}} dt \qquad (21)$$

Both equations produce similar errors. In fact, the interfacial area calculated at Na=13.3 s^{-1} using Eqs. 5 and 6 shows that both correlations produce similar results up to $\varepsilon_d < 0.6$, see fig. 5.

The correlation obtained for the system toluene-DIB and 77 wt. % sulphuric acid has been used to predict the interfacial area during aromatic nitrations using the correlations developed for the estimation of the interfacial tension, see Appendix 3.

3. OVERALL CONVERSION RATE FOR FAST NITRATION REGIME

Benzene, toluene and chlorobenzene nitrations under normal industrial conditions, typically with 15 mol % HNO_3, 30 mol % H_2SO_4 and 55 mol % H_2O, occurs in a two-phase system in which the organic phase is contacted with the mixed acid by agitation. Under these conditions, as has been confirmed by e.g. Schofield (1980), the reaction in the organic phase is negligible and the nitronium ion mechanism is applicable.

In order to develop an overall conversion expression, the following assumptions were made:

- Negligible mass transfer resistance in the organic phase, see Westerterp *et al.* (1984), if:

$$\frac{k_{L1}}{k_{L2}\cdot m\cdot E} >> 1 \qquad (22)$$

In view of the low solubility of the studied aromatic compounds in mixed acid with m≈(0.2-0.4)·10^{-3}, and mass transfer coefficients in the organic and acid phase being of the same order of magnitude, see Laddha and Degaleesan (1976), the enhancement factor E should be of the order of 10^3 to make this assumption invalid. So in approaching the regime of instantaneous reactions the resistance in the organic phase will be relevant.

- The Hinterland ratio Al is >>1. Al is the ratio of the bulk volume to the film volume in the reaction phase. For the case of reaction in the dispersed phase Al can be expressed as:

$$Al = \frac{\frac{\pi}{6} d_{32}^3}{\frac{\pi}{6}\left[d_{32}^3 - \left(d_{32} - \frac{D_{ArH}}{k_L}\right)^3\right]} \qquad (23)$$

The evaluation of this ratio can be done by using the correlation of Kronig and Brink (1950) for the dispersed phase mass transfer coefficient:

$$k_{L2} \approx k_d = \frac{17.9\, D_{ArH}}{d_{32}} \qquad (24)$$

see Appendix 2 for the derivation. Replacing eq. 24 into eq. 23 gives a Hinterland ratio of 6.3. The main problem of a small Hinterland coefficient is that film theory assumes a constant C_{HNO_3} at x=δ. For small values of Al and at high conversion of nitric acid, deviation may be expected due to depletion of nitric acid concentration: for example in the center of a drop. However, according to a numerical analysis carried out by Brunson and Wellek (1971), even though the Hinterland ratio is relatively small, if the fluid sphere is a liquid the film theory may be used with confidence and the effect of the depletion of the reactant initially in the dispersed phase, i.e. nitric acid, neglected. This is due to the fact that in liquid drops, the depth of penetration in general is small compared to the diameter, so that deviations are small as well. These assumtions being valid the general approximated solution, see Westerterp *et al.* (1984), for an irreversible nitration of order (1,1) is:

$$J_{ArH} = k_{L2}\, C^{i2}_{ArH}\, E_{ArH0} \tag{25}$$

where the enhancement factor E_{ArH0} can be calculated by trial and error from:

$$E_{ArH0} = \frac{Ha\sqrt{\frac{E_{ArH\infty} - E_{ArH0}}{E_{ArH\infty} - 1}}}{\tanh Ha\sqrt{\frac{E_{ArH\infty} - E_{ArH0}}{E_{ArH\infty} - 1}}}\left(1 - \frac{C^{L2}_{ArH}}{C^{i2}_{ArH}\cosh Ha\sqrt{\frac{E_{ArH\infty} - E_{ArH0}}{E_{ArH\infty} - 1}}}\right) \tag{26}$$

the Hatta number Ha being defined as:

$$Ha = \frac{\sqrt{k_2 \cdot D_{ArH} \cdot C^{L2}_{HNO_3}}}{k_{L2}} \tag{27}$$

and $E_{ArH\infty}$, the maximum possible enhancement factor for instantaneous reactions, is given by:

$$E_{ArH\infty} = 1 + \frac{D_{HNO_3} C^{L2}_{HNO_3}}{D_{ArH} C^{i2}_{ArH}} \tag{28}$$

Three limiting solutions can be obtained, see Westerterp *et al.* (1984):

Slow liquid-liquid reactions: In this case the rate of mass transfer is not enhanced by the occurring reaction and the reactions mainly proceeds in the bulk of the reaction phase, i.e.,

$$J_{ArH} = k_{L2}(C^{i2}_{ArH} - C^{L2}_{ArH}) \tag{29}$$

For such situations, it must be checked that the condition Ha < 0.3 holds in the reactor and that the concentration drop over the film of the component transferred is less the 5 %, or $C^{L2}_{ArH}/C^{i2}_{ArH} > 0.95$, see Steensma and Westerterp (1988). In this case the overall conversion rate expression is:

$$R = \varepsilon_{L2} \cdot k_2 \cdot C^{L2}_{ArH} \cdot C^{L2}_{HNO_3} \tag{30}$$

Fast liquid-liquid reactions with Ha > 2: In this case the rate of mass transfer is enhanced by the reaction and the bulk of the acid phase in which the reaction takes place is no more

important, i.e. the concentration of the aromatic component transferred into the acid phase becomes negligible. If $2 < Ha << D_{HNO_3} \cdot C_{HNO_3} / D_{ArH} \cdot C^{i2}_{ArH}$ holds then E = Ha and the conversion rate becomes:

$$R = a \cdot k_{L2} \cdot E \cdot C^{i2}_{ArH} = a \cdot \sqrt{k_2 \cdot D_{ArH} \cdot C^{L2}_{HNO_3}} \cdot C^{i2}_{ArH} \qquad (31)$$

Hence, J_{ArH} is no longer dependent of the mass transfer coefficient. In case Ha is not much smaller than $D_{HNO_3} \cdot C_{HNO_3} / D_{ArH} \cdot C^{i2}_{ArH}$, diffusion limitation of HNO_3 occurs and the enhancement factor must be calculated by iteration using eq. (26). As in the cases studied $Al \cdot Ha^2 >> 1$,the approximation $C^{L2}_{ArH} \approx 0$ holds.

Instantaneous liquid-liquid reactions: Now the reaction rate is so high that the aromatic compound and the nitronium ion do not occur simultaneously at the same place and the reaction zone reduces to a plane in the boundary layer of the reaction phase. Here:

$$R = a \cdot k_{L2} \cdot E_{ArH\infty} \cdot C^{i2}_{ArH} \qquad (32)$$

In this case the concentration drop in the non-reaction phase becomes important if $E_{ArH\infty}$ approximates to high values, i.e. 10^3-10^4; under such circumstances the assumptions derived previously are not anymore valid.

By modifying the sulphuric acid strength, it is possible to work in different regimes. Moreover, in a semibatch process the regime of nitration may change from mass transfer control to chemical control; or in a di or tri-nitration process the aromatic ring will be deactivated by the introduction of the nitro group and as a consequence the regime may change.

4. EXPERIMENTAL STUDY: MODEL VERIFICATION USING REACTION CALORIMETRY

In this work the regime of fast liquid-liquid reactions was studied in a reaction calorimeter (RC1). This apparatus provides an accurate measurement of the heat removal from the reactor, which through a heat balance is used to determine the rate of heat generation in the reaction mass and hence the rate of conversion. The precision of this calorimetric evaluation, see Bonvin and Saner (1988), depends on the correct representation of all the secondary heat effects like heat losses, stirring power supply, heat taken up by reactor wall and dilution heat, see Zaldívar *et al.* (1990). Here, the heat of dilution, which does play an important role in the total heat generated during nitration, has been evaluated using a model developed in previous work, see Zaldívar *et al.*, (1992). Furthermore, selectivity and yields were directly determined from concentration measurements by gas chromatography, see Molga *et al.*, (1993) and then compared to the reaction rate determined by calorimetric measurements, see Hernández *et al.*, (1993). Hence, two independent experiments, based on calorimetric determination and chemical analysis, were employed to obtain the experimental values of the conversion rates.

The slow liquid-liquid reaction regime was studied in previous work, see Zaldívar et al. (1995), and it takes place when low sulphuric acid strengths, i.e. below 60 % wt. H_2SO_4, are used.

The experiments in the reaction calorimeter were carried out in such a way as to assure the overall reaction rate was mass transfer controlled at least during the first part of the reaction. These conditions were achieved by operating in a semibatch mode and by using mixed acid of a high sulphuric acid strength of 70-80 wt. % H_2SO_4 in water. The operating conditions are summarised in Table 3.

Table 3. Isothermal nitration experiments in the mass transfer regime: operating and initial conditions.

Compounds	Temperatures (K)	x (% wt)	n_a (s^{-1})	Feeding time (hr)
Benzene, Toluene and Chlorobenzene	298.2-318.2	70-80	6.67-13.3	2-4

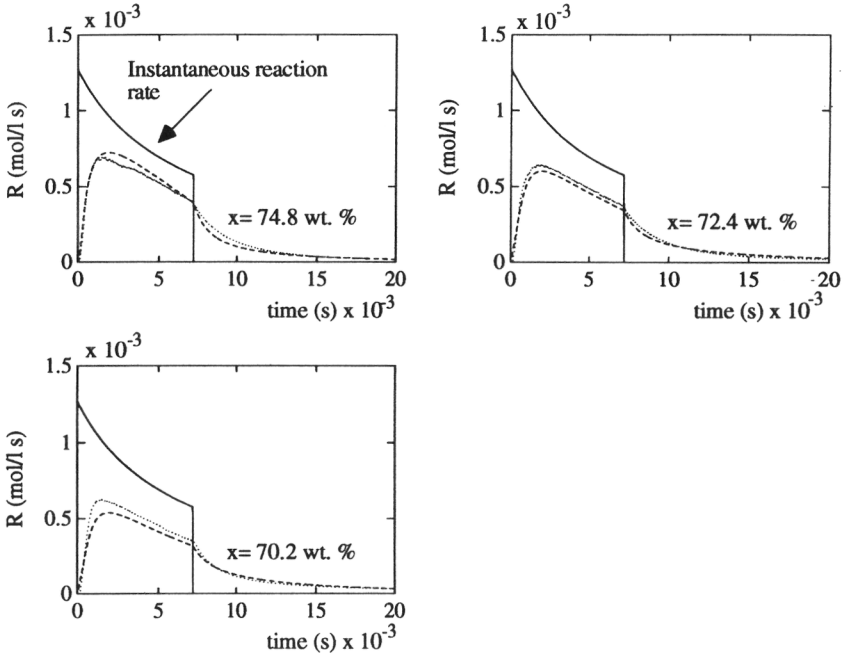

Figure 6. Experimental (·) and simulated (-), conversion rates in mol/l·s for semibatch toluene mononitrations.

4.1. Toluene mononitration experiments

A series of toluene mononitration experiments were carried out in the RC1 reaction calorimeter to study the influence on the overall conversion rate of operating and initial conditions like temperature, stirrer speed, feed rate and sulphuric acid strength.

Figure 6 shows the calculated and simulated reaction rates as a function of sulphuric acid strength, whereas in fig. 7 the measured and simulated concentration-time profiles for toluene o-mononitrotoluene (o-MNT), p-mononitrotoluene (p-MNT) and m-mononitrotoluene (m-MNT) are shown. The instantaneous reaction rate -no accumulation of nitric acid in the reactor- is also plotted. Mixed acids of different sulphuric acid strength, i.e. x= 74.8, 72.4 and 70.2 wt. %, were added in four hours. The reactor temperature and stirrer speed were 308.2 K and 6.67 s^{-1}, respectively. The slow starts of the reaction and the initial accumulation of nitric acid is caused by the relatively high solubility of nitric acid in the organic phase. This nitric acid is not available for the nitration as the reaction takes place in the acid phase.

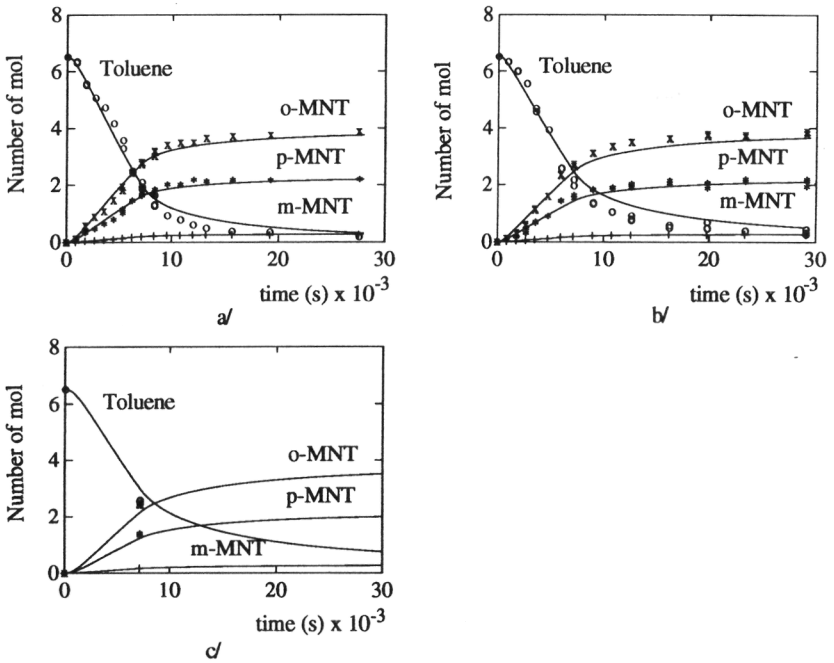

Figure 7. Experimental and simulated conversions for semibatch toluene mononitrations: a/ x = 74.8 wt. %; b/ x= 72.4 wt. %; c/ x= 70.6 wt. %.

Figure 8 shows the calculated and simulated conversion rates as a function of temperature for three semibatch toluene nitration experiments. The instantaneous reaction rate -no accumulation of nitric acid in the reactor- is also plotted. The mixed acid of sulphuric acid strength x=78.9 wt. % was added in two hours. The stirrer speed was 6.67 s^{-1}. As can be observed, as

temperature increases, the behaviour of nitration rate closely approaches to instantaneous reaction, which decreases as the volume increases. Even for the experiment at 308.2 K (fig. 8c) which during the intermediate period is practically limited by the feed rate, there is always an initial accumulation of nitric acid, see fig. 8d; this accumulation becomes more important as the temperature decreases reaching values which under adiabatic conditions, i.e. a cooling system failure, could produce temperature increases higher than 70 K.

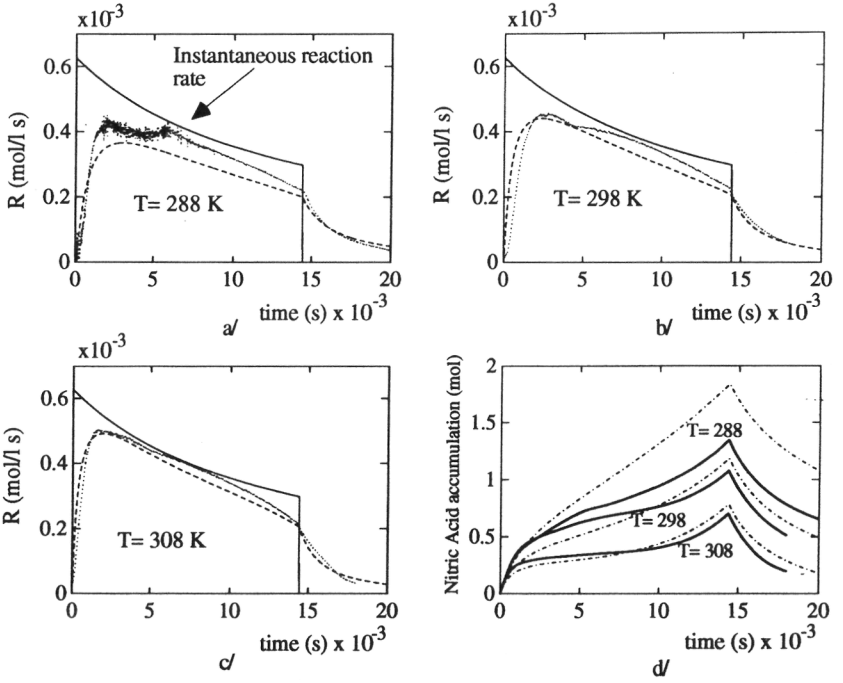

Figure 8. Experimental and simulated conversion rate in mol/l·s for semibatch toluene mononitrations: a/ T= 288 K; b/ T = 298 K; c/ T= 308 K. d/ Experimental and simulated nitric acid accumulation during the experiments.

4.2. Benzene mononitration experiments

A series of benzene nitration experiments were carried out in the RC1 to study this reaction. Figure 9 shows the experimental and simulated conversions for benzene and nitrobenzene during two experiments for different mixed acid compositions. The simulated accumulation of nitric acid is also shown. At a strength of 75.0 wt. % of sulphuric acid the maximum accumulation, which occurs at the end of the addition period, is 1.1 mol whereas in the experiment with an acid strength of 72.0 % the accumulation increases up to 1.7 mol. In both

experiments the mixed acid was added in two hours whereas the reactor temperature and the stirrer speed were 303.2 K and 8.33 s^{-1}, respectively.

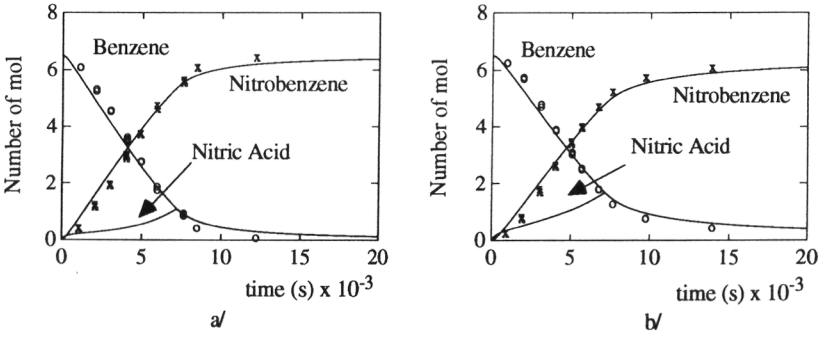

Figure 9. Experimental and simulated conversions for benzene and nitrobenzene during semibatch nitrations: a/ x= 75.0 wt. %; b/ x= 72.0 wt. %.

The experimental fact that under industrial conditions nitration rates of benzene and toluene are of similar magnitude when, in homogeneous conditions, the relation between the observed second order reaction rate is, at sulphuric acid strength of 70.0 wt %, approximately 1:8.5, is due to a combination of different factors that affect the overall conversion rate. The most important is the differences in solubilities, e.g. the relation at 298 K in sulphuric acid wt. 70.0 % is 1: 0.33. Moreover, the change of the physical and transport properties of the reaction mixture influences the interfacial area, mass transfer and diffusion coefficients, for example the relation between the diffusion coefficients of Benzene and Toluene at 298 K is 1:0.9; the relationship between the Sauter mean diameter for Benzene and Toluene in similar conditions is 1:0.96, which implies than Benzene droplets would be smaller and then the interfacial area would be slightly higher.

4.3. Chlorobenzene mononitration experiments

A chlorobenzene nitration experiment was carried out in the RC1 to study the reaction. The mixed acid with a sulphuric acid strength of 77.9 wt. % was added in two hours, the reactor temperature and the stirrer speed were 313.2 K and 6.67 s^{-1}, respectively.Figure 10 shows the experimental and simulated conversions for chlorobenzene and nitrochlorobenzenes. As can be observed no meta isomer was found experimentally in the gas chromatograpic analysis. In this case the nitric acid accumulation is higher than for benzene even though the reactor temperature and sulphuric acid strengths were higher.

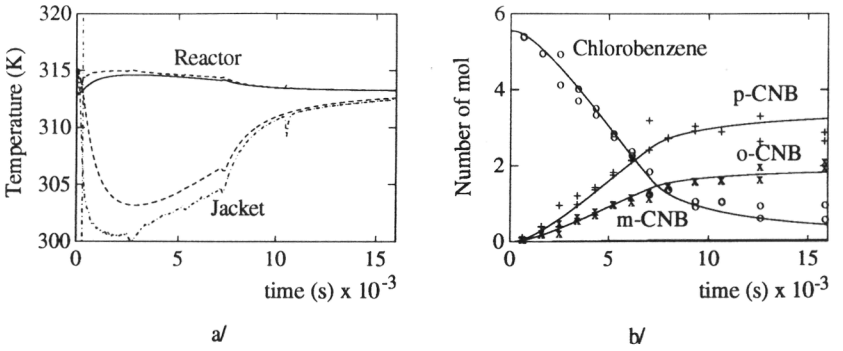

Figure 10. Experimental and simulated temperatures and conversions for chlorobenzene and mononitrochlorobenzenes during a semibatch nitration: a/ Reactor and jacket temperatures, b/ conversions of chlorobenzene, o-nitrochlorobenzene (o-CNB) and p-nitrochlorobenzene (p-CNB).

5. DISCUSSION AND CONCLUSIONS

The model employed, based on the effective interfacial area between two liquids and the description of mass transfer with reaction using the film model, is the simplest approach. Due to the complexity and non-idealities of the mixtures studied, and the data available, this model is adequate for the actual level of knowledge. The results indicate the nitration of benzene, toluene and chlorobenzene in the region of 70-80 wt. % of H_2SO_4 strength, temperatures between 298.2-318.2 K and in the bench scale reactor, occurs in the fast reaction regime. Under these conditions, the mass transfer rate does not directly influence the overall conversion; the conversion is affected by the interfacial area, the distribution coefficients, and the Hatta number.

The correlations obtained for the system toluene DIB- 77 wt. % sulphuric acid has been used to predict the interfacial area during aromatic nitrations. Effective interfacial area values determined in semibatch experiments indicate that the literature correlations can be used, although the constants deviate. This is probably caused by the specific properties of the investigated system of a strongly coalescing dispersion, no baffles in the RC1 reactor and the type of impeller installed, as well as by the literature investigated regions, close to the impeller and at low dispersed phase volume fractions. The correlations produce droplet diameters between 0.3-0.8 mm, with effective interfacial areas similar to those found by Fernandes and Sharma (1967) when they studied the two phase alkaline hydrolysis of 2-ethyl hexyl formate in 2 M NaOH solution.

The distribution coefficients of aromatic compounds limit the maximum possible concentration in acid reaction phase. The low solubility of aromatic compounds studied with $m_{ArH} \approx 10^{-4}$ allows us to neglect the mass transfer resistance in the non-reactive phase - it becomes

important for m·Ha>0.1 which would be the case for more reactive or more soluble aromatics, or at high sulphuric acid strengths at which the instantaneous reaction regime is entered into. Moreover, the nitric acid accumulation is due to these low values of m_{ArH}. Danger of accumulation is inminent if the conversion rate is lower than the molar feed rate per unit volume. Evaluation for typical parameters values yields the following criterion for the occurrence of accumulative conditions in our reactor: $a \cdot V \cdot m \cdot Ha < 2$, see Steensma and Westerterp (1991). These conditions hold in some of the experiments and can be observed for example in figs 8 and 9. Finally, another important value is the distribution coefficient of the nitric acid disolved in the aromatic phase. This nitric acid can not change into nitronium ion NO_2^+ - the nitrating agent - and, hence is not available for nitration.

NOTATION

a	interfacial area (m^2/m^3)
A	constant, see eq. 5
Al	Hinterland ratio, see eq. 23
B	constant, see eq. 6
C	concentration (mol/l)
d	droplet diameter (m)
d_{32}	Sauter mean diameter of droplets (m)
D	diffusion coefficient (m^2/s)
Da	impeller diameter (m)
E	Enhancement factor
F	surface area (m^2)
Ha	Hatta number
J_A	molar flux ($mol/m^2 \cdot s$)
k_L	mass transfer coefficient (m/s)
$k_{1,1}$	second order kinetic constant (l/mol·s)
k	pseudo-first order kinetic constant (1/s)
m	distribution coefficient
Na	impeller speed (rps)
q_a	acid addition rate (m^3/s)
R	overall rconversion rate (mol/l·s)
t	time (s)
u_t	terminal velocity (m/s)
V	volume (m^3)
We	Weber number
x	sulphuric acid strength

Greek letters

δ	film thickness
ε_d	dispersed phase volume fraction
γ	surface tension (N/m)
μ	kinematic viscosity (Pas)
$\in$	ratio

ρ density (Kg/m^3)
σ interfacial tension(N/m)

Subscripts and superscripts
A diisobutylene
a acid phase
ArH aromatic compound
B sulphuric acid
Be benzene
c continuous phase
d dispersed phase
i1 aqueous interphase
i2 organic interphase
L1 aqueous phase
L2 organic phase
m reaction mixture
o organic phase
To toluene

REFERENCES

Backes, H.M., J. J. M., E. Bender, and G. Maurer, 1990, Interfacial tensions in binary and ternary liquid-liquid systems, *Chem. Eng. Sci.* **45**,275-286.

Badachhape, R. B., M. K. Gharpurey and A. B. Biswas, 1965, Density and surface tension of phenol, (mono-, di-, and tri-) chlorophenols, salol and (o- and m-) chloronitrobenzenes, *J. Chem. Eng. Data* **10**, 143-145.

Bonvin, D. and Saner, U., 1988, On Line procedures for supervising the operation of batch reactors, *Computer Chem. Engng.* **12**, 371-376.

Brooks, B. W. and Richmond, H. N., 1994. Phase inversion in non-ionic surfactant-oil-water systems II. Drop size studies in catastrophic inversion with turbulent mixing. *Chem. Engng. Sci.* **49**, 1065-1075.

Brunson, R. J. and R. M. Wellek, 1971, Mass transfer inside liquid droplets and gas bubbles accompanied by a second-order chemical reaction, *AIChE Journal* **17**, 1123-1130.

Calderbank, P.H., 1958, Physical rate process in industrial fermentors,I. The interfacial area in gas-liquid contacting with mechanical agitation.*Trans. Inst. Chem. Engs.* **36**,43-48.

Calderbank, P.H. and Moo-Young, M.B., 1961, The continuous phase heat and mass-transfer properties of dispersions, *Chem. Eng. Sci.* **16**, 39-54.

Calderbank P.H., 1967, Mass Transfer in V.W. Uhl, J.B. Gray (eds), *Mixing Theory and Practice*, Academic Press, New York.

Chapman, J.W., P.R. Cox and A.N. Strachan , 1974, Two phase nitration of toluene III, *Chem. Eng. Sci.* **29**, 1247-1251.

Coulaloglou, C.A. and Tavlarides, L.L., 1976, Drop size distribution and coalescence frequencies of liquid-liquid dispersions in flow vessels. *AIChE J.* **22**, 289-297.

Delichatsios, M. A. and Probstein, R. F., 1976, The effect of coalescence on the average drop size in liquid-liquid dispersions. *Ind. Engng. Chem. Fundam.* **15**, 134-137.

De Santiago M. and Trambouze P, 1971, Applicabilité de la méthode chimique de measure de l'aire interfaciale, *Chem. Eng. Sci.* **26**, 1803-1815.

Donahue, D. J. and F. E. Bartell, 1952, The boundary tension at water-organic liquid interfaces, J. phys. Chem. 56, 480-484.

Fernandez J.B. and Sharma M.M., 1967, Effective interfacial area in agitated liquid-liquid contactors, Chem. Eng. Sci., 22, 1267-1282.

Giles J.W., Hanson C. and Marsland J.G., 1971, Drop size distribution in agitated liquid-liquid syatems with simultaneous interface mass transfer and chemical reaction, Proc. Int. Solv. Extr. Conference, Society of Chemical Industries, 94-111.

Good, R. J. and E. Elbing, 1970, Generalization of theory for estimation of interfacial energies, Industrial and Engineering Chemistry, 62, 54-78.

Handlos, A. E. and Baron, T., 1957, Mass and heat transfer from drops in liquid-liquid extraction. *AIChE J.* **3**, 127-136.

Hanson C. (ed.), 1971, *Recent advances in liquid-liquid extraction*, Pergamon, Oxford.

Hernández, H., J.M. Zaldívar and C. Barcons, 1993, Development of a mathematical model and a numerical simulator for the analysis and optimization of batch reactors, *Computer Chem. Engng.* **17S**, 45-50.

Hu, S. and Kintner, R. C., 1955, The fall of single liquid drops through water. *AIChE Journal* **1**, 42-48.

Johnson, A. I. and A. E. Hamielec, 1960, Mass transfer inside drops, *AIChE Journal* **6**, 145-149.

Kahlweit, M., 1962, Calculation of the interfacial tension between two phases of a binary system, *Z. phys. Chem.* **34**, 163-181.

Kolmogorov, A.N., 1949, The break-up of droplets in a turbulent stream. *Dokl. Akad. Nauk* **66**, 825-828.

Kronig, R. and Brink, J. C., 1960, On the theory of extractions from falling droplets, *Appl. sci. Res.* **A2**, 142-154.

Kumar, S., Kumar, R. and Gandhi, K. S., 1993, A new model for coalescence efficiency of drops in stirred dispersion. *Chem. Eng. Sci.* **48**, 2025-2038.

Laddha G.S. and Degaleesan T. E., 1976, *Transport phenomena in liquid extraction*, McGraw-Hill, New Delhi.

Li, B. and J. Fu, 1989, Prediction of interfacial tension of binary liquid mixtures from mutual solubility by the UNIQUAC method, *Chem. Eng. Sci.* **44**, 1519-1527.

Molga, E.J., C. Barcons and J.M. Zaldívar, 1993, Mononitration of toluene and quantitative determination of the isomer distribution by gas chromatography, *Afinidad* **50**, 15-20.

Molga, E., Zaldívar, J.M., and Hernández, H., 1994,Effective interfacial area in semibatch liquid-liquid stirred tanks reactors. JRC Ispra, TN n° I.94.xxx.

Okufi S., Perez de Ortiz E.S. and Sawistowski H., 1990, Scale-up of liquid-liquid dispersion in stirred tanks, *Can. J. Eng.* **68**,400-406.

Perry R.H. and C.H. Chilton, 1973, *Chemical Engineers' Handbook*, 5th Ed., MacGraw-Hill, New York.

Physical Properties Data Service, The Institute of Chemical Engineers, Rugby, UK.

Sankholdar, D.S. and Sharma, M.M., 1973, A new system for the measurements of effective interfacial area in agitated liquid-liquid contactors by the chemical method. *Chem. Eng. Sci.* **28**, 2089-2092.

Schofield, K., 1980, *Aromatic Nitration*, Cambridge University Press, Cambridge.

Schroeder, R. R. and Kintner, R. C., 1965, Oscillations of drops falling in a liquid field. *AIChE J.* **11**, 5-8.

Sprow, F.B., 1967, Distribution of drop sizes produced in turbulent liquid-liquid dispersions. *Chem. Engng. Sci.* **22**, 435-442.

Steensma, M. and K.R. Westerterp, 1988, Thermally safe operation of a cooled semi-batch reactor. Slow liquid-liquid reactions. *Chem. Eng. Sci.* **43**, 2125-2130.

Steensma, M. and K. R. Westerterp,1991, Thermally safe operation of a semibatch reactor for liquid-liquid reactions. Fast reactions, *Chem. Eng. Technol.* **14**, 367-375.

Tavlarides, L. L. and Stamatoudis, M., 1981, The analysis of interphase reactions and mass transfer in liquid-liquid dispersions, in *Advances in Chemical Engineering*, vol 11, Eds. T.B. Drew, G. R. Cokelet, J. W. Hoopes Jr. and T. Vermeulen, Academic Press, New York.

Treybal R.E., 1963, *Liquid Extraction*, 2nd edition, McGraw-Hill, New York.

Uhl V.W. and J.B. Gray (ed.), *Mixing: Theory and Practice*, vol. 1, Academic Press, New York (1966).

Villermaux J., 1981, Drop break-up and coalescence. Micormixing effect in liquid-liquid reactors, in *Multiphase chemical reactors VI Fundamentals*, Rodriguez, A.E., J. M. Calo, J. M.and Sweed, N. H. (eds.), Sijthoff et Noordhoff, Alphen aan den Rinj, 285-362.

Wellek, R. M. and Skelland, A. H. P., 1965, Extraction with single turbulent droplets. *AIChE J.* **11**, 557-560.

Wesselingh J.A., 1987, The velocity of particles, drops and bubbles, Chem. Eng. Process **21**, 9-14.

Westerterp, K.R., van Dierendonck, L.L. and de Kraa, J., 1963, Interfacial area in agitated gas-liquid contactors. *Chem. Eng. Sci.* **18**,147-176.

Westerterp, K.R., van Swaaij, W.P.M. and Beenackers, A.A.C.M., 1984, *Chemical Reactor Design and Operation*, J. Wiley & Sons, Chichester.

Zaldívar, J.M., H. Hernández and C. Barcons, 1990, Development of a numerical simulator for a reaction calorimeter. FISIM, RC1 version, JRC Ispra, TN n° I.90.109.

Zaldívar, J.M., H. Hernández, C. Barcons and R. Nomen, 1992, Heat effects due to dilution during aromatic nitrations by mixed acid in batch conditions, *J. of Thermal Analysis* **38**, 2575-2582.

Zaldívar, J.M., E. Molga , M. A. Alós, H. Hernández and K. R. Westerterp, 1995, Aromatic nitrations by mixed acid. Slow liquid-liquid reactions, 'submited for publication'

Appendix 1: Check on the validity of the assumed quasi-steady state for the interfacial area calculation

For non-steady state conditions using the Higbie penetration model the mass balance with a pseudo-first order irreversible reaction reads:

$$\frac{\partial C_A}{\partial t} = D_A \frac{\partial^2 C_A}{\partial x^2} - k\, C_A \qquad \text{(A1)}$$

with the boundary conditions:

$$t = 0\,;\ C_A = 0 \ \text{ at } \ 0 < x < \infty$$
$$t > 0\,;\ C_A = C_A^{i2} \ \text{ at } \ x = 0 \qquad \text{(A2)}$$
$$t > 0\,;\ C_A = 0 \ \text{ at } \ x \to \infty$$

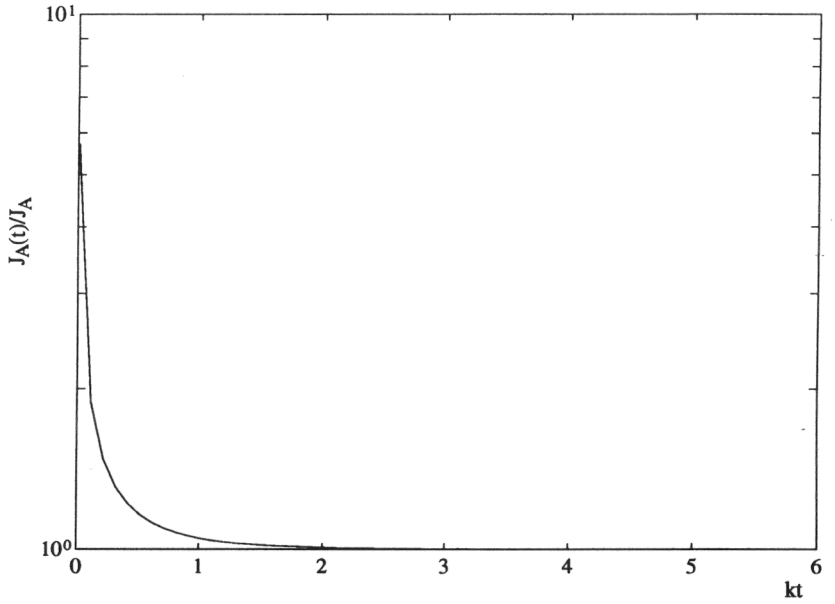

Figure A1. Ratio of the mass fluxes determined for steady and unsteady state conditions (constant concentration at the interface surface).

Solving of eq. A1 with the boundary conditions eq. A2 gives, for bulk concentration of A equal to zero,

the flux through the interface at time t as follows:

$$J_A(0,t) = C_A^{i2} \sqrt{k \cdot D_A} \left[\operatorname{erf}\left(\sqrt{k \cdot t}\right) + \frac{\exp(-k \cdot t)}{\sqrt{\pi \cdot k \cdot t}} \right] \qquad \text{(A3)}$$

The ratio of the non-steady state and steady state fluxes given by eq. A3 and eq. 11, respectively, is equal to:

$$\epsilon = \frac{J_A(0,t)}{J_A} = \mathrm{erf}\left(\sqrt{k \cdot t}\right) + \frac{\exp(-k \cdot t)}{\sqrt{\pi \cdot k \cdot t}} \qquad \text{(A4)}$$

The values of the ratio ϵ are plotted in fig. A1 as a function of time. For $k \cdot t > 2$ the mass transfer rate approaches a stationary minimum value given by eq. 11. The estimated value of k for the system used in our investigations - 77 wt.% of H_2SO_4 and DIB + toluene - is of order of magnitude of $k \approx 1\ s^{-1}$. In this case ratio ϵ becomes identical at 1 after a time as short as 1 s.

Appendix 2: Estimation of mass transfer coefficients in liquid-liquid systems

During the past decades a considerable amount of data has been collected on physical mass transfer in dispersed systems, for a review see Laddha and Degaleesan (1976) and Hanson (1971). The estimation of the overall mass transfer coefficient calls for a knowledge of the dispersed phase (k_d) and continuous phase (k_c) coefficients. These individual mass transfer coefficients have been correlated for many systems by analogy with heat transfer coefficients in terms of hydrodynamic behaviour and physical properties such as:

$$Sh \propto Re^{n_1} \cdot Sc^{n_2} \qquad \text{(A5)}$$

where Sh, Re and Sc are defined as,

$$Sh = \frac{k \cdot d}{D} \qquad \text{(A6)}$$

$$Re = \frac{d \cdot v \cdot \rho}{\mu} \qquad \text{(A7)}$$

$$Sc = \frac{\mu}{D \cdot \rho} \qquad \text{(A8)}$$

where d and v are a linear dimension and velocity characterizing the dispersion, e.g. drop size and drop velocity, D is the coefficient of molecular diffusion of the species considered and ρ and μ are the density and viscosity of the fluid. In the case of aromatic nitrations the reaction proceeds in the acid phase, hence the aromatic compound diffuses from the organic (L1) to the acid (L2) phase and reacts in the acid phase. Two different cases can be considered:

- the organic is the dispersed and the acid is the continuous phase, as for example in the slow liquid-liquid regime during batch nitrations, see Zaldívar *et al.* (1995).
- the organic is the continuous phase and the acid is the dispersed phase, as in the case of the semibatch nitrations in the fast regime.

The overall mass transfer coefficient, based on L1 and L2 phases respectively, can be written for physical transport without reaction as:

$$\frac{1}{k_{ov.}(L1)} = \frac{1}{k_{L1}} + \frac{1}{m \cdot k_{L2}} \qquad \text{(A9)}$$

$$\frac{1}{k_{ov.}(L2)} = \frac{m}{k_{L1}} + \frac{1}{k_{L2}} \qquad \text{(A10)}$$

The mass transfer resistance in the organic phase L1 can be neglected if the phase contains pure reactant without solvent as in the case of aromatic nitrations studied. If there is a solvent or a

product formed due to reaction and dissolved in the organic phase, the validity of neglecting the mass transfer resistance in the organic phase must be examined. In the case of mass transfer without chemical reaction in liquid-liquid dispersions, the order of magnitude of liquid mass transfer coefficients k_c and k_d lie normally in the range between 10^{-4} to 10^{-5} m/s, see Laddha and Degaleesan (1976), and they can, sometimes, arrive to lower values such as $5 \cdot 10^{-6}$ m/s in viscous solutions or in big drops, see Hanson (1971). As the value of m, see Zaldívar *et al.* (1995), is approximately 10^{-4} under the conditions studied, the overall mass transfer coefficient can be equated to k_{L2} and the resistance in the organic phase neglected. Hence, the two cases are:

- Continuous phase mass transfer coefficient:

The following empirical correlation developed by Calderbank and Moo-Young (1961) and experimentally validated in a wide range of operating conditions, see Uhl and Gray (1967), may be used to determine the mass transfer coefficient in the continuous phase k_{L2} in liquid-liquid dispersion systems, see De Santiago and Trambouze (1971):

$$k_{L2} = 0.13 \left(\frac{P \cdot \mu_c}{V_d \cdot \rho_c^2} \right)^{\frac{1}{4}} \left(\frac{\mu_c}{\rho_c \cdot D_{ArH}} \right)^{-\frac{2}{3}} \qquad \text{(A11)}$$

where P refers to the power dissipated by the stirrer,

$$P = \phi' \cdot \rho_m \cdot n_a^3 \cdot D_a^5 \qquad \text{(A12)}$$

and ϕ' may be considered as a constant and here $\phi'=2.2$, see Bourne et al. (1981) and Zaldívar et al. (1990).

Chapman *et al.* (1974) in a series of toluene nitration experiments using acid strengths between 76-79 % estimated the mass transfer coefficient to be $k_{L2} = 1.03 \cdot 10^{-5}$ m/s. This value is in agreement with typical values found in liquid-liquid systems, e.g.. Fernandes and Sharma (1967) found values between $1.13\text{-}1.6 \cdot 10^{-5}$ m/s for the system n-hexylacetate and 1M NaOH solution. Using the correlation eq. A11 and the experimental data from Chapman *et al.* (1974), the value obtained for k_{L2} is $1.1 \cdot 10^{-5}$ m/s, which is in agreement with that derived from the reported experiments in literature.

- Dispersed phase mass transfer coefficient:

In this case the mass transfer coefficient will depend on the behaviour of the drop and whether it is rigid or not, see Hanson (1971)

- For a rigid droplet Treybal (1963) presents the following relationship for spheres with no circulation and with transfer by pure molecular diffusion:

$$Sh_d = \frac{2 \cdot \pi^2}{3} \qquad \text{(A13)}$$

where Sh_d is the Sherwood number for the dispersed phase, defined as:

$$Sh_d = \frac{k_d \cdot d_{32}}{D} \qquad \text{(A14)}$$

and hence:

$$k_d = \frac{2 \cdot \pi^2 \cdot D}{3 \cdot d_{32}} \qquad \text{(A15)}$$

- For drops with internal circulation and/or oscillations, the mixing in the drop can be laminar or turbulent. For the regime of laminar circulation, the relation of Kronig and Brink (1950) is generally accepted, see Hanson (1971):

$$k_d = \frac{17.9 \cdot D}{d_{32}} \qquad \text{(A16)}$$

This correlation is restricted to regimes where Re < 1. Johnson and Hamielec (1960) found it can be used in some cases for higher values of Re. For drops with turbulent circulation the model of Handlos and Baron (1957), which has been experimentally verified by Wellek and Skelland (1965) and by Johson and Hamielec (1960), can be used as a good approximation.

$$k_d = 0.00375 \cdot u_t \left(\frac{\mu_c}{\mu_c + \mu_d} \right) \qquad \text{(A17)}$$

Schroeder and Kintner (1965) concluded no oscillations occur for Re<200 .

In the case of the reaction calorimeter, the usual drop diameter lies between 0.3-0.8 mm. In semibatch experiments the mixed acid is added into the reactor so the acid phase will be the dispersed phase.

Defining the interface number, see Wesseling (1987), as:

$$\sigma^* = \sigma \left(\frac{\rho_c^2}{g \cdot \Delta\rho \cdot \mu_c^4} \right)^{\frac{1}{3}} \qquad \text{(A18)}$$

which is a measure of the resistance of the interface against deformation, and calculating the diameter number according to Wesseling:

$$d^*_{max} = 4\sqrt{\sigma^*} \qquad \text{(A19)}$$

which applies for drops in liquids when $(\mu_d/\mu_c) \geq 2$; we find for a typical nitration reaction σ^* lies between 400-3500, whereas $d^* \approx$ 80-240. These values indicate the mixed acid drops do not behave as rigid drops. The power introduced by the turbine stirrer used varies between 0.2-3.2 kW/m^3. For liquids with low viscosities between 1 and 10 cP and high interfacial tensions between 25 and 45 mN/m the terminal velocity can be estimated with the correlation of Hu and Kinther (1955):

$$u_t = \sqrt{\frac{4 \cdot g \cdot d_{32} \cdot \Delta\rho}{3 \cdot \rho \cdot C_D}} \qquad \text{(A20)}$$

where C_D is a drag coefficient which is a function of the shape of the particle, the physical properties of the system and the Reynolds number. An estimate leads to a terminal velocity of 0.03 to 0.06 m/s and an internal Reynolds number between 1.5 and 20. For these values the general diagram derived by Wesselingh (1987) tell us the mixed acid drops behave as non-rigid drops with laminar circulation: as a consequence, correlation eq. (A16) should be used.

Appendix 3: Estimate of the interfacial tension between mixed acid and aromatic compounds

The liquid-liquid interfacial tension has a significant effect on the degree of dispersion and on the stability of the dispersed system. No method is available to predict interfacial tensions in multicomponent mixtures from pure component or binary data, see Backes *et al.* (1990). Therefore empirical correlations must be developed.

Antonow's rule, see Treybal (1963), says the interfacial tension between two saturated liquid phases equals the difference between their individual surface tensions with air:

$$\sigma_{12} = |\gamma_1' - \gamma_2'| \qquad \text{(A21)}$$

This equation is valid only for a restricted class of liquid pairs and can not be relied upon, see Treybal (1963). Donahue and Bartell (1952) proposed the following empirical correlation for a binary system,

$$\sigma_{12} = a - b \cdot \log (x_1'' + x_2') \qquad \text{(A22)}$$

where x''_1 refers to the molar concentration of the organic compound in the aqueous phase and x'_2 refers to the molar concentration of water in the organic phase; a and b are constants. This correlation was modified by Treybal (1963) for ternary systems into:

$$\sigma_{12} = a - b \cdot \log \left[x_1'' + x_2' + \frac{1}{2} (x_3' + x_3'') \right] \qquad \text{(A23)}$$

where x'_3 and x''_3 refer to the molar concentration of the solute in both phases. Good and Elbing (1970) proposed the following correlation:

$$\sigma_{12} = \gamma_1 + \gamma_2 - 2 \cdot \Phi_{12} \sqrt{\gamma_1 \cdot \gamma_2} \qquad \text{(A24)}$$

where Φ_{12} is an interaction parameter. For the prediction of Φ_{12} Good and Elbing developed a theoretical model based on intermolecular forces between the two liquid phases, such as the dipole-dipole force, hydrogen bonds and the Kihara dispersion potential. Recently, Li and Fu (1989) have proposed a new method for predicting the interfacial tension in binary mixtures, imaginating an interface of continuously changing concentrations in a direction normal to the interface, see Kahlweit (1962), and using activity coefficients of components in the interfacial region, calculated by the UNIQUAC method.

From this literature survey it is clear that an estimate of the interfacial tension between mixed acid and an aromatic mixture at the moment is not possible from pure or binary data due to the highly non-ideal behaviour of our mixtures.As a consequence, an empirical correlation fitted to experimental data seems the only solution. Equation A24 was chosen and Φ_{12} was used as fitting parameter. It is necessary to first calculate the surface tension of both phases:

Mixed acid surface tension. The surface tension of the mixed acid was calculated using experimental data from pure water and solutions of nitric and sulphuric acid at different concentrations and temperatures, see Perry and Chilton (1984), as:

$$\gamma_{L2} = \sum_{i=1}^{3} x_i \cdot \gamma_i + \frac{a_1 \cdot x_W \cdot x_N}{2 \cdot R \cdot T} (\gamma_W - \gamma_N)^2 + \frac{a_2 \cdot x_W \cdot x_S}{2 \cdot R \cdot T} (\gamma_W - \gamma_S)^2 \qquad \text{(A25)}$$

where $a_1 = 1.64 \cdot 10^5$ and $a_2 = 7.14 \cdot 10^5$, respectively. x_i and γ_i refer to the mass fraction and surface tension of the i-th compound. The surface tension was calculated as:

$$\gamma_i \text{ (N/m)} = A + B \cdot T + C \cdot T^2 \qquad \text{(A26)}$$

the constants A, B, C are listed in Table A1. Figure A2 shows the comparison between the experimental and calculated surface tensions for nitric acid solutions using eq. (A25).

Table A1. Constants for the calculation of the surface tension of mixed acid, γ_i (N/m).

Compound	A	B	C
H_2O	$9.77 \cdot 10^{-2}$	$-1.626 \cdot 10^{-5}$	$-2.35 \cdot 10^{-7}$
HNO_3	$8.39 \cdot 10^{-2}$	$-1.446 \cdot 10^{-4}$	0.0
H_2SO_4	$7.81 \cdot 10^{-2}$	$-7.846 \cdot 10^{-5}$	0.0

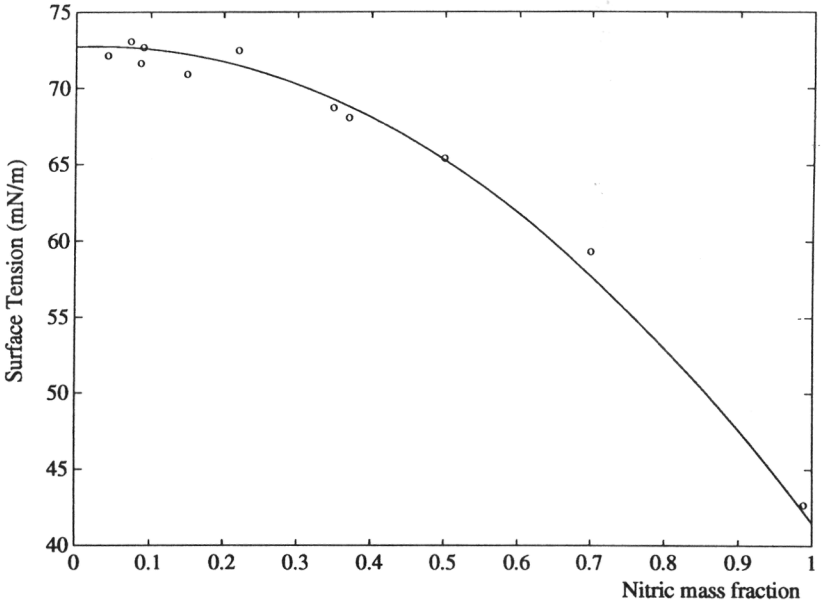

Figure A2. Experimental, see Perry and Chilton (1984), and correlated surface tension for water/nitric acid mixtures.

Aromatic phase surface tension. The surface tension of the organic phase was calculated using the Physical Properties Data Service (PPDS) and data from Badachhape *et al.* (1965), as:

$$\gamma_{L1} = \sum_{i} x_i \cdot \gamma_i \qquad \text{(A27)}$$

where x_i and γ_i refer to the mass fraction and surface tension of the i-th compound. The surface tension was calculated as:

γ_i (N/m)=A+B·T (A28)

the constants A and B are listed in Table A2.

Table A2. Constants for the calculation of the surface tension of organic mixtures, γ_i (N/m)

Compound	A	B
Benzene	$6.65 \cdot 10^{-2}$	$-1.283 \cdot 10^{-4}$
Nitrobenzene	$7.91 \cdot 10^{-2}$	$-1.193 \cdot 10^{-4}$
Toluene	$6.36 \cdot 10^{-2}$	$-1.197 \cdot 10^{-4}$
o-MNT	$7.75 \cdot 10^{-2}$	$-1.217 \cdot 10^{-4}$
m-MNT	$7.52 \cdot 10^{-2}$	$-1.153 \cdot 10^{-4}$
p-MNT	$6.91 \cdot 10^{-2}$	$-9.815 \cdot 10^{-5}$
Chlorobenzene	$6.80 \cdot 10^{-2}$	$-1.177 \cdot 10^{-4}$
o-MNC	$7.98 \cdot 10^{-2}$	$-1.163 \cdot 10^{-4}$
m-MNC	$8.84 \cdot 10^{-2}$	$-1.418 \cdot 10^{-4}$
p-MNC	$7.44 \cdot 10^{-2}$	$-1.045 \cdot 10^{-4}$

Calculated values deviated less than 5 percent, see Table A3, from experimentally determined surface tensions of mixtures of toluene and mononitrotoluenes.

Table A3. Experimental and calculated surface tensions in mN/m for organic mixtures at different temperatures.

Organic phase composition % wt	288.2 (K)		298.2 (K)		308.2 (K)		318.2 (K)	
	Exp.	Calc.	Exp.	Calc.	Exp.	Calc.	Exp.	Calc.
59% o-MNT, 4% m-MNT, 37% p-MNT	43.0	41.8	42.2	40.7	41.3	39.5	40.7	38.4
20% Toluene, 80% MNT's above composition	40.4	39.2	39.3	38.1	38.1	37.0	37.0	35.8

Table A4. Values of used in eq. (A29).

Compound	Φ_{ArH}
Benzene	0.739
Nitrobenzene	0.805
Toluene	0.737
MNTs	0.868
Chlorobenzene	0.697
MNCs	0.868

c/ Interfacial tension between organic and acid phases:

The value of Φ_{12} was obtained from data given by Good and Elbing (1970), see Table 4.The variation of Φ_{12} during the reaction was determined using the following correlation:

$$\Phi_{12} = x_{ArH} \cdot \Phi_{ArH} + x_{ArNO_2} \cdot \Phi_{ArNO_2} \qquad (A29)$$

where x_{ArH} and x_{ArNO_2} refer to the mass fractions of the aromatic compound being nitrated and the nitration products, respectively. Figure A3 shows experimental and calculated interfacial tensions using eq. (A29).

Figure A5 shows experimental versus calculated interfacial tensions using eq. (A34).

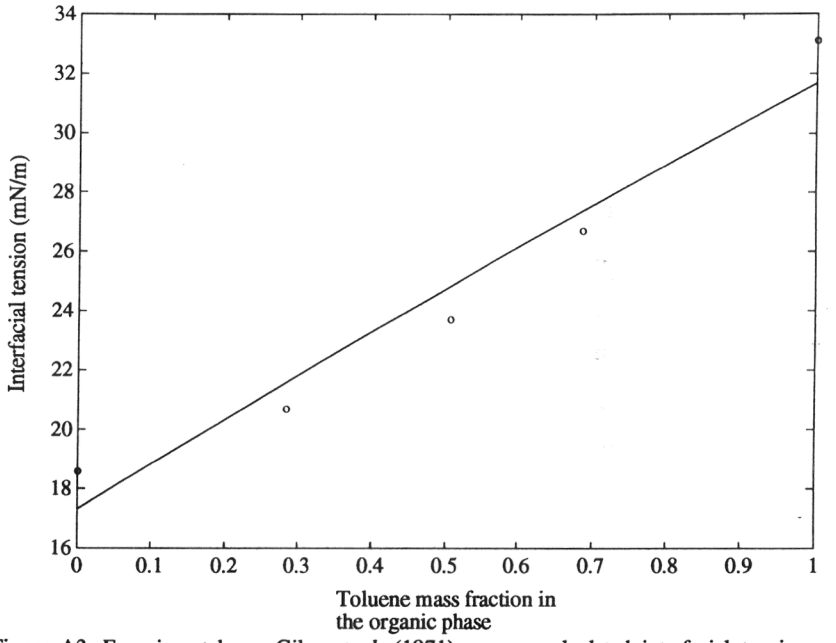

Figure A3. Experimental, see Giles *et al.* (1971), versus calculated interfacial tensions of sulphuric acid and water and mixtures of toluene and o-MNT.

CHAPTER 6

THE EFFECT OF PHASE INVERSION DURING SEMIBATCH AROMATIC NITRATIONS

ABSTRACT

The nitration of aromatic compounds by mixed acid has been selected as a specific case of heterogeneous liquid-liquid reactions. A series of experiments has been carried out to study the influences of different initial and operating conditions like temperature, stirrer speed, feed rate and sulphuric acid strength. The effect of phase inversion during semibatch nitrations is experimentally studied and analysed. The influence of various parameters is characterised. The implications to optimise nitrations are discussed from performance and safety points of view.

Keywords. Phase inversion, liquid-liquid dispersion, aromatic nitrations

1. INTRODUCTION

Despite aromatic nitrations in mixed acid being one of the oldest and most common industrial reactions, there is still a considerable number of problems in predicting their behaviour in semibatch reactors. The interdependence of reaction and mass transfer phenomena lead to a complex problem in characterising and scaling-up these processes. Furthermore, nitrations involve high exothermicity and side reactions.

An important phenomenon is phase inversion, which may occur in such systems. When two immiscible liquids are agitated a dispersion is formed by virtue of the continuous supply of energy by the stirrer. When the external supply of energy is stopped, the dispersion may remain stable or may disengage into two phases. In the first case, the dispersion is called an emulsion, while the term dispersion is normally applied to the second type.

After a transition period a dynamic equilibrium between break-up and coalescence is attained and a spectrum of drop sizes results. One of the phases becomes dispersed as droplets into the other, continuous phase. The type of dispersion depends on the volume fractions of the two liquids, their physical properties and the dynamic characteristics of the mixing process.

If more and more dispersed-phase material, as in the semibatch nitration process, is added to the stirred system, a point is eventually reached at which the addition of more dispersed phase causes an inversion: the continuous phase suddenly becomes the dispersed one and *viceversa.*

Notable for phase inversion is the ambivalent region, see Selker and Sleicher (1965) or the region, where the nature of the dispersion depends on history. The phase inversion points differ for the organic or the aqueous being dispersed. A hysteresis loop, termed the inside metastable area, characterises the ambivalence region, see fig. 1.

Inversion of phases is frequently accompanied either by a decrease or by an increase in the interfacial area. Fernandes and Sharma (1967) reported a change of 32% in the interfacial area, for the system 2M NaOH and 2 ethyl hexyl formate, depending on which phase was the continuous one. Luhning and Sawistowski (1971) reported a stepwise change in drop size at phase inversion in all systems studied and hence a change in interfacial area. In general, Clarke and Sawistowski (1978) found for solute-free systems that the interfacial area increased on inversion from the organic/aqueous (o/w) to the aqueous/organic (w/o) configuration, and decreased on inversion in the opposite direction.

Guillinger *et al.* (1988) found for phase inversion a step change in the viscosity of the dispersion, which produced a viscosity maximum at the inversion point for the system water-kerosene.

Some studies of phase inversion have been made in batch as well as in continuous systems, with and without mass transfer. Investigators have tried to determine the dependence of phase inversion on physical properties and geometrical and process parameters of the system. Apparently contradictory observations have been reported by researchers. In a recent review

Ganguly *et al.* (1992) concluded the phenomenon is still not well understood and more research should be dedicated to it.

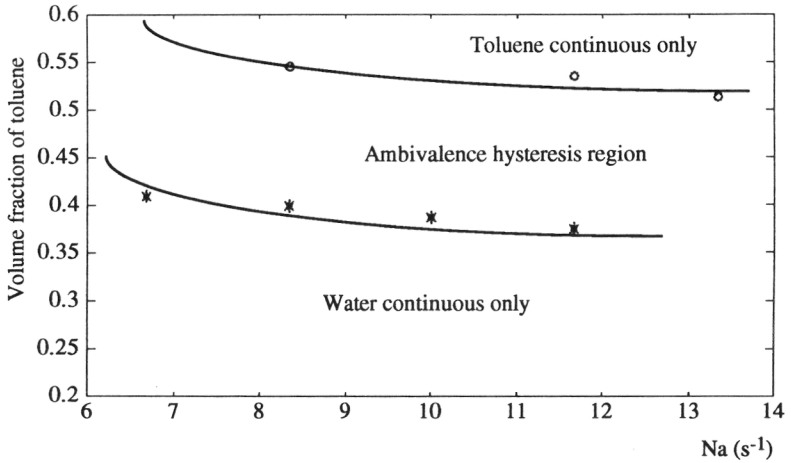

Figure 1. Inversion characteristics for Toluene T/Water W system: o is inversion from T/W to W/T; and * from W/T to T/W, see text for details on experimental data.

In the case of semibatch aromatic nitrations a phase inversion might produce an unexpected step change in the heat generated by the reaction mass, if the conversion rate were mass transfer controlled. Therefore, the identification and limits of stability of the dispersed phase under different conditions of volume fraction, species concentration, temperature and stirrer speed is important for the operation of semibatch nitration plants. In this study the phase inversion phenomenon was investigated to determine the main parameters which affect the dynamic behaviour of semibatch aromatic nitrations at inversion. Preliminary experiments to separate the effects of different factors were carried out, like experimental determination by the chemical method, of the interfacial area during phase inversion with the similar system toluene with diisobutylene (DIB) and 77 wt % sulphuric acid, see Zaldivar *et al.* (1995b), and a continuous evaluation of the effective heat transfer parameters for non-reactive heterogeneous mixtures of toluene and benzene and 70 wt % sulphuric acid.

Some nitration experiments in which phase inversion took place are presented and analysed using previous experimental results. The contribution to the increase in conversion rate is studied in view of the previous experiments.

2. EXPERIMENTAL PHASE INVERSION DETECTION

In phase inversion studies, the experimental procedure is quite important. In discontinuous type studies two methods are used, see Ganguly *et al.* (1992):

- For batch studies measured volumes of both phases are put into the vessel and mixing is started. The agitator speed is increased till inversion occurs. The experiment is repeated for different volume fractions of the two phases.
- In a semibatch study a certain volume of one of the liquids is put into the vessel and subjected to stirring at a constant speed. The second liquid is added and dispersed while the first liquid remains continuous. At some hold-up the phase inversion occurs. Several techniques are commonly used for the detection of inversion like conductivity measurement or visual and photographic observations. Of these, the first method is the most popular.

We were interested in the study of phase inversion during semibatch aromatic nitrations and used conductivity measurement, see fig. 2b, and also a second method based on the change of reactor and jacket temperature due to the change of the overall heat transfer coefficient. For the second method we introduced a constant power of 23 W via an electrical resistance during the experiments, see fig. 2a and Appendix 1 for a discussion on this method.

Table 1. Characteristics of the equipment.

Vessel	Diameter T (m)	Height H (mm)	Volume V (l)	Agitator type	Impeller Diameter D_a (mm)	Impeller speed n_a (s^{-1})
Reactor RC1	115	200	2.0	FB45IP	59.0	6.6-13.3

Note: four-bladed 45° inclined paddle impeller, vessel unbaffled

Phase inversion was studied in the RC1 reactor which characteristics are given in Table 1. Heterogeneous non-reactive mixtures of water/toluene or sulphuric acid of 70.0 wt. %/benzene or toluene were chosen to determine the phase inversion point. The aqueous phase was added to the organic phase and phase inversion was detected measuring the electrical conductivity. The experimental procedure was chosen to simulate the experimental conditions during nitrations. In a set of separate experiments toluene was added to water to check the ocurrence of the hyteresis effect and the ambivalent region, see fig. 1.

Tables 2 and 3 summarise the experimental results. For the system toluene-sulphuric acid, the experimental reproducibility was studied by repeating the same experiment. As can be seen in Table 3 the reproducibility of the experiments was usually within the range of $\varepsilon = 0.02\text{-}0.03$.

Table 2. Volume fraction ε at phase inversion for the system toluene-water and water-toluene, T=308.2 K

n_a (s^{-1})	$\varepsilon_{toluene}$	$\varepsilon_{toluene}$
6.67	0.41	-
8.33	0.40	0.55
10.0	0.39	-
11.67	0.38	0.54
13.33	-	0.51

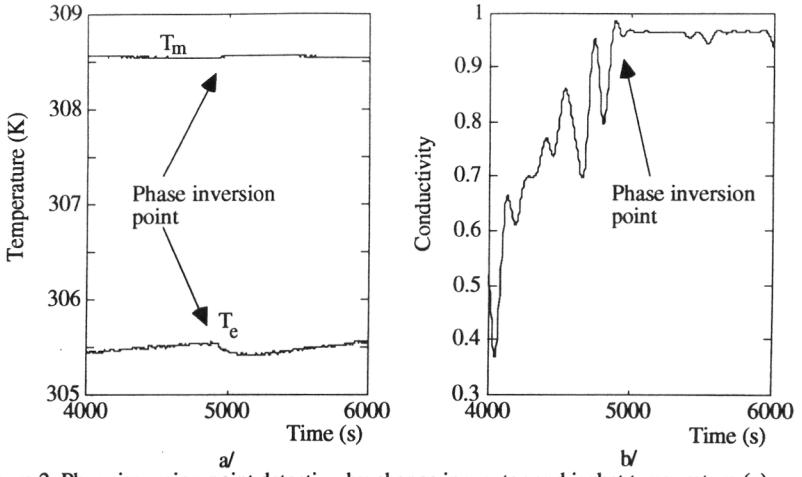

Figure 2. Phase inversion point detection by change in reactor and jacket temperature (a), or by change in conductivity (b) for the system toluene-70 wt % sulphuric acid and a stirrer speed of 8.33 s^{-1}. For (b) we have an arbitrary scale between 0 and 1.

Table 3. Volume fraction ε at phase inversion for the systems toluene-70 wt % sulphuric acid, T=308.2 K and benzene-70 wt % sulphuric acid , T=298.2 K.

n_a (s^{-1})	$\varepsilon_{toluene}$	$\varepsilon_{benzene}$
5.0	0.70	0.64
	0.72	
5.83	0.70	0.63
6.67	0.66	0.60
	0.65	
8.33	0.58	0.54
	0.58	
10.0	0.56	-
	0.52	
11.67	0.52	-
13.33	0.49	-

3. MODELLING PHASE INVERSION. PREPARATORY EXPERIMENTS AND MODEL VALIDATION

Phase inversion may affect semibatch nitrations by modifying:

- the internal heat transfer coefficient h_0 due to a change in physical and transport properties of the mixture,
- the conversion rate due to a change in the interfacial area 'a', and/or mass transfer coefficient k_L.

To characterise these effects separately, different experiments were carried out. The effective heat transfer parameter US was evaluated for non-reactive heterogeneous mixtures of toluene and benzene and 70 % wt. sulphuric acid. The interfacial area at phase inversion was measured with the chemical method with a similar system like aromatic nitrations; Toluene and Diisobutylene/77 wt. % sulphuric acid, see Zaldívar *et al.* (1995b).

3.1. Effective heat transfer parameters in liquid-liquid systems

The heat flow to the jacket is proportional to the temperature difference between the reaction mixture T_m and the jacket T_e:

$$q_{removed} = U \cdot S \, (T_m - T_e) \cdot \Psi \qquad (1)$$

where US depends on the fluids properties, operating conditions, and the geometry of the system. Ψ is a correction factor which takes into account the temperature variation of the heat transfer fluid between the inlet and outlet in the jacket. Experimentally US is evaluated with calorimetric methods: heat flow calorimetry has been demonstrated to be a useful technique, see Bourne *et al.*(1981).

We will check whether the mathematical model to predict the effective heat transfer parameter, previously developed and tested for pure liquids, see Zaldívar *et al.* (1990) can be used for liquid-liquid dispersions. Furthermore, the effect of phase inversion phenomena on this parameter is studied.

The effective heat transfer parameter can be divided into:

The overall heat transfer coefficient: The overall heat transfer coefficient is expressed as the inverse of the sum of the three main resistances of the film at the wall in the reaction mixture $1/h_0$, the wall thermal conductivity $1/h_w$ and on the film in heat transfer fluid $1/h_1$:

$$U = \left(\frac{1}{h_0} + \frac{1}{h_w} + \frac{D_0}{D_1 \cdot h_1} \right)^{-1} \qquad (2)$$

where D_0 and D_1 are the internal and external diameter of the reactor wall.

Correlations for the film transfer coefficients are obtained from the Nusselt equation:

$$h_i = \theta_{1i} \frac{\lambda}{D} \, Re^{\theta_{2i}} \cdot Pr^{\theta_{3i}} \cdot Vi^{\theta_{4i}} \qquad (3)$$

The characteristic parameters (θ_{ji}'s) depend on the shape factors and fluid-dynamic regime, whereas the transport and physical properties of the reaction mixture and the heat transfer fluid are taking up in the dimensionless numbers. Using the Nusselt equation, the external heat transfer coefficient can be expressed as:

$$h_1 = \theta_{11} \frac{\lambda_e}{D_t} \left(\frac{\rho_e \cdot D_t \cdot Q_e}{S_t \cdot \mu_e} \right)^{\theta_{21}} \left(\frac{\mu_e \cdot Cp_e}{\lambda_e} \right)^{\theta_{31}} \left(\frac{\mu_e}{\mu_{\text{at the wall}}} \right)^{\theta_{41}} \qquad (4)$$

Experimentally from more than 400 experiments it was found, see Zaldívar *et al.* (1990), for the RC1 reaction calorimeter the characteristic parameters are: θ_{11}=1.11, θ_{21}=0.29, θ_{31}=0.33 and θ_{41}= 0.14.

In the case of the internal heat transfer coefficient we have:

$$h_0 = \theta_{10} \frac{\lambda_m}{D_0} \left(\frac{D_a^2 \cdot \rho_m \cdot n_a}{\mu_m} \right)^{\theta_{20}} \left(\frac{\mu_m \cdot Cp_m}{\lambda_m} \right)^{\theta_{30}} \left(\frac{\mu_m}{\mu_{\text{at the wall}}} \right)^{\theta_{40}} \quad (5)$$

For a turbine impeller using five different fluids, Bourne *et al.* (1981) found that θ_{10}=0.42, θ_{20}=0.69, θ_{30}=0.33 and θ_{40}=0.14 over range of 8 < Re < 4600. Similar results were obtained in the reaction calorimeter, see Zaldívar *et al.* (1990).

Heat transfer area : The heat transfer area is the surface wetted by the reaction mixture; it can be calculated as a function of the reaction mixture volume and the stirring or vortex formation by:

$$S = S_0 + \Delta S_v \quad (6)$$

where S_0 is the surface without agitation and ΔS_v is the surface increase due to the vortex. A correlation for ΔS_v was obtained by Zaldívar *et al.* (1990).

3.2. Experimental validation for liquid-liquid systems

Two procedures were adopted to evaluate the effective heat transfer parameter. The first consisted of adding periodically certain quantities to the reactor mass and evaluating US, see Appendix 1. The second consisted of introducing a compound to the reactor at constant rate and a known amount of heat q_i; US was determined following the procedure described in Appendix 1.

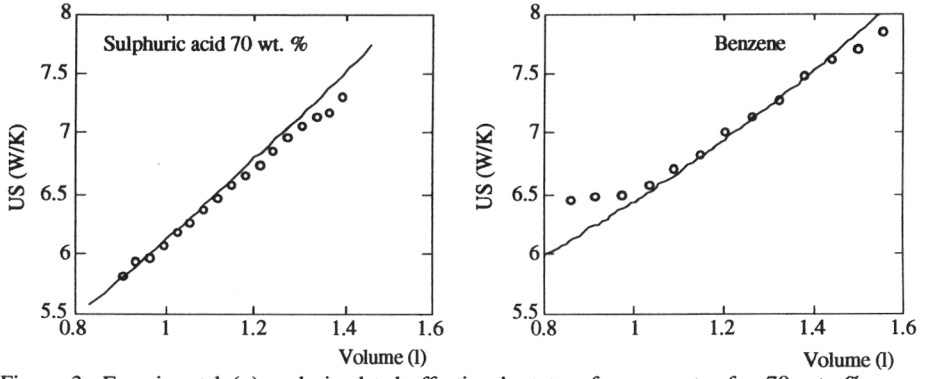

Figure 3. Experimental (o) and simulated effective heat transfer parameter for 70 wt. % sulphuric acid solution and benzene. T= 308.2 K and $n_a = 8.33\ s^{-1}$.

- Pure compounds and homogeneous mixtures: The effective heat transfer parameter for pure compounds and homogeneous mixtures was determined with the first procedure. Figure 3 shows the experimental and calculated results for 70.0 wt. % sulphuric acid and benzene. The agreement is satisfactory and the relative error lower than 10 %.

- Heterogeneous mixtures: The heterogeneous non-reactive mixtures of water-toluene, 70 wt. % sulphuric acid-toluene or benzene were chosen to study the overall heat transfer coefficient in liquid-liquid dispersions and the effect of phase inversion phenomena. The two types of experiments described previously were carried out. The phase inversion point was measured by detecting the change in the conductivity measurement. Figures 4 and 5 show the evaluated effective heat transfer parameters using both procedures for benzene-70 wt % sulphuric acid and toluene-70 wt % sulphuric acid.

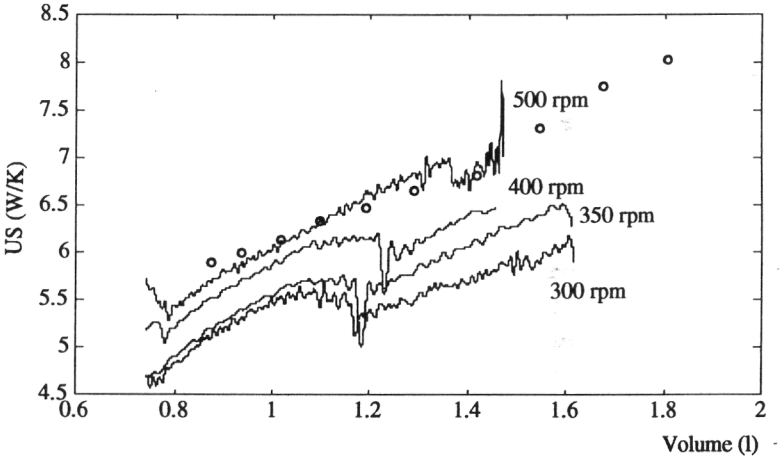

Figure 4. Experimental effective heat transfer for the mixture benzene-70 wt %sulphuric acid. The symbol 'o' indicates periodical addition of aqueous sulphuric acid to 640 g of benzene and the evaluation of US. T = 308.2 K. The lines indicate the experiments with a continuous evaluation of US, see Appendix 1.

As can be seen from experimental data, there is a change in the effective heat transfer parameter during phase inversion and also, the slope of US changes after phase inversion. Figure 6 shows two similar experiments with different phase inversion points. Similar behaviour in the effective heat transfer parameter is observed when phase inversion occurs and in the point at which it occurs there is a change in the effective heat transfer parameter. This delay time in phase inversion experiments was studied by Gilchrist *et al.* (1989) ; they found experimentally that it is sensitive to a wide range of parameters. In all the experiments carried out, going from organic to aqueous phase as the continuous phase, the effective heat transfer parameter decreases at phase inversion point.

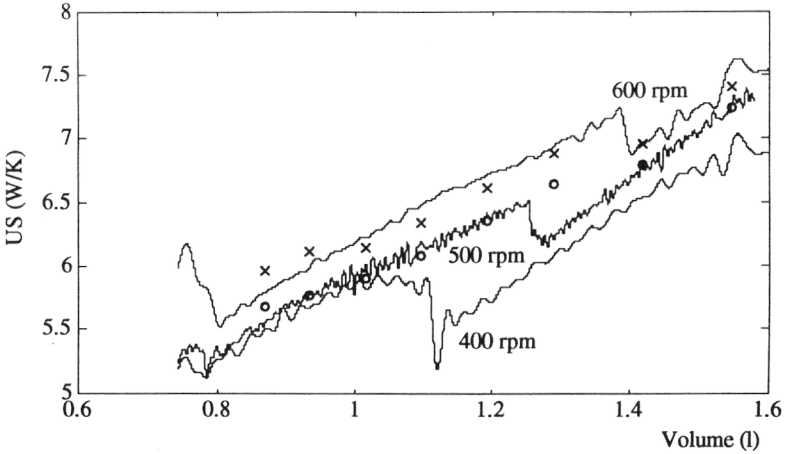

Figure 5. Experimental effective heat transfer for the mixture toluene-70 wt % sulphuric acid. The symbols 'o' and 'x' indicate the experiments with periodical addition of aqueous sulphuric acid to 631 g of toluene and evaluation of US. T = 308.2 K. The lines indicate experiments with continuous evaluation of US.

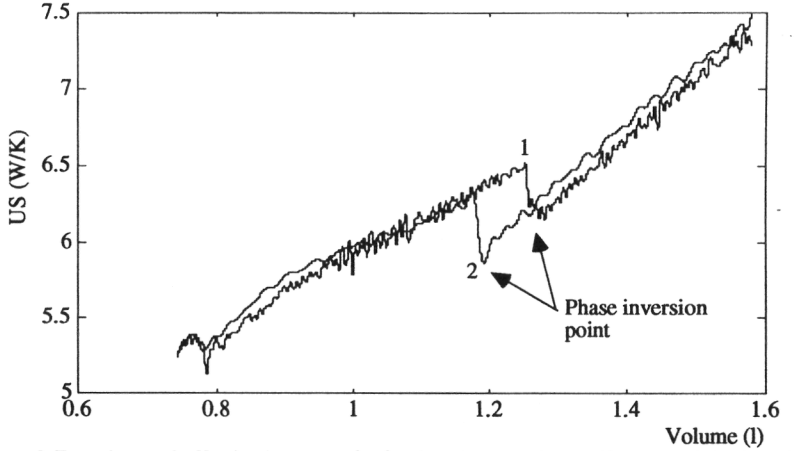

Figure 6. Experimental effective heat transfer for the mixture toluene-70 wt % sulphuric acid in two similar experiments. The addition of aqueous sulphuric acid to 0.74 l of toluene was carried out at constant rate. T = 308.2 K, and n_a=6.67 s^{-1}.

This change in US at phase inversion is caused by a change in the local internal heat transfer coefficient h_0 due mainly to the viscosity changes as observed experimentally by Guillinger *et al.* (1988). To calculate the viscosity of the mixture during phase inversion, different correlations, see Appendix 2, were checked and the best fit was obtained with the correlation from Leviton and Leighton (1936) which is an extension to Taylor's equation (1932); it has

been employed previously by Kumar *et al.* (1991). Figures 7 and 8 show the experimental and calculated effective heat transfer parameters. It can be concluded the classical approach, followed in this work for the prediction of the proportionality factor of Newton's law in jacketed agitated vessels, produces accurate results and can be extended to immiscible liquid systems by only modifying the transport properties.

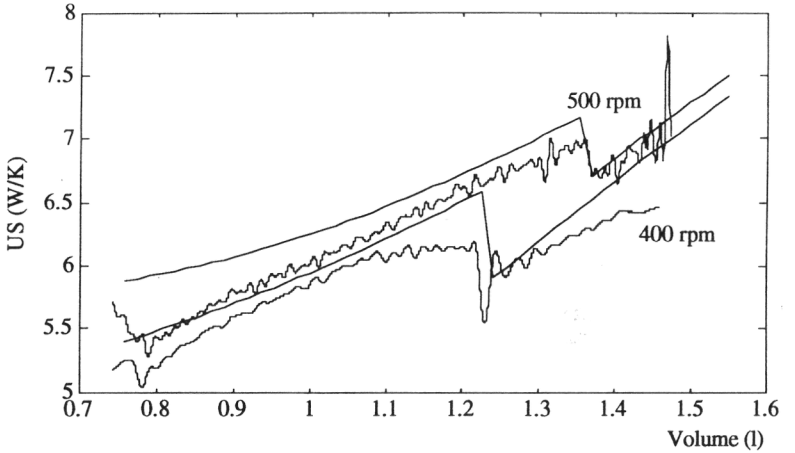

Figure 7. Experimental and simulated effective heat transfer parameters for the system benzene-70 wt % sulphuric acid.

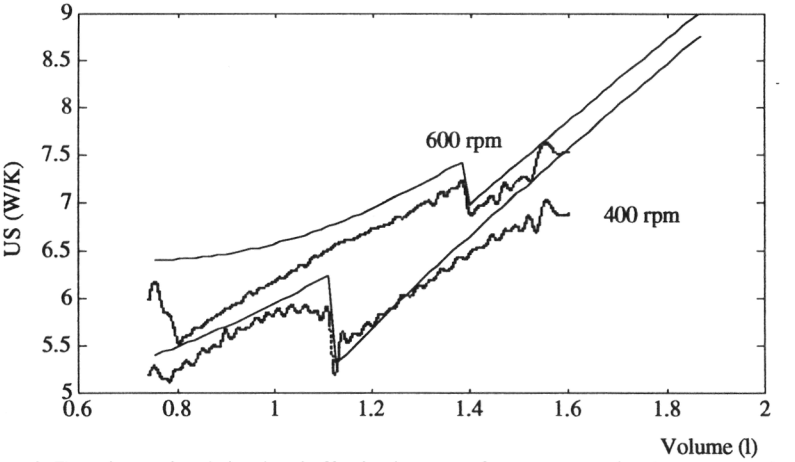

Figure 8. Experimental and simulated effective heat transfer parameters for the system toluene-70 wt % sulphuric acid.

3.3. Effect of phase inversion on the interfacial area: experimental study

The interfacial area per unit volume of dispersion can be calculated from:

$$a = \frac{6 \cdot \varepsilon_d}{d_{32}} \tag{7}$$

where d_{32} is given by:

$$d_{32} = A \cdot f(\varepsilon_d) \cdot We^{-0.6} \cdot D_a \tag{8}$$

and $f(\varepsilon_d)$ normally is a linear correlation:

$$f(\varepsilon_d) = 1 + B \cdot \varepsilon_d \tag{9}$$

The constant B can vary between 2.0 to 9.0. The validity of such a correlation has been questioned for dispersions with a volume fraction higher than 0.3, see Brooks and Richmond (1994): they recommended the correlation developed theoretically by Delichatsios and Probstein (1976). In this case the function of the dispersed phase volume fraction in Eq. 8 is:

$$f(\varepsilon_d) = \left(\frac{\ln(c_2 + c_3 \cdot \varepsilon_d)}{\ln c_2} \right)^{\frac{-3}{5}} \tag{10}$$

where $c_2 = 0.011$ is a constant related to the cut-off velocity in the Gaussian probability function and c_3 is a constant proportional to the ratio of coalescence to break-up coefficients. c_3 allows for differences in collision efficiencies in different systems. The value of c_3 must be determined empirically and differs from system to system; it should be of the order of 1.0.

In the case of phase inversion, the volume fraction of the dispersed phase and the Weber number We will change, where:

$$We = \frac{\rho_c \cdot n_a^2 \cdot D_a^3}{\sigma} \tag{11}$$

In the aromatic nitrations, if the acid phase becomes the continuous one, the density ρ_c will increase and as a consequence also We, which implies that d_{32} decreases and the interfacial area increases.

To study the change in interfacial area at phase inversion a series of experiments were carried out using the system toluene + DIB and 77.0 wt. % H_2SO_4. To check for phase inversion phenomena conductivity measurements as well as on-line heat transfer estimations were used. Phase inversion was observed in the experiment with $n_a = 6.67 s^{-1}$ at 6950 s, which corresponds to an $\varepsilon_d = 0.541$, just before the end of acid addition at 7200 s. This phenomenon is probably the cause of the observed significant difference between the values of the interfacial area calculated using the data from the semibatch period with acid addition and the batch period, see Molga *et al.* (1994). Phase inversion has not been observed at higher agitation speeds even if the dispersed phase volumetric fraction was as high as 0.6.

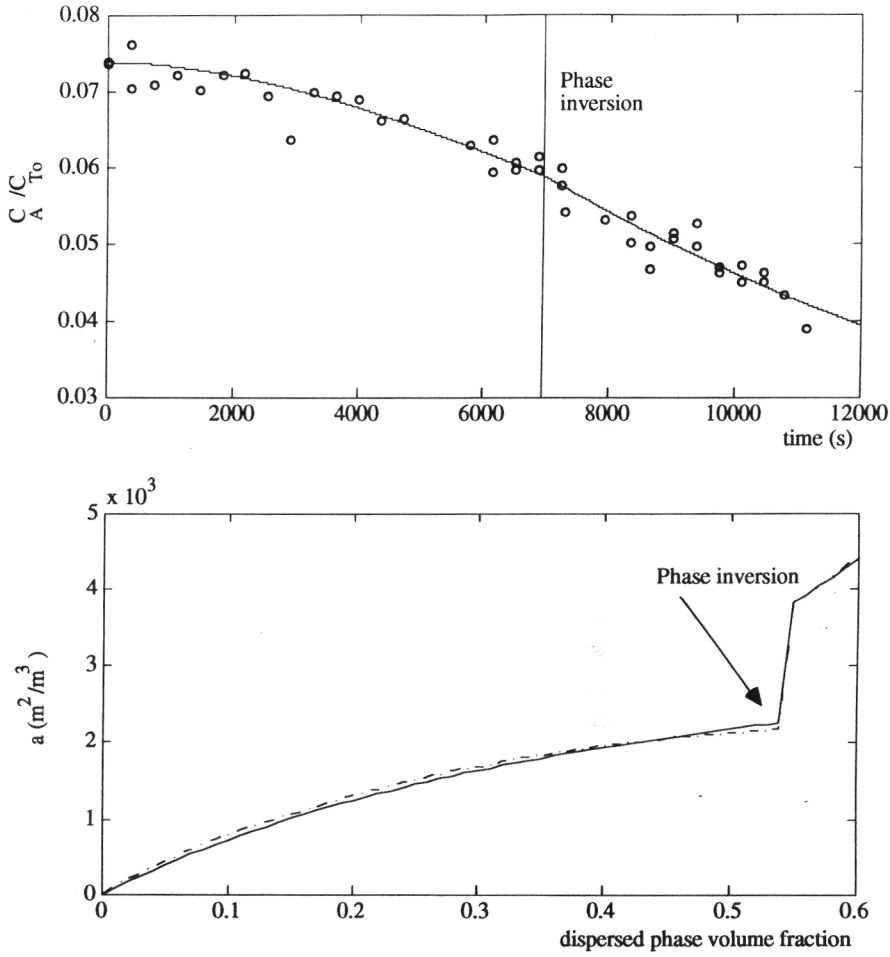

Figure 9. a/ Concentrations of DIB in a RC1 reactor in semibatch and batch operation n_a = 6.67 s^{-1}. b/ Interfacial area calculated with linear and non-linear dependences on the volume fraction.

To check the effect of phase inversion on the interfacial area, the parameters of eq. 8 were fitted to the experimental data assuming a linear dependence on the volume fraction and the dependence described by Delichatsios and Probstein (1976), respectively. The values of the fitted constants are A=0.431, B=2 for the linear dependence and A=0.321 c_3=0.847 for the correlation from Delichatsios and Probstein (1976), respectively. Figure 9a shows the experimental and calculated values for the reactive extraction of diisobutylene with aqueous sulphuric acid, see Zaldívar *et al.* (1995b) for experimental details, whereas in fig. 9b the

calculated values for the interfacial area are shown using the fitted curves. As can be seen in fig 9a, there is no difference between the fit of the linear dependence and the correlation of Delichatsios and Probstein (1976) and both predict a similar increase in the interfacial area of approximately 69 % and 75 %, respectively. The reason for this high increase - Fernandes and Sharma (1967) reported a change of 32% of the interfacial area in the system 2M NaOH and 2 ethyl hexyl formate - is probably due to the high density difference between the organic and the aqueous phases of 843 against 1678 kg/m^3, which changes the Weber number from 410 to 817.

4. CONVERSION RATES AND PHASE INVERSION PHENOMENA

Benzene, toluene and chlorobenzene nitration under normal industrial conditions, typically 15 mol % HNO_3, 30 mol % H_2SO_4 and 55 mol % H_2O, occurs in a two-phase system and under stirring. It has been confirmed by various authors, see Schofield (1980) and the references therein, that reaction is negligible in the organic phase and that the nitronium ion mechanism is applicable.

Furthermore, in the region of industrial interest with a 70 to 80 wt. % sulphuric acid strength and 298 to 318 K it was demonstrated that the nitration of benzene, toluene and chlorobenzene occurred in the fast regime, see Zaldívar *et al.* (1995b).

In this case the rate of mass transfer is enhanced by the reaction and the bulk of the reaction phase becomes less important, i.e. the concentration of the aromatic component transferred into the acid phase becomes negligible at even short distances from the interface. The Hatta number is defined as:

$$Ha = \frac{\sqrt{k_2 \; D_{ArH} \; C^{L2}_{HNO_3}}}{k_{L2}} \qquad (12)$$

If $2 < Ha << (D_{HNO_3} C_{HNO_3})/(D_{ArH} C^{i2}_{ArH})$, then the enhancement factor E equals Ha and the conversion rate becomes, see Westerterp *et al.* (1984):

$$J_{ArH}\, a = a \; k_{L2} \; E \; C^{i2}_{ArH} = a \sqrt{k_2 \; D_{ArH} \; C^{L2}_{HNO_3}} \; C^{i2}_{ArH} \qquad (13)$$

Hence, J_{ArH} no longer depends on the mass transfer coefficient. In case of Ha not much smaller than $(D_{HNO_3} C_{HNO_3})/(D_{ArH} C^{i2}_{ArH})$, diffusion limitation of HNO_3 occurs and the enhancement factor has to be calculated by iteration, see Westerterp *et al.* (1984).

In case of phase inversion, the interfacial area change plays an important role since the conversion rate is directly proportional to it. If E = Ha holds the conversion notlonger depends on the mass transfer coefficient. In view of the different nature of the mass transfer after

inversion - from the continuous phase to the droplet or from the droplet to the continuous phase - it may be possible the Ha number, which is inversely proportional to k_{L2}, changes and hence the nitration regime.

If the Hatta number decreases or k_{L2} increases, we may go to the slow regime, in which the rate of mass transfer is not enhanced anymore by reaction and the nitration proceeds in the bulk of reaction phase. Also it might be possible to arrive into the instantaneous regime, where no chemical limitations seem to exist. For an instantaneous reaction the conversion rate is so high that the reaction zone reduces to a plane in the boundary layer of the reaction phase.

5. EXPERIMENTAL STUDY. MODEL VERIFICATION WITH REACTION CALORIMETRY

To study phase inversion phenomena and their influence on the conversion rate, a series of toluene nitration experiments were carried out in the RC1 reaction calorimeter. This apparatus enables an accurate measurement of the heat removal from the reactor, which through a heat balance is used to determine the rate of heat generation in the reaction mass and hence the rate of conversion, see Reisen and Grob (1985). The precision of these calorimetric measurements, see Bonvin and Saner (1988), depends on the correct representation of all the secondary heat effects like heat losses, stirring power supply, heat taken up by reactor wall and dilution heat, see Zaldívar et al. (1990). In this particular case, the heat of dilution was evaluated using a model previously developed, see Zaldívar *et al.* (1992). Also selectivity and yields were directly determined from concentration measurements by gas chromatography, see Molga *et al.* (1993), and compared to the reaction rate estimated from the calorimetric measurements, see Hernández *et al.* (1993). Hence, two independent methods were employed to obtain experimental conversion rates.

To study the influence of phase inversion on the conversion rate, the previously developed model to calculate the effective heat transfer parameter was employed. Hence, the change of this parameter was taking into account to evaluate the conversion rates from experimental temperature profiles.

Figure 10 shows experimental and simulated rates profiles versus time for four different toluene nitration experiments, whereas in fig. 11 the experimental and simulated conversions of toluene to o-MNT, m-MNT and p-MNT are shown. Phase inversion took place at 12600, 4260, 4900 and 4400 s or volume fractions 0.455, 0.424, 0.475 and 0.470, respectively. In all the experiments the initial continuous phase was the organic phase and the stirrer spped was 6.67 s^{-1}. As can be observed, phase inversion increases suddenly the reaction rate, which is in accordance with the previously studied effects on the interfacial area. The simulated results gave as increases in interfacial area 42, 54, 40 and 45 %, respectively. These increases are lower than those found using the system Toluene(DIB)-77 wt % H_2SO4 which is coherent in

view of the differences in the physical properties, mainly the density difference between the phases. The behaviour of the reaction rate during phase inversion not only depends on the increase of the interfacial area, but also on the nitric acid accumulated during the process, see fig 11 for the simulated concentration profiles of nitric acid.

Phase inversion was simulated as a one step phenomenon, starting at a previously calculated moment in accordance with the experimental data. As can be seen, experimental phase inversion seems to be a slow process. This is in agreement with the findings of McClarey and Ali Mansoori (1978) who showed for systems with large density differences between the phases, that inversion took place over a range of volume fractions rather than at a single point.

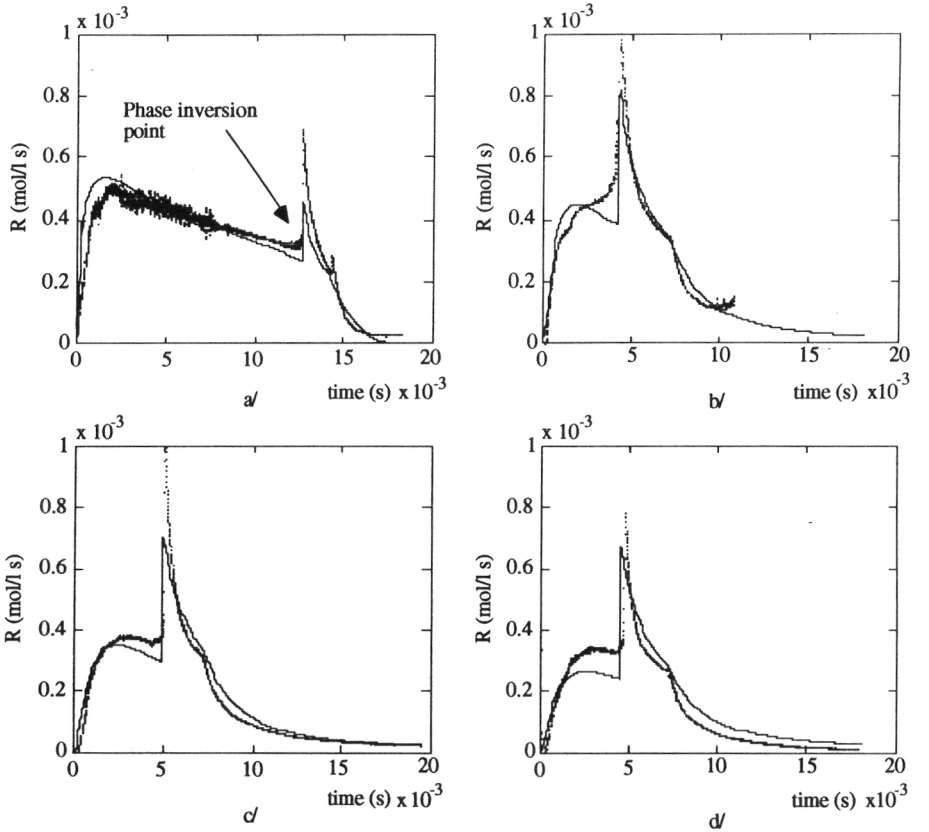

Figure 10. Experimental and simulated conversion rates for some semibatch nitration experiments in which phase inversion took place. **a/** x =78.9 wt. %, feed time 4 h, and T = 318.2 K. **b/** x = 68.02 wt.%, feed time 2 h and T_{sp} = 308.2 K. **c/** x = 66.1 wt.%, feed time 2 h and T = 308.2 K. **d/** x = 63.9 wt.%, feed time 2 h and T = 308.2 K.

From simulations it seems the increase in interfacial area is not the only parameter responsible for the increase in conversion rate. The best results, see figs. 10 and 11, were obtained using the correlation of Kronig and Brink (1950) for non-rigid droplets when the acid phase is the

dispersed phase, whereas that of Calderbank (1967) was best when phase inversion occurs and the acid phase becomes the continuous phase, see Zaldívar *et al.* (1995b). The simulations showed after the initial period, the reaction entered into the fast regime with Ha numbers between 3 and 10 and k_{L2} between 10^{-6} and 10^{-5} m/s. As phase inversion occurs and mixed acid phase becomes the continuous phase, the calulated value of k_{L2} decreases to values between 10^{-5} and 10^{-4} m/s and the system enters into the slow regime in which the conversion rate can be expressed as:

$$R = a \cdot k_{L2} \cdot C_{ArH}^{i\,2} \qquad (14)$$

which means $E \approx 1$. In this situation the conversion rate depends on the overall mass transfer coefficient, which produces an increase in the conversion rate even though the regime has changed from fast to slow. Experimental evidence is needed to confirm it.

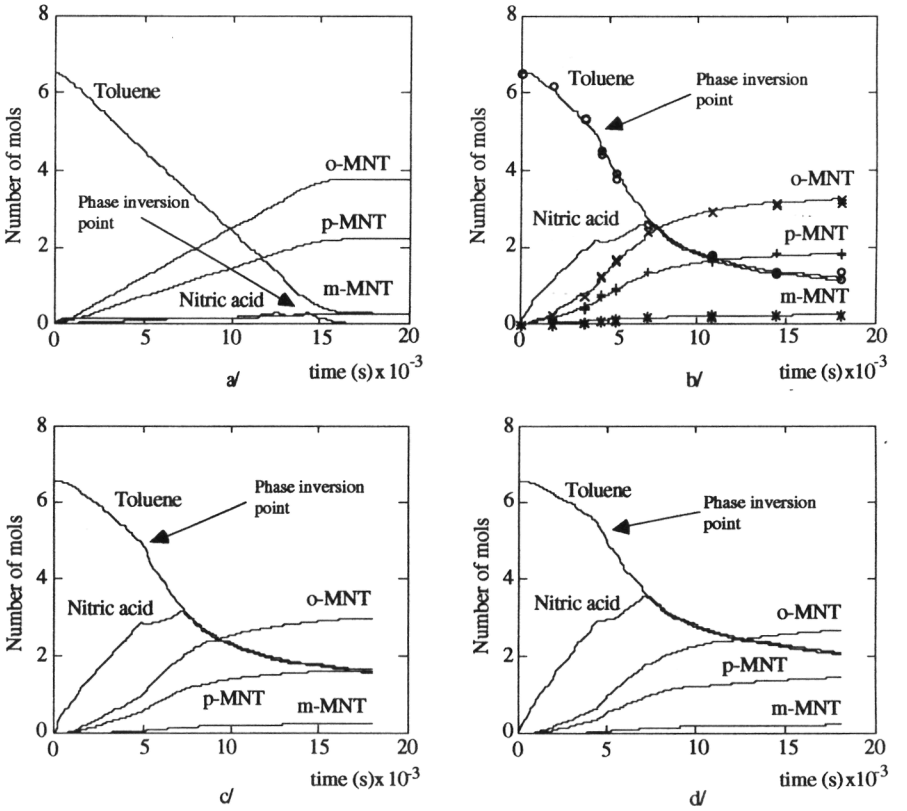

Figure 11. Experimental and simulated conversion profiles of the reactants for the above described semibatch nitrations in which phase inversion took place.

The calculated effective heat transfer parameters, using the correlations previously developed for heterogeneous liquid-liquid mixtures of aromatics and sulphuric acid solutions, are shown in fig. 12: phase inversion under these circumstances seems to produce a relatively small change; the principal contribution to an US increase is the continuous addition of fresh mixed acid during the semibatch process, thus increasing the volume of the reactor and hence the heat transfer surface, see the differences between the 4 h dosing time, experiment in fig. 12a, and 2 h dosing time, experiments in fig. 12c and d.

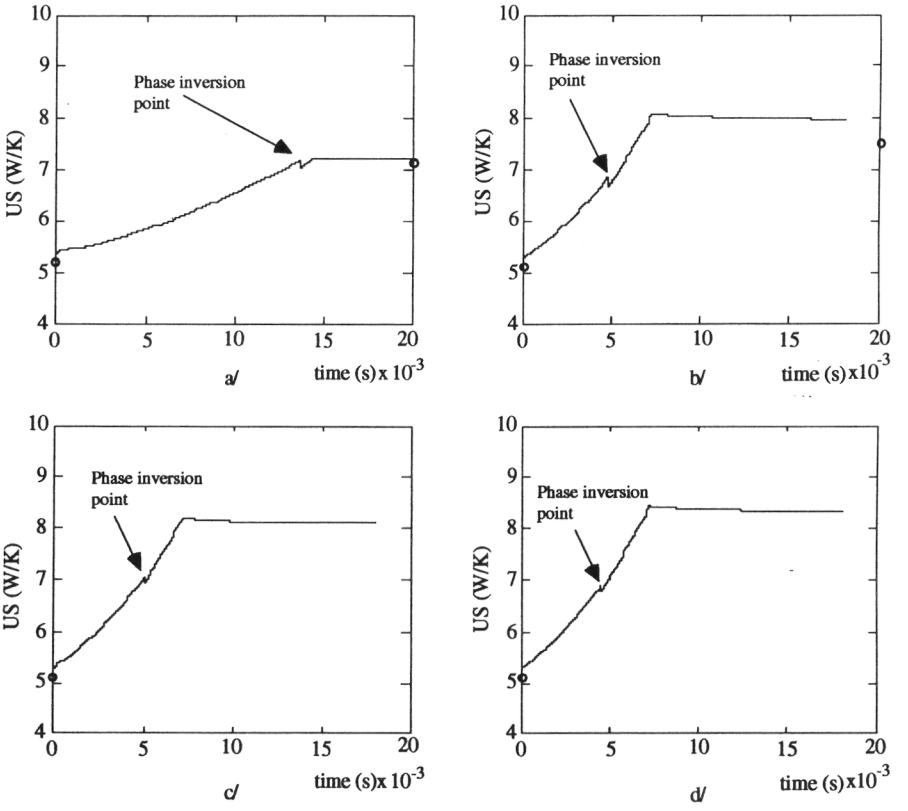

Figure 12. Experimentally and simulated effective heat transfer parameters for the above described semibatch nitrations in which phase inversion took place.

6. CORRELATION OF THE PHASE INVERSION POINT

The determination of the phase inversion point is complicated by the existence of an ambivalence region, in which what phase is dispersed depends on the method by which the

dispersion was formed and the time delays that may occur in these systems. All agitated heterogeneous liquid-liquid systems exhibit this hysteresis. For these reasons, only few attempts have been made to quantify the parameters controlling phase inversion. Quinn and Sigloh (1963) found that for dispersions of organic liquids in water the volume fraction of organic phase at phase inversion could be correlated by:

$$\varepsilon_{d_{PI}} = \varepsilon_{d_0} + \frac{C'}{P} \qquad (15)$$

where ε_{d_0} and C' are constants. ε_{d_0} is the asymptotic value of the volume fraction at which the stirrer speed no longer affects the phase inversion point and the latter is only related to the physical properties of the dispersion. P is the power introduced by the stirrer; for the highly turbulent regime it can be expressed by:

$$P = \phi \cdot \rho_m \cdot n_a^3 \cdot D_a^5 \qquad (16)$$

where ϕ may be considered constant in the system studied; in our case ϕ =2.2, see Zaldívar et al. (1995). Substituting eq. (16) into eq. (15) and rearranging gives:

$$\varepsilon_{d_{PI}} = \varepsilon_{d_0} + \frac{C''}{\rho_m \cdot n_a^3} \qquad (17)$$

Droplet size in a dispersion is determined by droplet breakup, droplet collision and droplet coalescence. Arashmid and Jeffreys (1980) assumed phase inversion will occur when the coalescence frequency is equal to the collision frequency, that is, every collision results in a coalescence. Hence, if T is the ratio between the coalescence and collision frequencies, phase inversion occurs when T=1. Using the expression deduced by Misek (1964) for the collision frequency and the expression deduced by Howarth (1967) for the coalescence frequency, Arashmid and Jeffreys arrived to the following expression:

$$T = \frac{C'''}{\varepsilon_d \cdot d_{32}^2 \cdot n_a^{\alpha}} \qquad (18)$$

where C''' and α are constants that depend on the characteristics of the stirrer and the physical properties of the mixture. Experimental results agreed well with this equation although incorrect forms for the collision frequency, see Guilinger *et al.* (1988) and for the coalescence frequency, see Tavlarides and Stamatoudis (1981), were used.

In both models the ambivalence region can be represented adjusting the constants in eq. (17) and eq. (18) depending whether the initial dispersed phase is the organic or the aqueous. Figure 13 shows the experimental and calculated results using eq. (18) for the different systems studied. The constants C''' and α were obtained by non-linear regression over the experimental points in Tables 2 and 3and are: $C''' = 2.26 \cdot 10^{-4}$ and $\alpha = 2.7$ for the Water-Toluene system, $C''' = 1.42 \cdot 10^{-4}$ and $\alpha = 2.7$ for the Toluene-Water,. $C''' = 1.05 \cdot 10^{-3}$ and $\alpha = 3.3$ for the Toluene-70 wt. % Sulphuric acid and $C''' = 8.7 \cdot 10^{-4}$ and $\alpha = 3.3$ for Benzene-

70 wt. % Sulphuric acid. As can be seen the influence of stirrer speed, represented in the constant α, change from one system to the other.

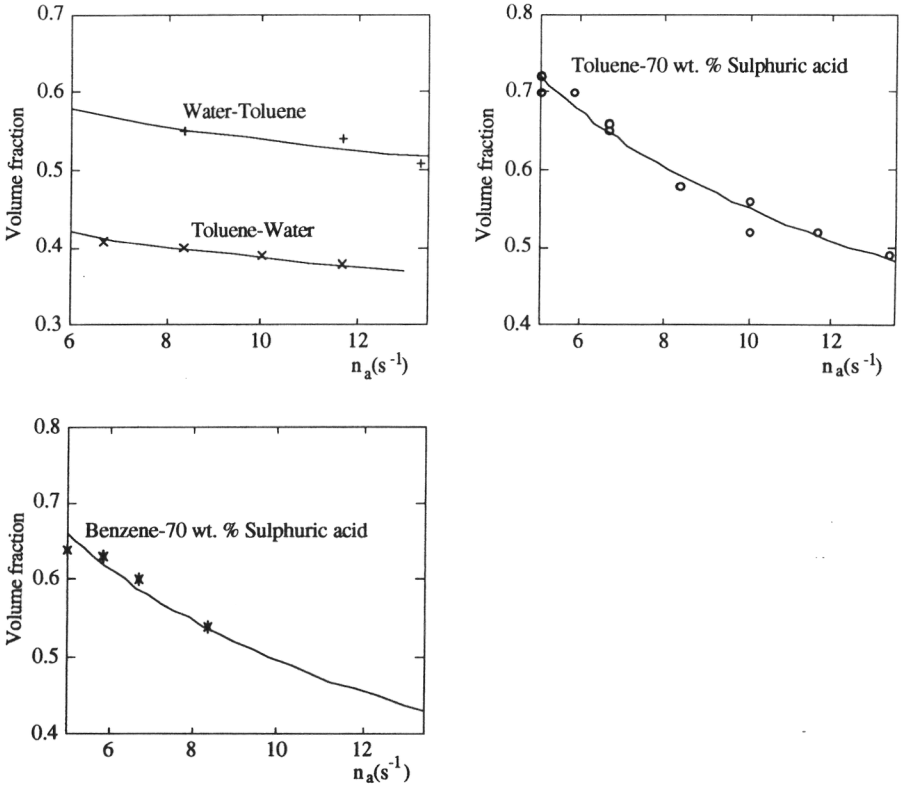

Figure 13. Experimental and calculated phase inversion points for the systems (+) Water-Toluene, (x) Toluene-Water, (o)Toluene-70 wt. % Sulphuric acid, (*)Benzene-70 wt. % Sulphuric acid. For data see Tables 2 and 3.

During semibatch aromatic nitrations the compositions of organic and aqueous phase change as reaction proceeds. As can be seen from concentration data in fig. 11 at the phase inversion point, the composition of the reaction mixtures was different. Therefore, the correlations developed by previous authors can not be used to predict the phase inversion point.

7. CONCLUSIONS

The accumulation of unreacted nitric acid in semibatch aromatic nitrations can be dangerous if accompanied by a phase inversion due to the fact that the rate may increase suddenly, since the reaction rate is usually mass transfer controlled under industrial operating conditions. The main

parameter responsible for this increase in conversion rate is the interfacial area that increases if the continuous phase change to acid with the accompanying change in density of both phases.
The inside heat transfer coefficient influences the heat removal rate. The change of this parameter is correlated to the change in physical and transport properties of the mixture during phase inversion. Here, the viscosity plays an important role.
The correlation developed by Arashmid and Jeffreys (1980) can be used to predict the phase inversion point in systems with constant composition. However, it is not possible to use it for reacting systems, in which phases compositions change continuously, i.e. in semibatch aromatic nitrations. Unfortunately, the prediction of the phase inversion point is difficult since it depends on the stirrer speed, temperature, interfacial tension, etc. Moreover it exhibits hysteresis phenomena and in some cases inversion takes place over a range of volume fractions rather than at a single point, i.e. it is not an instantaneous phenomenon. More attention will be dedicated to this aspect in future research.
The mathematical model derived can be used to predict the influence of phase inversion on the dynamic behaviour of a nitrator, the mass transfer coefficient should be investigated further to clarify whether it changes during phase inversion.

NOTATION

a	interfacial area (m^2/m^3)
A	constant (eq. 9)
c_3	constant (eq. 10)
C	concentration ($kmol/m^3$)
Cp	Specific heat capacity ($J \cdot Kg^{-1} \cdot K^{-1}$)
d_{32}	Sauter mean diameter of droplets (m)
D	diffusion coefficient (m^2/s)
D_a	impeller diameter (m)
D_0	internal reactor diameter (m)
D_1	external reactor diameter (m)
E	Enhancement factor
F	molar flow (mol/s)
h	partial heat transfer coefficient ($W \cdot m^{-2} \cdot K^{-1}$)
Ha	Hatta number
J_A	molar flux ($mol/m^2 \cdot s$)
k_L	mass transfer coefficient (m/s)
k_2	measured 2nd order rate constant ($m^3/kmol \cdot s$)
m	distribution coefficient
M	mass (kg)
n	Molar hold-up
n_a	impeller speed (rps)
q	thermal flow (W)
Q	volumetric flow (m^3/s)
R	overall reaction rate ($kmol/m^3 \cdot s$)

S	heat transfer surface (m^2)
t	time (s)
T	temperature (K)
U	overall heat transfer coefficient ($W \cdot m^{-2} \cdot K^{-1}$)
US	effective heat transfer parameter($W \cdot K^{-1}$)
V	volume (m^3)
x	sulphuric acid strength

Greek letters

ε_d	dispersed phase volume fraction
γ	surface tension (Nw/m)
λ	thermal conductivity ($W \cdot m^{-1} \cdot K^{-1}$)
μ	viscosity ($Kg \cdot m^{-1} \cdot s^{-1}$)
ρ	density (Kg/m^3)
σ	interfacial tension(Nw/m)

Subscripts and superscripts

0,1	internal and external sides
A	Diisobutylene
a	acid phase
ArH	aromatic compound
B	Sulphuric acid
c, d	continuous and dispersed phases
e	jacket
i1,i2	aqueous and organic interphase
L1,L2	aqueous and organic phase
m	reaction mixture
o	organic phase
PI	phase inversion
t	hydraulic
To	Toluene
w	reactor wall

REFERENCES

Arashmid, M. and Jeffreys, G. V., 1980, Analysis of the phase inversion characteristics of liquid-liquid dispersions. *AIChE Journal* **26**, 51-55

Barnea, E. and Mizrahi ,J., 1976, On the "effective" viscosity of liquid-liquid dispersions. *Ind. Eng. Chem. Fundam.* **15**, 120-125.

Barnea, E. and Mizrahi, J., 1973, A generalized approach to the fluid dynamics of particulate systems. Part 1. General correlation for fluidization and sedimentation in solid multiparticle systems. *The Chem. Eng. J.* **5**, 171-189.

Bonvin, D., de Vallière, P. and Rippin, D.W.T., 1989, Application of estimation techniques to batch reactors- I. Modelling thermal effects. *Computer Chem. Engng.* **13**, 1-9.

Bonvin, D. and Saner, U., 1988, On line procedures for supervising the operation of batch reactors, *Computer Chem. Engng.* **12**, 371-376.

Bourne, J.R., Buerli, M. and Regenass, W., 1981, Heat transfer and power measurements in stirred tanks using heat flow calorimetry. *Chem. Eng. Sci.* **36**, 347-354.

Brooks, B. W. and Richmond, H. N., 1994. Phase Inversion in non-ionic surfactant-oil-water systems II. Drop size studies in catastrophic inversion with turbulent mixing. *Chem. Engng. Sci.* **49**, 1065-1075.

Calderbank P.H., 1967, Mass Transfer in V.W. Uhl, J.B. Gray (eds), *Mixing theory and practice*, Academic Press, New York.

Choudhury, S. Utiger, L. and Riesen, R., 1990, Heat transpot in agitated vessels: scale-up methods. Chem. Ing. Tech. 62, 154-168.

Clarke, S.I., and Sawistowski H.,1978, Phase inversion of stirred liquid/liquid dispersions under mass transfer conditions.*Trans IChem E* **56**, 50-55.

Delichatsios, M. A. and Probstein, R. F., 1976, The effect of coalescence on the average drop size in liquid-liquid dispersions. *Ind. Engng. Chem. Fundam.* **15**, 134-137.

Fernandez J.B. and Sharma M.M., 1967, Effective interfacial area in agitated liquid-liquid contactors, *Chem. Eng. Sci.* **22**, 1267-1282.

Ganguly, K., Ray, P. and Mitra, A., 1992, Phase inversion studies in liquid dispersions- a review. *IEI Journal* **72**, 49-54.

Gilchrist, A., Dyster, K. N., Moore, I.P.T., Nienow, A. W. and Carpentier, K. J., 1989, Delayed phase inversion in stirred liquid-liquid dispersions. *Chem. Eng. Sci.* **44**, 2381-2384.

Guilinger T.R., Grislingas A. K. and Erga O., 1988, Phase inversion behavior of water-kerosene dispersions. *Ind. Eng. Chem. Res.* **27**, 978-982.

Hernández, H., Zaldívar, J.M. and Barcons, C., 1993, Development of a mathematical model and a numerical simulator for the analysis and optimization of batch reactors.*Computers Chem. Engng.* **17S**, 45-50.

Hoffman, W., 1989, Qdos Qflow Qaccu and all these things. Proceedings of the RC1 3rd International User's Forum, St. Moritz (CH).

Howarth, W. J., 1967, Measurement of coalescence frequency in an agitated tank. *AIChE Journal* **13**, 1007-1013.

Kronig, R. and Brink, J. C., 1950, On the theory of extractions from falling droplets. *Appl. sci. Res.* **A2**, 142-154.

Kumar, S., Kumar, R. and Gandhi, K. S., 1991, Alternative mechanisms of drop breakage in stirred vessels. *Chem. Engng. Sci.* **46**, 2483-2489.

Laity, D. S. and Treybal, R. E., 1957, Dynamics of liquid agitation in the absence of an air-liquid Interface. *A.I.Ch.E. Journal* **3**, 176-180.

Leviton, A. and Leighton, A., 1936, *J. Phys. Chem.* **40**, 71

Luhning, R. W. and Sawistowski, H., 1971, Phase inversion in stirred liquid-liquid systems, *Solvent Extraction Proceeding ISEC* **11**, 873-887.

McClarey, M. J. and Ali Mansoori, G., 1978, Factors affecting the phase inversion of dispersed immiscible liquid-liquid mixtures. *AIChE Symposium Series*, vol. 74, 134-139.

Misek, T., 1964, Coallescence of drops in an agitated liquid-liquid extractor. *Collection Czeck. Chem. Comm.* **29**, 2086-2093.

Molga, E., Barcons, C. and Zaldívar, J.M., 1993, Mononitration of toluene and quantitative determination of the isomer distribution by gas chromatography. *Afinidad* **50**, 15-20.

Molga, E., Zaldívar, J.M., and Hernández, H., 1994, Effective interfacial area in semibatch liquid-liquid stirred tanks reactors. Joint Research Center-Ispra site, Technical Note n° I.94.99.

Perry R.H. and C.H. Chilton, 1984, *Chemical Engineers' Handbook*, 6th Ed., MacGraw-Hill, New York.

Quinn, J. A. and Sigloh, D. B., 1963, Phase inversion in the mixing of immiscible liquids. *Can. J. Chem. Eng.* **42**, 15-18.

RC1 Operating Instructions, 1989, Mettler AG, Switzerland.

Reisen, R. and B. Grob, 1985, Reaction calorimetry in chemical process development. *Swiss Chem.* **7**, 39-43.

Rietema K., 1982, Science and technology of dispersed two-phase systems. *Chem. Engng. Sci.* **37**, 1125-1150.

Selker, A. H. and Sleicher, C. A., 1965, Factors affecting which phase will disperse when immiscible liquids are stirred together.*Can. J. Chem. Eng.***43**, 298-301.

Tavlarides, L. L. and Stamatoudis, M., 1981, The analysis of interphase reactions and mass transfer in liquid-liquid dispersions, in *Advances in Chemical Engineering*, vol 11, Eds. T.B. Drew, G. R. Cokelet, J. W. Hoopes Jr. and T. Vermeulen, Academic Press, New York.

Taylor G.I., 1932, The viscosity of a fluid containing small drops of another fluid. *Proc. Roy. Soc.*, Ser. A, **138**, 41-48.

Uhl V.W. and J.B. Gray (ed.), 1966, *Mixing: Theory and Practice*, vol. 1 and 2, Academic Press, New York.

Vand V., 1948, Viscosity of solutions and suspensions. *J. Phys. Chem.* **52**, 277-321.

Vanderveen, J.M., 1960, M.S. Thesis, Dept. of Chem Engr. University of California, Berkeley Lawrence Radiation Lab. Rept. UCRL 8733.

Vermeulen, T., Williams, G.M. and Langlois, G.E., 1955, Interfacial area in liquid-liquid and gas-liquid agitation. *Chem. Eng. Prog.* **51**, 85F-94F.

Villermaux, J., 1982, *Génie de la réaction chimique*, Technique et Documentation Paris.

Westerterp, K.R., van Swaaij, W.P.M. and Beenackers, A.A.C.M., 1984, *Chemical Reactor Design and Operation*, J. Wiley & Sons, Chichester.

Zaldívar, J.M., H. Hernández and C. Barcons, 1990, Development of a numerical simulator for a reaction calorimeter. FISIM, RC1 version, Joint Research Center-Ispra site, Technical Note n° I.90.109.

Zaldívar, J.M., H. Hernández, C. Barcons and R. Nomen, 1992, Heat effects due to dilution during aromatic nitrations by mixed acid in batch conditions.*J. of Thermal Analysis* **38**, 2575-2582.

Zaldívar, J.M., E. Molga , M. A. Alós, H. Hernández and K. R. Westerterp, 1995a. Aromatic nitrations by mixed acid. Slow liquid-liquid reactions, 'submited for publication'.

Zaldívar, J.M., E. Molga , M. A. Alós, H. Hernández and K. R. Westerterp, 1995b. Aromatic nitrations by mixed acid. Fast liquid-liquid reactions, 'submited for publication'.

Appendix 1: Continuous determination of the effective heat transfer parameter U S

Different experimental and empirical methods have been proposed to evaluate the effective heat transfer parameter US; heat flow calorimetry has been demonstrated to be a useful technique, see Bourne *et al.* (1981), and is widely used. The method consists in introducing a known amount of heat q_i in the reaction mass by means of an electrical resistance and comparing the area under the curve of a plot of $(T_m-T_e)\Psi$ against time over the period of the calibration, see RC1 Operating instructions, while keeping the reactor temperature constant via the control system:

$$U \cdot S = \frac{q_i}{(T_m-T_e)\cdot\Psi} \qquad \textbf{(A1)}$$

The correction factor Ψ takes into account the temperature variation of the heat transfer fluid through the jacket and can be obtained by means of a local heat balance:

$$\Psi = \left[\frac{1-\exp\left(\frac{-U\cdot S}{Q_e\cdot Cp_e}\right)}{\frac{U\cdot S}{Q_e\cdot Cp_e}} \right] \qquad \textbf{(A2)}$$

The effective heat transfer parameter is determined at the start of the experiment, before chemical reaction starts, and at the end, when all the reagents have been consumed. Linearity between these two points is assumed for further evaluations. This simplification may produce important errors when the measured power is used to estimate kinetic parameters, for scale-up procedures, for implementation of temperature control strategies, etc. To solve this problem different approaches can be used, between them the application of model-based estimation techniques, see Bonvin *et al.* (1989), continuous calibration, see Hoffman (1989), etc.

Here a continuous calibration method, based on a mathematical model previously developed and validated for the RC1 reaction calorimeter, see Zaldívar *et al.* (1990), was used to estimate US during phase inversion studies using non-reactive mixtures. The formulation of the energy balance for the reactor contents enables us to determine time dependence of the temperature of the reactor mixture, see Hernández *et al.* (1993), assuming there is no heat of reaction:

$$\frac{dT_m}{dt} = \frac{1}{\Gamma_m}\left[q_E + U\cdot S\,(T_m-T_e)\,\Psi + q_a + q_l + q_i \right] \qquad \textbf{(A3)}$$

where the different thermal flows taken into account are q_E, for mass addition, q_a, for the agitation, q_l, for the exchange with the surroundings, q_i, for the input by the calibration heater; Γ_m is the thermal capacity of the reaction mixture and internal wetted devices in the reactor.

The continuous calibration method consists of adding a well known and constant amount of heat q_i to the mixture, by means of an electric heater during the entire experiment. The term of heating/cooling by mass addition can be determinated from the enthalpy difference between the feed stream and the reaction mixture as follows:

$$q_E = -\sum_{j \in A_L}^{N_L} F_{E_j} \int_{T_m}^{T_{E_j}} Cp_j \cdot dT \qquad \text{(A4)}$$

where F_{Ej} is the molar input flow of j and:

$$F_{E_j} = \sum_{j \in A_L}^{N_L} Q_k \cdot C_{E_j} \quad ; \quad k=1,...,N_E \qquad \text{(A5)}$$

where Q_k is the mass flow of k-th input stream and C_{Ej} is the concentration of j in mol/kg.

The power supplied by stirring was previously evaluated by Zaldívar *et al.* (1990), being:

$$q_a = 2.2 \cdot \rho_m \cdot n_a^3 \cdot D_a^5 \qquad \text{(A6)}$$

whereas the term of heat losses is proportional to the temperature difference between the mixture and the surroundings, see the Mettler RC1 operating instructions:

$$q_l = 0.1(T_{amb} - T_m) \qquad \text{(A7)}$$

The thermal capacity of the reaction mixture is calculated as the product of the number of moles and the specific heat of the species in the reactor, including the thermal capacity $\Gamma_b = 69$ J/K of the devices wetted by the mixture:

$$\Gamma_m = \sum_{j \in A_L}^{N_L} n_{m_j} \cdot Cp_{L_j} + \Gamma_b \qquad \text{(A8)}$$

By registering the reactor, jacket, dosing and ambient temperatures plus the calibration heat introduced, it is possible after filtering the signal to estimate US continuously during the addition and hence, to check the influence of phase inversion.

Appendix 2: Physical and transport properties of liquid-liquid dispersions

Correlations for Newtonian liquid-liquid mixtures and their effective viscosity, density, specific heat capacity, thermal conductivity, diffusitivity and interfacial tension have been derived. The test for the adequacy of the methods used for calculating the average viscosity and density has been the relation between the Power number and the Reynolds number for single-phase data. In this relation the average density and viscosity for dispersions are introduced. For newtonian liquids this is perfectly satisfactory.

Interfacial tension and diffusitivity in multicomponent mixtures still cannot be predicted correctly, so experimental data and empirical correlations must be used, see Zaldívar *et al.* (1995a, 1995b). The arithmetic, average density of a liquid-liquid mixture is calculated using the volume fraction of each phase, see Uhl and Gray (1966):

$$\rho_m = \varepsilon_d \cdot \rho_d + (1-\varepsilon_d) \cdot \rho_c \qquad \text{(A9)}$$

The average specific heat capacity of the mixture can be calculated using the mass fraction of each phase:

$$Cp_m = \frac{M_c \cdot Cp_c + M_d \cdot Cp_d}{M_c + M_d} \qquad \text{(A10)}$$

Estimates of the thermal conductivity of liquid-liquid emulsions can be made using Tareef's correlation, see Perry and Chilton (1984), which has been recomended by Choudhury *et al.* (1990) for this type of systems:

$$\lambda_m = \lambda_c \frac{2\cdot\lambda_c + \lambda_d - 2\cdot\varepsilon_d(\lambda_c - \lambda_d)}{2\cdot\lambda_c + \lambda_d + \varepsilon_d(\lambda_c - \lambda_d)} \qquad \text{(A11)}$$

The effective viscosity of a heterogeneous system μ_m is related to the viscosity of the continuous phase μ_c and is increased due to the presence of the dispersed particles or droplets. At low concentrations or $\varepsilon_d \rightarrow 0$ they manifest themselves only by being impermeable for the continuous phase. This effect was derived by Einstein, see Rietema (1982), to be:

$$\mu_m = \mu_c (1 + 2.5\cdot\varepsilon_d) \qquad \text{(A12)}$$

Vand (1948), taking into account the hydrodynamic interaction of the flow fields around the neighbouring particles, derived an expression for rigid, dispersed particles and low concentrations:

$$\mu_m = \mu_c \exp\left[\frac{2.5\cdot\varepsilon_d}{1-0.61\cdot\varepsilon_d}\right] \qquad \text{(A13)}$$

When the dispersed particles are droplets or gas bubbles, one might expect the hydrodynamic interaction between the flow fields of neighbouring particles is less strong. On the basis of experiments different correlations based on the Einstein or Vand equations have appeared in literature, see Uhl and Gray (1966) and Rietema (1982) for a review, which are summarised in Table A1.

Table A1. Effective viscosity for Liquid-Liquid mixtures.

Author	Correlation
Taylor, 1932	$\mu_m = \mu_c \left[1+2.5 \cdot \varepsilon_d \left(\frac{\mu_d+0.4 \cdot \mu_c}{\mu_d+\mu_c} \right) \right]$
Leviton and Leighton, 1936	$\mu_m = \mu_c \exp\left[2.5 \left(\frac{\mu_d+0.4 \cdot \mu_c}{\mu_d+\mu_c} \right) \left(\varepsilon_d+\varepsilon_d^{\frac{5}{3}}+\varepsilon_d^{\frac{11}{3}} \right) \right]$
Vermeulen et al., 1955	$\mu_m = \frac{\mu_c}{1-\varepsilon_d} \left(1+\frac{1.5 \cdot \mu_d \cdot \varepsilon_d}{\mu_d+\mu_c} \right)$
Laity and Treybal, 1957	$\mu_m = \frac{\mu_c}{1-\varepsilon_d} \left(1+\frac{6.0 \cdot \mu_d \cdot \varepsilon_d}{\mu_d+\mu_c} \right)$
Vanderveen, 1960	$\mu_m = \frac{\mu_c}{(1-\varepsilon_d)^{1.5}} \left(1+\frac{\mu_d \cdot \varepsilon_d}{\mu_d+\mu_c} \right)^{1.5}$
Barnea and Mizrahi, 1975	$\mu_m = \mu_c \cdot B \left[\frac{\frac{2}{3} B + \left(\frac{\mu_d}{\mu_c}\right)}{B + \left(\frac{\mu_d}{\mu_c}\right)} \right]$ where $B=\exp\left[\frac{5 \cdot \varepsilon_d \cdot A}{3 (1-\varepsilon_d)} \right]$ and $A=\left(\frac{\mu_d+0.4 \cdot \mu_c}{\mu_d+\mu_c} \right)$
Barnea and Mizrahi, 1976	$\mu_m = \mu_c \cdot \exp\left[\frac{2.5 \cdot \varepsilon_d}{1-\varepsilon_d} \left(\frac{\mu_d^*+0.4 \cdot \mu_c}{\mu_d^*+\mu_c} \right) \right]$

Barnea and Mizrahi (1976) carried out an experimental study on the effective viscosity of relatively coarse and unstable liquid-liquid dispersions like water/silicone oil, toluene/glycerine and tetradecane/ethylene glycol in a dispersion range limited to ε_d lower than 0.33 and they found the experimental results corroborate their correlation. Similar results could be obtained using the relation of Leviton and Leighton (1936). In fact, numerical comparison of both equations reveals a reasonable agreement in the range of ε_d between 0 and 0.5. Barnea and Mizrahi (1976) use μ_d^* as an adjustable parameter representing the "effective" viscosity of the dispersed phase.

European Commission

EUR 16266 – Mathematical modelling and numerical simulation of aromatic nitrations by mixed acid in discontinuous reactors

J. M. Zaldivar

Luxembourg: Office for Official Publications of the European Communities

1995 – 184 pp. – 16.0 x 23.0 cm

Scientific and Technical Research series

ISBN 92-827-4107-9

This work deals with the mathematical modelling and numerical simulation of aromatic nitrations in discontinuous reactors, and the experimenta work carried out to characterise the model, as well as to verify the simulated results.
The model employed, based on the effective interfacial area between the two liquids and the description of mass transfer with reaction using the film model is used.Theoretical model predictions are compared with experimental results and the effect of the different parameters is discussed. From the comparisons between model and experimental results it can be concluded that it is possible to extrapolate data from homogeneous nitration experiments and to interpret the dynamic behaviour of discontinuous nitration processes of benzene, toluene and chlorobenzene in the different reaction regimens. Furthermore, the accumulation of unreacted nitric acid in semibatch aromatic nitrations can be dangerous if accompanied by a phase inversion due to the fact that the heat rate production may increase suddenly, since the conversion rate is usually mass transfer controlled under industrial operating conditions. The main parameter resposible for this increase is the interfacial area that increases if the continuous phase changes to acid phase.